

Vol. 6 No. 1 Tahun 2023

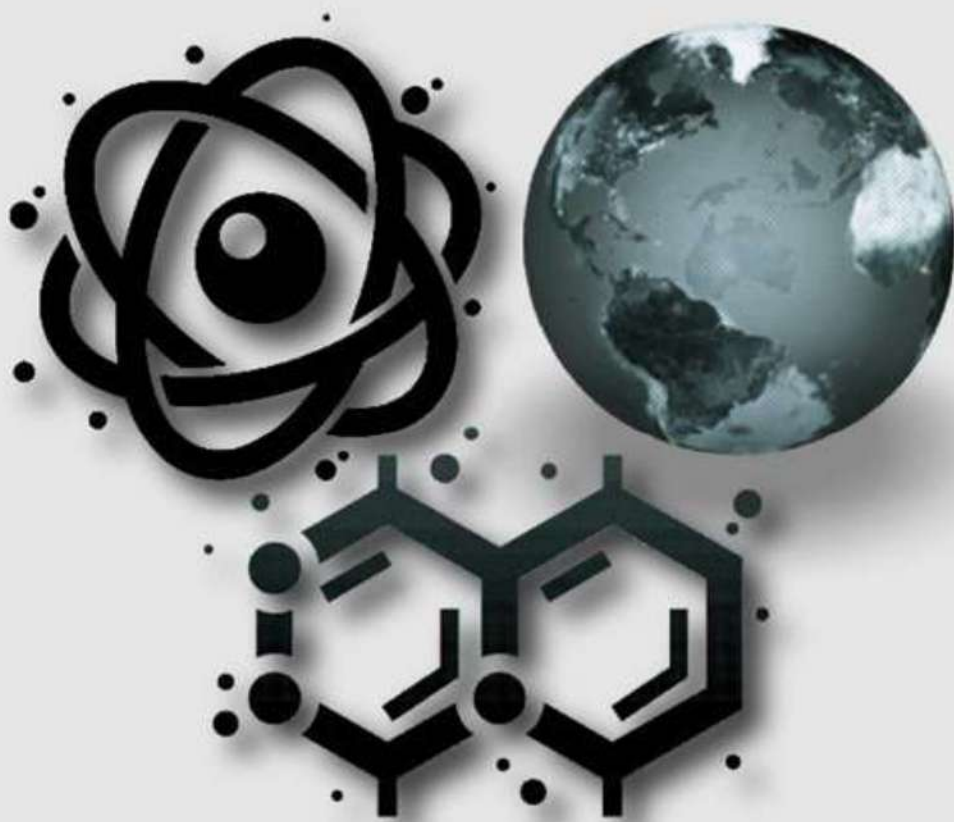
P-ISSN : 2621-0215

E-ISSN : 2621-489X

# Al-Fiziya



Journal of Materials Science, Geophysics,  
Instrumentation and Theoretical Physics



Published by  
Program Studi Fisika  
Fakultas Sains dan Teknologi  
Universitas Islam Negeri Syarif Hidayatullah Jakarta

**AL-FIZIYA:**  
Journal of Materials Science, Geophysics, Instrumentation,  
and Theoretical Physics

**Vol. 6, No. I, 2023**

**EDITORIAL IN CHIEF**

Dr. Sitti Ahmiatri Saptari

**MANAGING EDITOR**

Muhammad Nafian, M.Si

**REVIEWER**

Fitri Indah Sari, Ph.D

Ikhwan Nur Rahman

Dhita Azzahra Pancorowati

Muhammad Yusro

Dewi Lestari, M.Si

Mada Sanjaya W.S

Nizar Septian, M.Si

Dr. Rina Dwi Indriana, S.Si., M.Si

Agustya Adi Martha

Imam Wahyutama

Rofiqul Umam, M.Si., Ph.D

Dr. Humbang Purba

**SECTION EDITOR**

Saipudin, M.Si.

Biaunik Niski Kumila, M.Sc.

Pradityo Riyadi, M.Si

Arif Tjahjono, M.Si

Edi Sanjaya, M.Si

**LAYOUT EDITOR**

Ryan Rizaldy, M.Si.

**Alamat Redaksi**

Gedung Fakultas Sains dan Teknologi Lt. 3

Jl. Ir. H Juanda No.95 Ciputat 15412 Tangerang

Telp. (6221)743731, (6221)7493315

Email: [al-fiziya@uinjkt.ac.id](mailto:al-fiziya@uinjkt.ac.id)

**Published by**

Program Studi Fisika, Fakultas Sains dan Teknologi  
Universitas Islam Negeri Syarif Hidayatullah Jakarta

## PENGANTAR REDAKSI

Assalamu'alaikum, Wr. Wb.

Puji Syukur kita panjatkan kehadiran Allah SWT, dengan terbitnya Al-Fiziya: Journal of Materials Science, Geophysics, Instrumentation, and Theoretical Physics Vol 6, No. I, 2023 dengan nomor ISSN: 2621-0215 dan E-ISSN: 2621-489X sebagai jurnal penelitian dan pengembangan ilmu fisika yang diterbitkan oleh Program Studi Fisika Fakultas Sains dan Teknologi UIN Syarif Hidayatullah Jakarta. Jurnal ini menyajikan artikel-artikel penelitian dan pengembangan terkini baik dalam Bahasa Indonesia maupun Bahasa Inggris di bidang fisika murni dan terapan, antara lain bidang fisika material, geofisika, fisika instrumentasi, dan fisika teori. Jurnal ini merupakan sarana publikasi bagi dosen dan para peneliti yang bergerak di bidang penelitian dan pengembangan ilmu fisika. Dengan demikian, melalui penerbitan jurnal ini kami memberikan kesempatan seluas-luasnya bagi siapapun yang ingi berpartisipasi dalam menyampaikan buah pikirannya melalui tulisan atau artikel yang akan kami muat pada edisi berikutnya.

Artikel yang masuk akan melalui proses seleksi oleh dewan editor dan *review* yang melibatkan mitra bestari baik dari para dosen ahli dibidangnya berdasarkan kesesuaian isi dan bobot karya ilmiah. Untuk informasi lengkap submit dan tata cara penulisan dalam Al-Fiziya: *Journal of Material Science, Geophysics, Instrumentation, and heoretical Physics* dapat dilihat pada pedoman penulisan artikel di halaman akhir penerbitan atau dapat mengakses website kami di <http://journal.uinjkt.ac.id/index.php/al-fiziya>. Atas nama dewan redaksi, kami mengucapkan terimakasih atas dukungan dan partisipasi dari semua pihak hingga terbitnya Al-Fiziya: *Journal of Materials Science, Geophysics, Instrumentation, and Theoretical Physics*.

*Editorial in chief*  
**SITTI AHMIATRI SAPTARI**

## Daftar Isi

Vol. 6, No. 1, 2023

Pengantar Redaksi .....	i
Daftar Isi .....	ii
<b>Hidayah Fajria, Ferry Setiawan, Dhimas Wicaksono.</b> The Effect Of Nickel Electroplating Time On Aluminium 2024 To Its Mechanical Property .....	1 – 8
<b>Chandra Febriyanto, Ferry Setiawan, Ikbal Rizki Putra.</b> Testing the Banding Strength of Carbon Fiber Composite using the vacuum infusion and Vacuum Bagging Method on the UAV Skywalker 1900 Fuselage Material .....	9 – 19
<b>Abu Ammar, Muhammad Yusril, Prasepvianto Estu Broto.</b> Prototype of Automatic Tractor Control Navigation System Using ESP 32 Microcontroller .....	20 – 29
<b>Lamin Rene Loua, Dewi Lestari, Elvan Yuniarti, Rista.</b> Design and Control Underwater Robot Based on Smartphone .....	30 – 39
<b>Nanda Ridki Permana, Belista Gunawan.</b> 3D Visualization of Geothermal System Structure Based on Inversion Model of Gravity Data. Case Study: Mt. Salak Region, West Java.....	40 – 49
<b>Nur Fitriani, Siti Ahmiatri Saptari, Elvan Yuniarti.</b> Library Visitor Noise Monitoring System Design With Warning Using LED and Telegram....	50 – 59
<b>Suwondo, Mill Sartika Indah, Afzalurrahman Assalam, Muhammad Nafian, Andika Perbawa.</b> Lithofacies Interpretation Of Sediment Rocks In The Cipamingkis River Outcrop, Jonggol Area, Bogor District, West Java .....	60 – 70
<b>Pradityo Riyadi, Arkanu Andaru, Muhammad Nafian, .</b> 2D Joint Inversion of Gravity and Magnetic Data to Evaluate a Geological Structure in Tanimbar Island .....	71 – 78

---

## The Effect of Nickel Electroplating Time on Aluminum 2024 to Its Mechanical Property

Hidayah fajria<sup>1</sup>, Ferry Setiawan<sup>1,\*</sup>, Dhimas Wicaksono<sup>1</sup>

<sup>1</sup>College of Aerospace Technology of Yogyakarta, Indonesia

\*[ferry.setiawan@sttkd.ac.id](mailto:ferry.setiawan@sttkd.ac.id)

---

Submitted: January ; Revised: May ; Approved: July ; Available Online: september

---

**Abstract.** Nickel plating is an excellent way to protect aluminum components from corrosion and wear. Nickel plating offers several advantages over other protective coatings for aluminum parts. It is extremely cost-effective compared to other options like powder coating or painting. The purpose of this research on nickel electroplating on aluminum was to determine the effect of time on the mechanical properties in the form of the hardness value of the specimen. The SEM-EDX test was carried out on the specimen with the highest hardness test value to determine the microstructure and elemental composition of the coating. The materials used in this study were nickel as a coating and aluminum 2024 as a coated material. Fixed variables used in this study include voltage (25 V), electrode distance (20 cm), water (2400 ml), salt (40gr), vinegar (1600 ml), aluminum 2024, and nickel. The independent variable is the variation of coating time, namely 10, 15, and 20 minutes. The results of this study showed that the highest hardness value was found in specimens with 10 minutes of immersion time with a value of 198.31 HV and the lowest hardness value was obtained by sample with 20 minutes of immersion time with a value of 132.81 HV. After the SEM-EDX test, it was found that the microstructure of the layer was containing pitting (defects) and highest element found in the layer was Nickel with a mass of 84.07% and an atomic number of 55.29%.

**Keywords:** *aluminium 2024, nickel electroplating, hardness analysis, elemental analysis.*

**DOI :** [10.15408/fiziya.v6i1.30508](https://doi.org/10.15408/fiziya.v6i1.30508)

### INTRODUCTION

The technique of depositing metals from aqueous solutions onto substrate without the use of an external current source is known as electroless plating, which is sometimes referred to as autocatalytic plating (1,2). Brenner and Riddel invented this procedure in 1946 for the deposition of nickel-phosphorous alloys (3), and it has several industrial uses (4–6). Electroless nickel-boron plating is an instance of that method that

©2022 The Author (s) This is an Open-access article under CC-BY-SA license  
(<https://creativecommons.org/licenses/by-sa/4.0/>)

Al-Fiziya: Journal of Materials Science, Geophysics,  
Instrumentation and Theoretical Physics  
P-ISSN: 2621-0215, E-ISSN: 2621-489X

utilizes either sodium borohydride (7,8) or dimethylamineborane (DMAB) (9,10) as a reducing agent. The resultant alloys contain a substantial quantity of co-deposited boron.

The ability to plate non-conducting materials as well as metals is one of the most essential characteristics of electroless nickel plating, as is the production of continuous coatings with completely homogenous thickness regardless of substrate shape (11). Therefore, the electroless nickel plating is the superior and interesting electroplating methods to produce high hardness (around 750 hv100 in the as-deposited state) (12,13), good wear resistance (14–16), good corrosion behavior (6,12–14,16,17) metal alloy. Due to this, electroless nickel-boron coatings are applicable in a wide range of industries, including those in the chemical and petroleum industries, plastic injection, optical, aircraft, weapons, automotive, and electronics (11,18).

Aluminum alloy 2024 is one of the metal alloys which is mostly utilized by aircraft manufacturers as a material for aircraft components due to its excellent mechanical property which has a high strength to weight ratio. Apart from airplanes, aluminum 2024 is also often used as a material for making motorcycle components. Electroless plating on Aluminum alloys gives them mechanical qualities (wear resistance) that enable their usage in mechanical applications. But it is difficult to use this method for plating aluminum since sodium borohydride is very unstable, save in very alkaline conditions. As a result, the plating bath typically has a pH greater than 9, which is unsuitable for aluminum. In addition, because they are conducted at temperatures that are too high for aluminum alloys, heat treatments created for electroless nickel coatings (typically at 400 °C for 1 h) are not appropriate (19). Therefore, specific methods for improving electroless nickel-boron coating characteristics without negatively affecting the resistance of the aluminum substrate were discovered (15,20).

There have been previous studies of the characteristics of electroless nickel coatings on aluminum alloys (17,19–22) , However, there aren't many works that specifically address how the properties of electroplating change with time. In addition, coating nickel on an aluminum mixture without harming the mixture's structure required a relatively complicated and complex approach, which was used in earlier studies.

In this study, a simple technique has been utilized to generate metal alloy structures with lower structural defects compared to previous work (23). This work introduces a straightforward technique for coating metal alloys that has an excellent rate of effectiveness in terms of diminishing structural imperfections. In this study, nickel plating on an alloy of aluminum was conducted at various coating times of 10, 15, and 20 minutes. The effect on the mechanical properties was then examined following the study of the structure..

## **RESEARCH METHODS**

Electroplating is a process used to manipulate the properties of a substrate by coating it with another metal. The results obtained in the electroplating process are influenced by many variables, including the solution used, the temperature of the solution, the duration of the plating, the voltage between the two electrodes, the condition of the (23)electrodes used, and so on. Electroplating is made by passing an electric current through a solution between metals or other conductive materials. Two metal plates are the anode and cathode connected to the positive and negative terminals of the direct current (DC) source. The metal connected to the positive pole is called the

anode and the metal connected to the negative pole is called the cathode. When a voltage source is used in the electrolyte, the positive pole emits ions that move in solution (electrolyte) towards the cathode and are referred to as cations. The negative pole also gives off ions, moving towards the anode and is referred to as anion. The scheme of electroplating mechanism is shown in **Figure 1**.

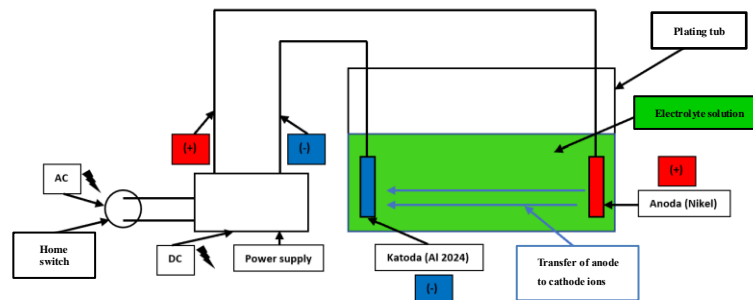


**Figure 1 Electroplating mechanism scheme**

Aluminum alloy 2024 is one of the metal alloys which is mostly utilized by aircraft manufacturers as a material for aircraft components due to its excellent mechanical property which has a high strength to weight ratio. Apart from airplanes, aluminum 2024 is also often used as a material for making motorcycle components. The element content of aluminum 2024 is shown in **Table 1**.

**Tabel. 1 Aluminium 2024 element content**

Element	Percentage (%)
Aluminium	90.7-94.7
Chromium	0.1
Copper	3.8-4.9
Ferrit	0.5
Magnesium	1.2-1.8
Mangan	0.3-0.9

The Vickers Hardness Test is to determine the resistance of the material associated with a smaller indenter, so that the results are more detail compared to using other hardness testing methods. The Vickers value is obtained using the formula 1 and 2:

$$D = \frac{(d1+d2)}{2} \quad \text{Formula 1}$$

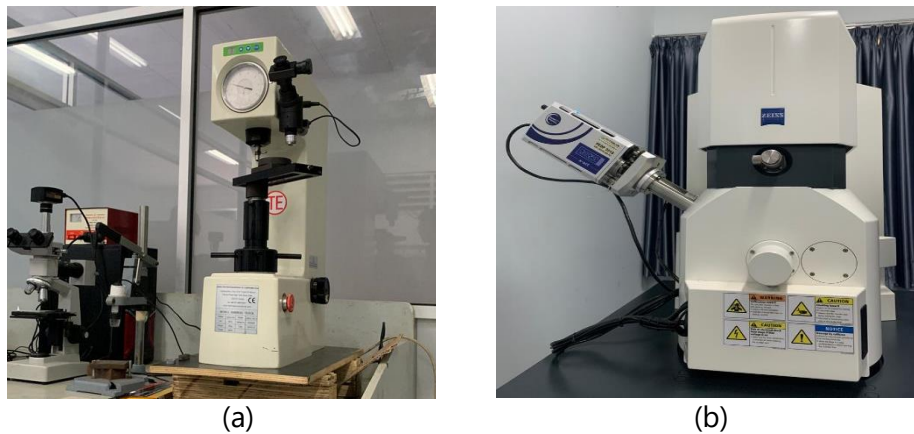
$$HV = \frac{1.854F}{D^2} \quad \text{Formula 2}$$

where:

- D : Mean diagonal tracking (mm),
- d1 : Side diagonal tracking 1 (mm),
- d2 : side diagonal tracking 2 (mm),
- HV : Hardness Vickers value (kgf/mm<sup>2</sup>), (HV), and
- F : Maximum force (Newton).

Scanning Electron Microscope (SEM) is an electron microscope designed to directly observe the surface of solid objects. SEM has a magnification of 10 – 3,000,000 times. Due to its combination of high magnification, large depth of field, good resolution, the SEM test is widely used to determine the composition and crystallographic information of a material surface.

This research was carried out by making electroplating tools. After carrying out the manufacturing process, all tools were calibrated both in the system and measuring instruments. After making sure everything is in good condition, the next step is to carry out the nickel-plating process on the aluminum base material and carry out hardness testing and SEM testing. Figure 2 shows the instruments used during the test:



**Gambar. 2 (a) Hardness testing instrument, (b) SEM-EDX instrument**

## RESULT AND DISCUSSION

The data from this study came from hardness tests on 3 electroplated specimens and SEM tests on specimens with the highest hardness values.

### 1. Hardness analysis

**Figure 3** shows the hardness Vickers values of samples with variation of nickel electroplating time.

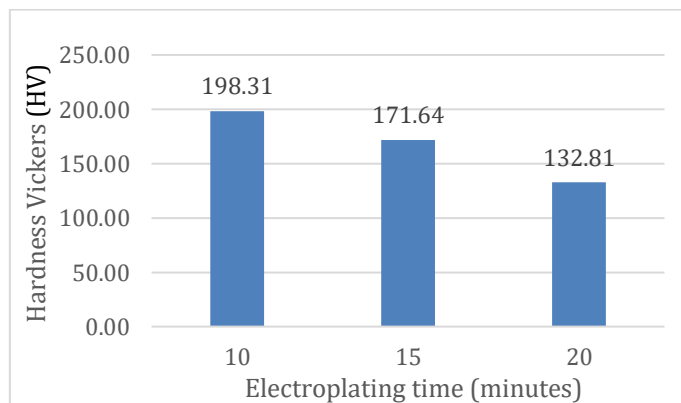


**Figure 3 The Hardness result of samples with nickel electroplating time variations of 10, 15 and 20 minutes.**



**Figure 3** shows the results of the average hardness value of each time variation. The sample with an immersion time of 10 minutes has the highest hardness Vickers value of 198.31 HV. Otherwise, the sample with longest immersion time (20 minutes) has the lowest hardness Vickers value of 132.81HV.

## 2. SEM-EDX Analysis

SEM test was carried out with a magnification of 1000 times. The microstructure of the electroplated layer obtained on the specimen with an immersion time of 10 minutes was obtained by Figure 4.

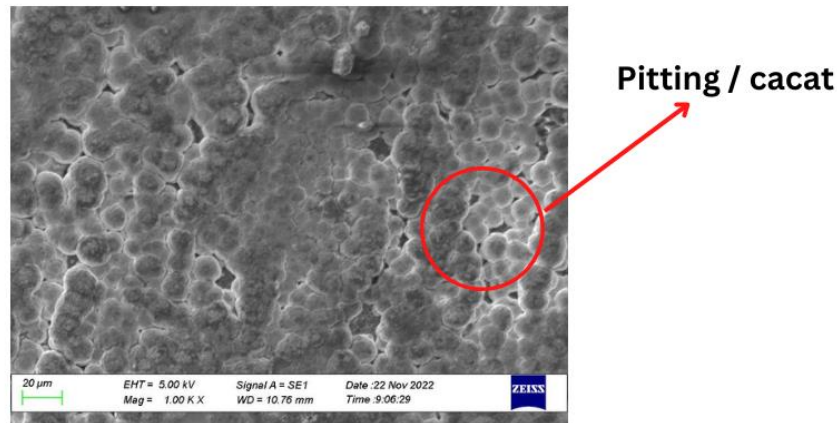


**Figure 4 SEM image of sample with immersion time of 10 minutes**

From the SEM result, it can be observed that the nickel was successfully coated to the Aluminum 2024. Nickel particles that stick to aluminum form bubbles that are layered and interrelated. However, there are also unrelated bubbles that form cavities in each of them. After carrying out the EDX test on the layer, it can be observed that it is these cavities that allow oxygen and carbon to be trapped in the layer. This can be caused by reactions that occur during the coating process.

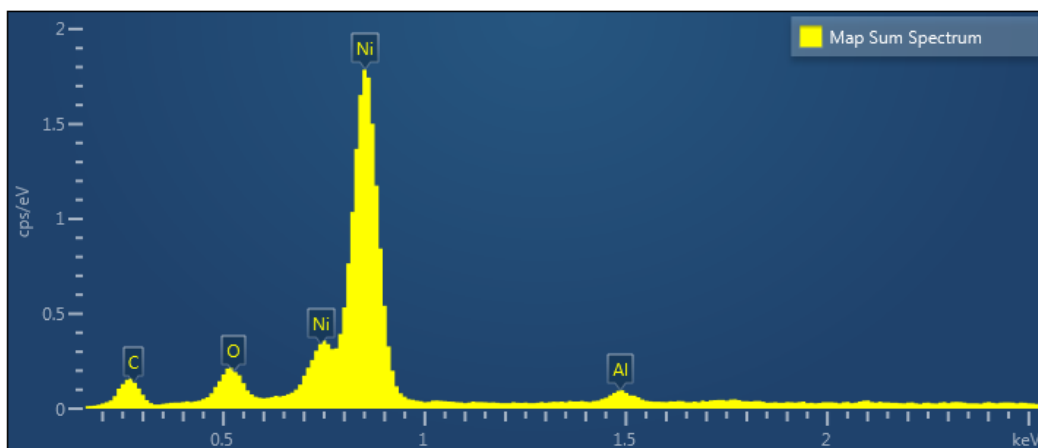


**Figure 5 Elemental analysis result of sample with immersion time of 10 minutes**

**Figure 5 and Table 2** show the elemental analysis of sample with immersion time of 10 minutes. The largest element contained in the sample is nickel element with a composition of 84.07 wight % 55.29 atomic %.

**Table 2. Elemental analysis of sample with immersion time of 10 minutes**

Element	Weight %	Atomic %
Ni	84.07	55.29
O	4.86	11.73
C	9.60	30.87
Al	1.47	2.11

### CONCLUSION

The nickel electroplating to alumunium 2024 was successfully performed with the immersion time variations of 10, 15 and 20 minutes. Hardness analysis result states that the immersion time variation affect the hardness property of samples. The shorter immersion time of 10 minutes shows the higher hardness value of 198.31 HV compared to the sample with the longer immersion time of 20 minutes which has the lower hardness value of 132.81 HV. The hardness value decreases along with the increasing immersion time due to the emergence of pitting (defects) on the electroplated layer. SEM image of 10 minutes immersion sample shows that the microstructure of the specimen layer is hollow and there are some impurities attached to it. The cavities and impurities are identified as oxygen and carbon analyzed from the EDX result. With the presence of pitting (defects), it causes the decrease of hardness value of the specimen and easily produce the brittle nickel coating on the specimen.

### REFERENCES

1. Wei X, Roper DK. Tin Sensitization for Electroless Plating Review. *J Electrochem Soc.* 2014;161(5):D235–42.
2. Chintada VB, Koon R, Raju Bahubalendruni MVA. State of Art Review on Nickel-Based Electroless Coatings and Materials. Vol. 7, *Journal of Bio- and Tribo-Corrosion.* Springer Science and Business Media Deutschland GmbH; 2021.
3. Brenner A, Riddell GE. Nickel Plating on Steel by Chemical Reduction. Vol. 37. 1946.
4. Luganov V, Mishra B, Baimakhanova S, Akpanbayev R. Chemical Enrichment of Nickel Sulfide. *International Journal of Nonferrous Metallurgy.* 2016;05(01):1–8.
5. Mainier FB, Fonseca MPC, Tavares SSM, Pardal JM. Quality of Electroless Ni-P (Nickel-Phosphorus) Coatings Applied in Oil Production Equipment with Salinity. *Journal of Materials Science and Chemical Engineering.* 2013;01(06):1–8.

6. Durodola BM, Olugbuyiro JAO. Effect of Some Plating Variables on Zinc Coated Low Carbon Steel Substrates. Vol. 10, Journal of Minerals & Materials Characterization & Engineering. 2011.
7. Loandbing YL, Hwang' J. Decomposition of NaBH<sub>4</sub> in an Electroless Nickel Bath. Vol. 33, Ind. Eng. Chem. Res. 1994.
8. Sürdem S, Eseroğlu C, Çitak R. A parametric study on the relationship between NaBH<sub>4</sub> and tribological properties in the nickel-boron electroless depositions. Mater Res Express. 2019 Dec 4;6(12).
9. Dimethylamine Borane.
10. Ellsworth AA, Walker A V. Role of the Reducing Agent in the Electroless Deposition of Copper on Functionalized SAMs. Langmuir. 2017 Sep 5;33(35):8663–70.
11. Vitry V, Sens A, Kanta AF, Delaunois F. Wear and corrosion resistance of heat treated and as-plated Duplex NiP/NiB coatings on 2024 aluminum alloys. Surf Coat Technol. 2012 Apr 15;206(16):3421–7.
12. Park SG, Lee YS, Rha SK. High-purity Ni electroless plating on screen-printed anodized Al substrates. Journal of the Korean Physical Society. 2016 Jul 1;69(2):164–8.
13. López JR, Méndez PF, Pérez-Bueno JJ, Trejo G, Stremmsdoerfer G, Meas Y. The effect of boron content, crystal structure, crystal size on the hardness and the corrosion resistance of electrodeposited Ni-B coatings. Int J Electrochem Sci. 2016 Jun 1;11(6):4231–44.
14. Véronique V, Abdoul-Fatah K, Adeline S, Fabienne D. Tribological characterization of electroless nickel-boron coatings. In: Advanced Materials Research. 2012. p. 808–13.
15. Vitry V, Delaunois F, Dumortier C. Mechanical properties and scratch test resistance of nickel-boron coated aluminium alloy after heat treatments. Surf Coat Technol. 2008 Apr 15;202(14):3316–24.
16. Bekish YuN, Poznyak SK, Tsybul'skaya LS, Gaev'skaya T V., Kukareko VA, Mazanik A V. Electrodeposited Ni–Co–B Alloy Coatings: Preparation and Properties. J Electrochem Soc. 2014;161(12):D620–7.
17. Cheng AY, Sheu HH, Liu YM, Hou KH, Hsieh PY, Ger M Der. Effect of pretreatment process on the adhesion and corrosion resistance of nickel-boron coatings deposited on 8620H alloy steel. Int J Electrochem Sci. 2020 Jan 1;15(1):68–79.
18. Sampath S, Ravi VP, Sundararajan S. An Overview on Synthesis, Processing and Applications of Nickel Aluminides: From Fundamentals to Current Prospects. Vol. 13, Crystals. MDPI; 2023.
19. Moon G, Lee E. Combined effects of optimized heat treatment and nickel coating for the improvement of interfacial bonding in aluminum-iron alloys hybrid structures. Applied Sciences (Switzerland). 2021 Feb 2;11(4):1–15.
20. Vitry V, Yunacti M, Mégret A, Khalid HA, Staia MH, Montagne A. Selection of New Heat Treatment Conditions for Novel Electroless Nickel-Boron Deposits and Characterization of Heat-Treated Coatings. Coatings. 2023 Jan 1;13(1).
21. Hieu DN, Ha My DN, Thu VT, Hung NQ, Chung DN, Thuat NT. Selected-area growth of nickel micropillars on aluminum thin films by electroless plating for applications in microbolometers. Journal of Science: Advanced Materials and Devices. 2017 Jun 1;2(2):192–8.
22. Chang X, Zhang X Bin. Study on electroless nickel plating process and property of aluminum alloy. In: Advanced Materials Research. 2013. p. 60–3.
23. Fatir FS, Sehonon, Setiawan F. Analisis Pengaruh Pelapisan Nikel Pada Material Aluminium Seri 2024 Terhadap Kekuatan Tarik Dan Kekerasan Dengan Metode

Elektroplating. *Teknika STTKD: Jurnal Teknik, Elektronik, Engine [Internet]*. 2023  
Jul 31;9(1):174–80. Available from:  
<https://jurnal.sttkd.ac.id/index.php/ts/article/view/611>

---

## Testing the Bending Strength of Carbon Fiber Composites using the Vacuum Infusion and Vacuum Bagging Method on the UAV Skywalker 1900 Fuselage Material

Chandra Febriyanto<sup>1</sup>, Ferry Setiawan<sup>1\*</sup>, Ikbal Rizki Putra<sup>1</sup>, Dimas Aditya Mahendra<sup>1</sup>

<sup>1</sup>College of Aerospace Technology of Yogyakarta, Indonesia

\*[ferry.setiawan@sttkd.ac.id](mailto:ferry.setiawan@sttkd.ac.id)

---

Submitted: January ; Revised: April ; Approved: June ; Available Online: September

---

**Abstract.** The growing popularity of Unmanned Aerial Vehicles (UAV) requires modern engineers to create products swiftly and affordably. This study evaluated the Skywalker 1900 UAV's bending strength of carbon fiber composite materials with lycal epoxy resin. Carbon fiber and lycal resin composites will be created utilizing vacuum infusion printing and vacuum bagging techniques for test specimens. To establish the bending strength value of the fuselage material, a sample of specimens for testing will be created utilizing these two techniques. This test will use the three-point bending method. Regarding a different test, microphotos, it can be seen from this microstructure that the second-phase particle size, shape, and distribution are crucial for understanding the material's properties. Vacuum bagging and vacuum infusion printing each produced test specimen results that were compared, and the best result was then sought between the two techniques. Testing produced the results, with the two printing techniques and microphotos producing the best vacuum bagging outcomes. Specimen i1 had the lowest yield in the vacuum bagging procedure, with a bending stress value of 1017.74Mpa, whereas specimen b2 had the most outstanding value (1201.90Mpa). The micro photo test can then be observed in the vacuum bagging printing process; the resin in the bagging has improved fiber penetration.

**Keywords:** UAV, Composite, Carbon fiber, Vacuum infusion, Vacuum bagging, Bending test.

**DOI :** [10.15408/fiziya.v6i1.30562](https://doi.org/10.15408/fiziya.v6i1.30562)

### INTRODUCTION

The utilization of Unmanned Aerial Vehicle (UAV) technology has proliferated. UAV, commonly known as drones, are pilotless aircraft that can be operated remotely from a computer system or other vehicles on land, sea, or air [1]–[6]. Drones have various applications, including mapping [7]–[9]. Drone technology has been instrumental in territory mapping in Indonesia, an archipelagic nation [7].

A vehicle's wing development is a multi-stage process that includes wing profile selection, geometric calculations, structural design, material maintenance, numerical analysis, and manufacturing [10], [11]. One of the most challenging difficulties in aviation is determining how to progress. Structures that are lightweight but sufficiently strong to sustain the imposed loads. Materials that can accommodate this are required. Composite materials are an essential component of modern airplane designs. One of the significant factors contributing to the continued development of the UAV industry is the innovation of structures and materials, particularly the advent of composite materials used in UAV construction [12]

Composite is a material made from two or more components, and each composite possesses unique mechanical characteristics based on the materials used to create it. Depending on the type of binding material and the reinforcing material, the mechanical strength characteristics of the composite can vary. Various fiber materials are reinforced in fiber-reinforced composites (reinforcing materials) [13]–[19].

Carbon fibers are used in UAV fuselages to reduce weight while maintaining material strength. Materials with at least 90% carbon by weight are known as carbon fibers. Graphite fibers with a carbon content exceeding 95% are the most commonly used type of carbon fiber. Applications that require strength, rigidity, lightweight, and fatigue resistance are suitable for carbon fibers[20].

Several methods are used to manufacture composite materials, including vacuum bagging, spray-up, hand layup, pressure bagging, infusion, continuous extrusion, and injection molding. This technique involves vacuum infusion and vacuum bagging to create composites, which is relatively straightforward. Manufacturing composite materials using vacuum infusion involves pressing matrix, fiber, and other layers into the mold while utilizing an airtight bag, merging the layers into a composite material[10], [17], [20]–[29].

Vacuum bagging is one of the most commonly used methods, along with hand lay-up. This method is an improvement over the manual hand lay-up method, as it involves lamination and vacuum steps to eliminate excess resin and trapped air from the lamination [21], [22].

## RESEARCH METHODS

In this research, vacuum infusion and vacuum bagging methods were used. Figure 1 showed a specimen using the vacuum-assisted resin infusion and vacuum bagging processes. Dry fibers are placed between the fixed mold and a plastic bag in the vacuum-assisted resin infusion. Then, resin is injected after the space inside the plastic bag is put under low pressure, and the process continues until the entire fiber is impregnated with resin. On the other hand, in the vacuum bagging process, dry fibers are placed between the fix mold, and resin is manually applied evenly using a brush onto the fiber surface [10].



**Figure 1.** Shows The UAV Fuselage For Which Test Specimens Will Be Produced

**The specimen manufacturing process utilizes the vacuum infusion method.**

The composite manufacturing process begins with determining and preparing carbon fibers. Carbon fibers are purchased online with dimensions of 1.5x0.5 meters. After obtaining the carbon fibers, they are cut and shaped according to the size of the vacuum infusion specimen mold.

The mold used is made of glass and has a box-shaped dimension of 40x35 cm. The mold is then cut on the edges to facilitate the airflow in and out. Before placing the fibers, the mold is coated with a wax mold release to prevent the resin from sticking to the mold. Next, the fibers are arranged in 2 layers. Peel ply is then applied over the carbon fibers and installed flow media. Hoses are connected to the in and out parts and covered with plastic bags sealed with dodol adhesive to ensure no air leakage occurs during infusion.

The resin and catalyst are mixed in a 3:1 ratio (catalyst to resin by weight) and manually stirred for approximately 5 minutes to ensure a uniform mixture. The resin is poured into a glass container, and the vacuum infusion machine is activated. The in-hose is inserted into the glass container to allow the resin to flow into the mold. Once the resin flows through the hose, it is sealed with dodol adhesive to prevent air from entering the mold, ensuring a smooth vacuum process.

The next step is to wait approximately 6 hours for the composite to cure. After the specified time has passed, the vacuum machine is turned off. The composite is left to rest for 18 hours before removing the plastic bag and extracting the composite from the mold. Once removed from the mold, the composite undergoes material forming to meet ASTM testing size requirements using milling machines and sandpaper before being subjected to bending tests. The formed specimens are now ready for bending tests, completing the manufacturing process of the composites [14].

**The process of specimen fabrication utilizes the vacuum bagging method.**

This research involves several sequential stages. The initial step is to determine and prepare the carbon fibers for the composite. Carbon fibers are purchased online with dimensions of 1.5x0.5 meters. After obtaining the carbon fibers, they are cut and shaped according to the size of the vacuum-bagging specimen mold. The mold used is made of glass and has a box-shaped dimension of 40x35 cm. It is then cut in the middle to allow air to exit. Before placing the fibers, the mold is coated with a wax mold release to prevent the resin from sticking. The following process involves arranging the threads in a single layer. The resin and catalyst are mixed in a 3:1 ratio (based on resin weight) and manually

stirred for approximately 5 minutes to ensure a homogeneous mixture. This mixture is then evenly applied to the previously arranged carbon fibers. The carbon fibers are then re-arranged in another single layer, and the resin-catalyst mixture is again evenly spread.

A breder cloth is placed over the carbon fibers to strengthen the composite structure. Hoses are attached to the middle part of the mold to allow air to be removed, and then the mold is covered with a plastic bag sealed with dodol adhesive to prevent air leakage into the mold. Next, the composite is left to cure for approximately 6 hours. After the curing period, the vacuum machine is turned off, and the composite is left to rest for 18 hours before removing the plastic bag and extracting the composite from the mold. Once successfully removed from the mold, the composite undergoes material forming to meet ASTM testing size requirements using milling machines and sandpaper as preparation for testing. The formed specimens are then ready to be tested in bending tests.

In the final stage, data from all tests are collected and recorded for further analysis and discussion in this research. All these stages are carried out to achieve accurate and reliable results in this composite study.

## RESULTS AND DISCUSSION

### A. Research Result

This section displays the data processing results of the tests carried out. The data from this study were sourced from bending tests and micro-photos using six specimens. For data analysis, it takes the average value of each variation used (Figure 2).

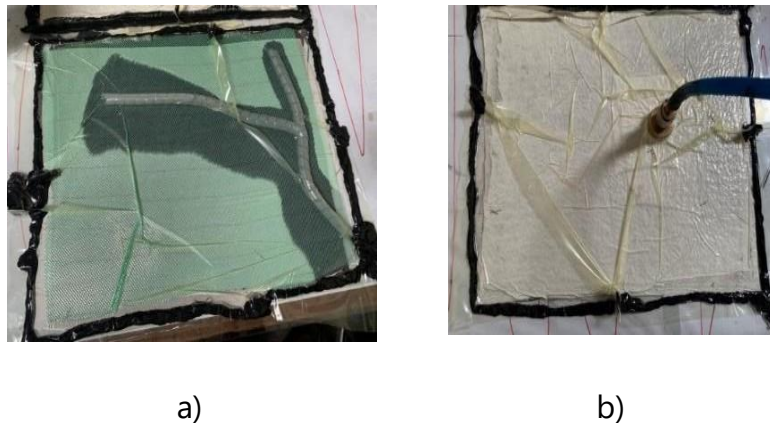


**Figure 2.** a) Vacuum Infusion b) Vacuum Bagging Processes

The results follow after the vacuuming process for 6 hours and then left for 18 hours (Figure 3).



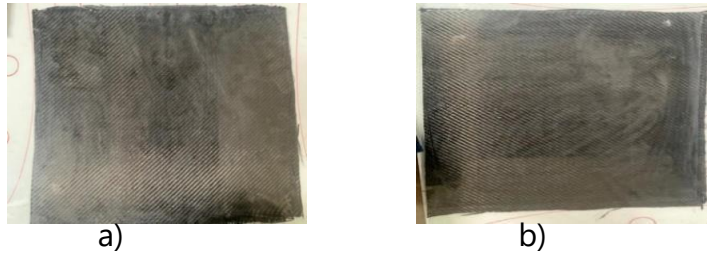


**Figure 3.** The Results a) The Vacuum Infusion b) Vacuum Bagging Processes

Then, cut the specimen using a CNC router to get precise sizes according to ASTM D790 (Figure 4).

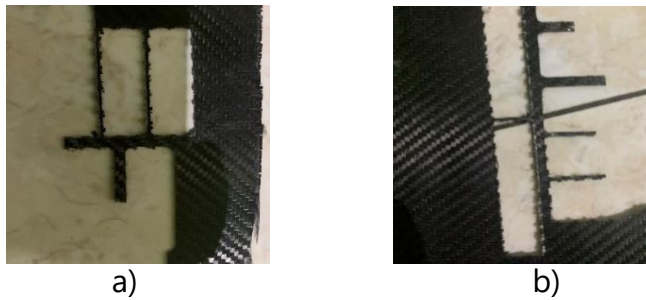


**Figure 4.** Results Of Cutting Using CNC Router a). Vacuum Infusion Cutting Results b) Vacuum Bagging Cutting Results

### ***Bending Test***

After the results of cutting composite materials using a CNC router and according to ASTM D790-17 for bending strength testing (Figure 5)

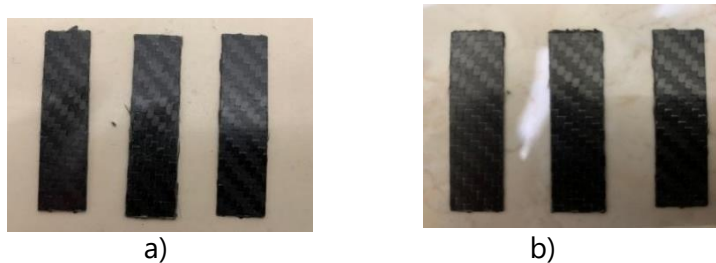


**Figure 5.** Specimens of the vacuum infusion and vacuum bagging method a).specimen vacuum infusion method b) specimen vacuum bagging method

Photos of the bending test results can be seen in Figure 6.

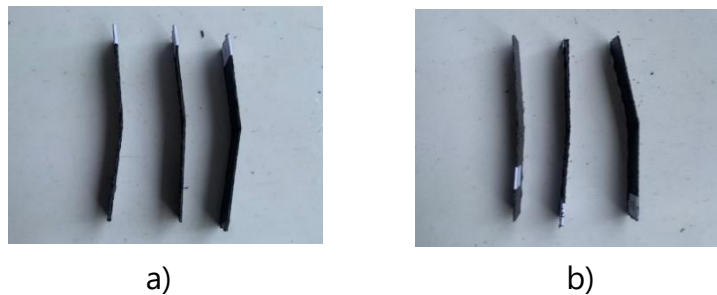


**Figure 6.** Documentation of the results of a) Vacuum infusion bending test results b) Vacuum bagging bending test results

**Table 1.** Shows the comparison of the vacuum infusion and vacuum bagging methods.

Variation	Bending Strength (MPA)	Bending Strength Average (MPA)
Vacuum Infusion method	1017,74	1110,25
	1182,56	
	1130,43	
Vacuum Bagging Methode	1079,00	1159,75
	1201,90	
	1198,37	

Table 1 shows the average carbon fiber bending test results using the vacuum infusion and bagging methods. The average bending strength results are obtained at 1110.25 MPa in carbon fiber using the vacuum infusion method. Using the vacuum bagging method, carbon fiber's average bending strength is obtained at 1159.75 MPa. In this bending test, the increase in bending strength from the vacuum infusion to the vacuum bagging method reached 0.045%.

**a. Specimen Metode Vacuum Infusion**

Figure 7 represents the bending test results of carbon fiber using the vacuum infusion method with three specimens. The highest bending stress was achieved at 1182.56 MPa in specimen 2, while the lowest bending stress was recorded at 1017.74 MPa in specimen 1.

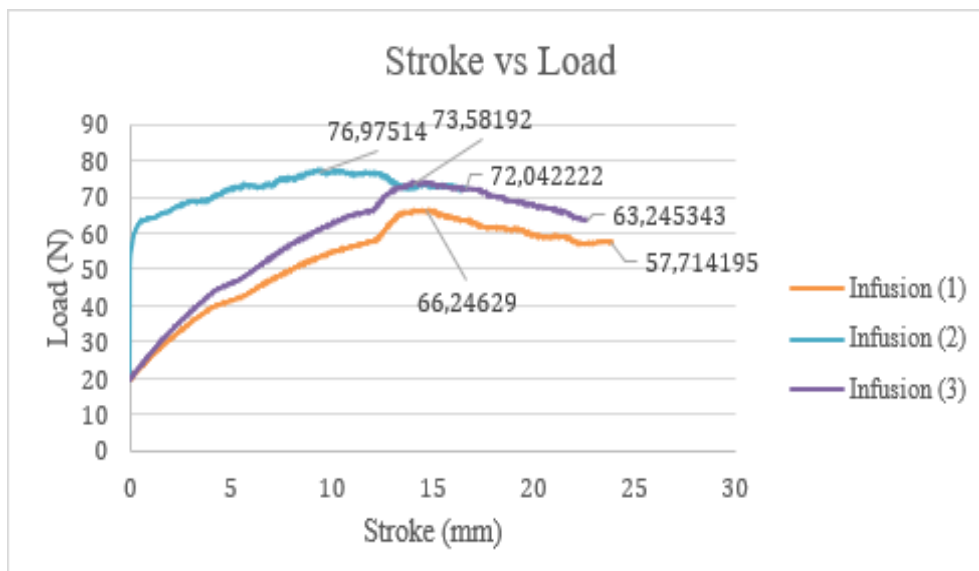


**Figure 7.** Load vs. stroke Chart of The Vacuum Infusion Method

**b. Specimen metode vacuum bagging**

Figure 8 shows the results of the bending test of carbon fiber using the vacuum bagging method with three specimens. The highest bending stress was achieved at 1201.90 MPa in specimen 2, while the lowest bending stress was recorded at 1079.00 MPa in specimen 1.

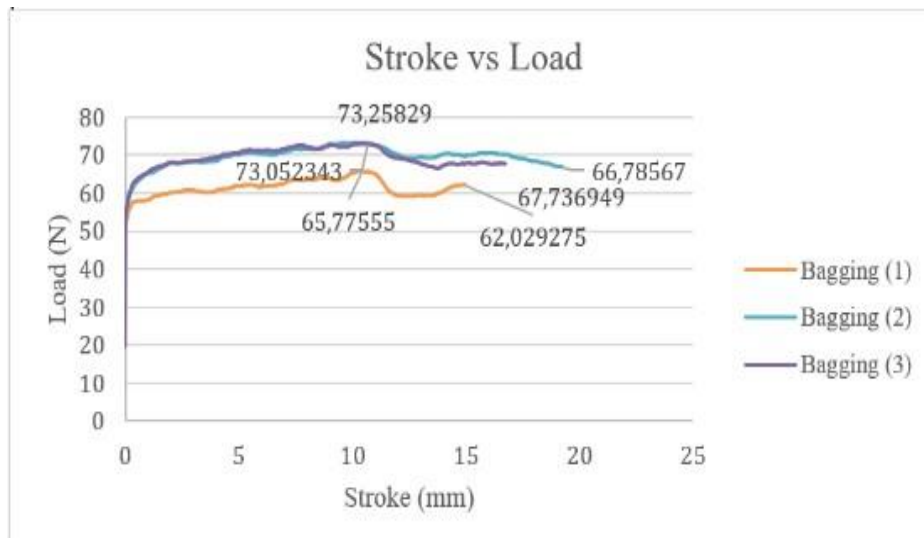


**Figure 8.** Load vs. Stroke Chart of the Vacuum Bagging Method

### Micro Photo

The best variation was achieved using the vacuum bagging method in the bending strength testing. This is because, during the manual resin application, it was evenly distributed using a brush. On the other hand, the vacuum infusion method showed imperfect resin penetration into the fibers due to poor application, caused explicitly by uneven resin distribution through the spiral hoses, primarily positioned in the middle. The vacuum bagging method produced better results with fewer voids. This can be observed from the micrograph of the specimens at 70x magnification shown below.

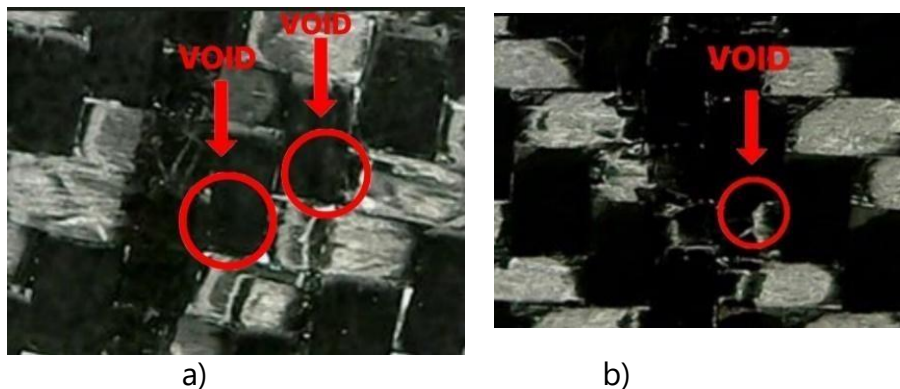


**Figure 9.** a). Micro vacuum infusion photo results b). Photographs of micro vacuum bagging

Figure 9 shows that the vacuum infusion method has more voids, and the vacuum bagging method has fewer voids. This is caused during the manufacturing process.

### B. Discussion of results

The discussion of the results of the bending test and microphotographs shows that the best method to be used in the manufacture of composite materials for the UAV Skywalker 1900 fuselage is the vacuum bagging method because the highest results are from the results of making specimens in the form of samples and then bending tests by ASTM

D790, the best results are obtained. By vacuum bagging. The micro photo shows that the vacuum bagging method receives the best penetration between resin and fiber. The vacuum infusion process did not go well due to the uneven application of the wax, as seen in the image below.



**Figure 10.** Application Of Resin Vacuum Infusion

**Figure 10** shows that resin application tends to flow downward so that it is not evenly distributed at the top when applying resin to the fiber. To manufacture the vacuum infusion method, place the spiral hose on the side like the letter U so that it is evenly distributed in the infusion method.

## CONCLUSION

The bending strength testing results of the specimens indicate that the vacuum infusion method achieved the highest bending strength at 1182.56 MPa, while the lowest bending strength reached 1017.74 MPa. On the other hand, the bending strength testing with the vacuum bagging method had the highest bending power at 1201.90 MPa, and the lowest bending strength was recorded at 1079.00 MPa.

Based on the results and discussions, the best method for manufacturing carbon fiber composite materials for the UAV Skywalker 1900 fuselage is the vacuum bagging method. This method provides higher bending strength compared to the vacuum infusion method. The use of vacuum infusion encountered challenges in resin penetration into the fibers, mainly due to uneven resin application through spiral hoses, particularly caused by the position of the spiral hoses in the middle, resembling the letter T. Thus, the vacuum bagging method is considered more effective, producing composites with better mechanical properties for UAV fuselage applications. These results offer essential insights for improving and developing the composite material manufacturing process based on the desired needs and technical requirements.

## SUGGESTION

For future researchers, it is recommended to focus on developing lighter materials that maintain high bending strength. Carbon fiber composite materials have the potential to be used in various applications, including UAV fuselages. By optimizing the weight-to-bending strength ratio, composite materials will become more efficient and deliver better performance in their applications.

Additionally, for improvements in the vacuum infusion method, the following researchers can consider placing the spiral hoses on the sides, forming a U shape. With this improved placement, resin distribution into the fibers will be even more during

infusion. This will help enhance resin penetration into the fibers and reduce the possibility of structural weaknesses caused by uneven resin distribution in the previous method. Consequently, vacuum infusion can be optimized to produce better carbon fiber composite materials.

## REFERENCES

- [1] Z. Jiang *et al.*, "A Prototype Design and Sea Trials of an 11,000 m Autonomous and Remotely-Operated Vehicle Dream Chaser," *J Mar Sci Eng*, vol. 10, no. 6, Jun. 2022, doi: 10.3390/jmse10060812.
- [2] H. G. Nguyen *et al.*, "Land, sea, and air unmanned systems research and development at SPAWAR Systems Center Pacific," in *Unmanned Systems Technology XI*, SPIE, May 2009, p. 73321I. doi: 10.1117/12.818994.
- [3] G. Y. Pardomoan, A. Asyraf, and Y. I. Jenie, "Micro Aerial Vehicle as an Aircraft Inspection System based on Computer Vision," in *AIAA AVIATION 2022 Forum*, American Institute of Aeronautics and Astronautics Inc, AIAA, 2022. doi: 10.2514/6.2022-3406.
- [4] M. Jagtap and B. V Asewar, "Weed control efficiency with herbicide application by the combination of Drone and Knapsack sprayer in wheat (*Triticum aestivum* L.) Climate Smart Agriculture-Rainfed Farming View project Nitrogen management in maize View project," 2022. [Online]. Available: <http://www.thepharmajournal.com>
- [5] M. E. Geringer *et al.*, "Deep-sea biology in undergraduate classrooms: Open access data from remotely operated vehicles provide impactful research experiences," *Front Mar Sci*, vol. 9, Jan. 2023, doi: 10.3389/fmars.2022.1033274.
- [6] K. M. Al-Sofy and S. A. Al-Talib, "Investigation of cartesian routing for unmanned aerial vehicle networks," in *IOP Conference Series: Materials Science and Engineering*, IOP Publishing Ltd, Nov. 2020. doi: 10.1088/1757-899X/928/2/022002.
- [7] M. A. Negara *et al.*, "Perbandingan Hasil Pemotretan Foto Udara Menggunakan Drone Industrial Dengan Drone Basic," 2021.
- [8] T. F. Abiodun, "Usage Of Drones Or Unmanned Aerial Vehicles (Uavs) For Effective Aerial Surveillance, Mapping System And Intelligence Gathering In Combating Insecurity In Nigeria Terrorist Attacks And The Influence Of Illicit Or Hard Drugs:Implications To Border Security In West Africa View project Security Intelligence Cooperation and the Coordinated War on Terror Among Nigeria's Security Agencies :Panacea to Stable National Security View project." [Online]. Available: [www.abjournals.org](http://www.abjournals.org)
- [9] M. Zeybek, "Exciting Advances in UAV Mapping and Geospatial Technology! Structural Analysis of Tbeti Church View project Landslide Monitoring and Assessment for Highway Retaining Wall View project." [Online]. Available: <https://www.researchgate.net/publication/371125669>
- [10] F. Setiaawan *et al.*, "Manufacture Of UAV Skywalker 1900 Flying Vehicles Made Of Composites", doi: 10.15408/fiziya.v5i2.30531.
- [11] G. Kanesan, S. Mansor, and A. Abdul-Latif, "Validation of UAV wing structural model for finite element analysis," *J Teknol*, vol. 71, no. 2, pp. 1–5, 2014, doi: 10.11113/jt.v71.3710.
- [12] U. Fasel, D. Keidel, L. Baumann, G. Cavolina, M. Eichenhofer, and P. Ermanni, "Composite additive manufacturing of morphing aerospace structures," *Manuf Lett*, vol. 23, pp. 85–88, Jan. 2020, doi: 10.1016/j.mfglet.2019.12.004.
- [13] B. B. Vatandaş and R. Gümürük, "Interlayer Bonding Behaviours Of Continuous Carbon Fiber Reinforced Peek Composites 3d Printed In Vacuum Making Tree Pruning Machine View Project Experimental And Numerical Investigation Of The Wear Failure Occurred In

- Erosion Shield Of Helicopter Rotor Blades Under Low-Velocity Impact Effect View Project." [Online]. Available: <https://www.researchgate.net/publication/370765862>
- [14] A. Dođru and H. E. Yalkin, "Production Of Polymer Matrix Sandwich Composite Materials by Vacuum Infusion Method And Comparison of Mechanical Properties Production and Characterization of Hybrid Composites by Additive Manufacturing Method View project." [Online]. Available: <https://www.researchgate.net/publication/359000008>
- [15] M. A. Irfa'i, Dzulkiflih, R. Ismail, and A. N. F. Ganda, "Effect of the orientation carbon-glass fiber reinforced polyester composite on bending strength for runner foot prosthesis applications," *IOP Conf Ser Mater Sci Eng*, vol. 1034, no. 1, p. 012147, Feb. 2021, doi: 10.1088/1757-899x/1034/1/012147.
- [16] M. R. Ricciardi *et al.*, "A new cost-saving vacuum infusion process for fiber-reinforced composites: Pulsed infusion," *J Compos Mater*, vol. 48, no. 11, pp. 1365–1373, 2014, doi: 10.1177/0021998313485998.
- [17] S. H. Permatasari, "Analysis Of Mechanical Properties Fiber Composite E-Glass Ew 135 Cloth-Resin Lycal With Vacuum Infusion Method," 2017. [Online]. Available: <https://www.researchgate.net/publication/327239422>
- [18] N. S. Binti Mohd Hafidz and M. S. Bin Mohamed Rehan, "Experimental testing of oil palm fibre composite manufactured via vacuum bagging method," in *IOP Conference Series: Materials Science and Engineering*, Institute of Physics Publishing, Mar. 2019. doi: 10.1088/1757-899X/488/1/012009.
- [19] Ş. YILDIZHAN, "Effects of vacuum infusion configuration on homogeneity of glass fiber reinforced polymer composites for automotive components," *European Mechanical Science*, vol. 7, no. 1, pp. 1–6, Mar. 2023, doi: 10.26701/ems.1166710.
- [20] F. Hazhari, F. Setiawan, T. Dirgantara, and S. Yogyakarta, "Pengaruh Kekuatan Tarik Dan Kekuatan Bending Komposit Hybrid Dan Non-Hybrid Menggunakan Metode Vacuum Bagging," *Indonesian Journal of Mechanical Engineering*, vol. 2, 2022, [Online]. Available: <https://politap.ac.id/journal/index.php/injection>
- [21] M. Azissyukhron and S. Hidayat, "Perbandingan Kekuatan Material Hasil Metode Hand Lay-up dan Metode Vacuum Bag Pada Material Sandwich Composite."
- [22] A. Prakoso and F. Amrullah, "Analisa Kekuatan Struktur Dan Pembuatan Fuselage UAV Dengan Metode Vacuum Bagging," *Conference SENATIK STT Adisutjipto Yogyakarta*, vol. 6, Dec. 2020, doi: 10.28989/senatik.v6i0.432.
- [23] K. Abdurohman, T. Satrio, N. L. Muzayadah, and Teten, "A comparison process between hand lay-up, vacuum infusion and vacuum bagging method toward e-glass EW 185/lycal composites," in *Journal of Physics: Conference Series*, Institute of Physics Publishing, Nov. 2018. doi: 10.1088/1742-6596/1130/1/012018.
- [24] M. Rahman, A. A. Jasani, and M. A. Ibrahim, "Flexural Strength of Banana Fibre Reinforced Epoxy Composites Produced through Vacuum Infusion and Hand Lay-Up Techniques - A Comparative Study," *International Journal of Engineering Materials and Manufacture*, vol. 2, no. 2, pp. 31–36, Jul. 2017, doi: 10.26776/ijemm.02.02.2017.02.
- [25] A. Saifullah, M. Jufri, D. Kurniawati, and R. Chandra, "Mechanical Properties of Layered-Carbon Fiber Reinforced with Vacuum Infusion Process," *Journal of Energy Mechanical Material and Manufacturing Engineering*, vol. 6, no. 1, pp. 33–40, Apr. 2021, doi: 10.22219/jemmm.v6i1.16428.
- [26] K. Ramachandran, C. L. Gnanasagaran, and A. Vekariya, "Life cycle assessment of carbon fiber and bio-fiber composites prepared via vacuum bagging technique," *J Manuf Process*, vol. 89, pp. 124–131, Mar. 2023, doi: 10.1016/j.jmapro.2023.01.068.

- [27] L. Xu, A. Jiang, Z. Yang, H. Guan, H. Jia, and M. Min, "Mechanical properties of CFF/MC/SF composite prepared using vacuum infusion impregnation method," *Results Phys*, vol. 7, pp. 1016–1021, 2017, doi: 10.1016/j.rinp.2017.02.042.
- [28] T. S. Nurtiasto, F. A. Wandono, N. L. Muzayadah, and R. Fazabik, "Variation of Mesh Peel Ply and Gelcoat on Mechanical Properties of Carbon Twill-Vinyl Ester Composites Using Vacuum Assisted Resin Infusion Manufacturing Method," in *Journal of Physics: Conference Series*, Institute of Physics, 2022. doi: 10.1088/1742-6596/2243/1/012048.
- [29] A. Doğru and H. E. Yalkin, "Production of Polymer Matrix Composite Materials by Vacuum Infusion Method and Non-Destructive Inspection of Products Production and Characterization of Hybrid Composites by Additive Manufacturing Method View project," 2016. [Online]. Available: <https://www.researchgate.net/publication/358999812>

---

## Prototype of Automatic Tractor Control Navigation System Using ESP32 Microcontroller

Abu Ammar<sup>1,\*</sup>, Muhammad Yusril<sup>2</sup>, Prasepvianto Estu Broto<sup>3</sup>, dan Ihsan<sup>4</sup>

<sup>1</sup>Alauddin State Islamic University Makassar, Indonesia.

[\\*ur.abuammar99@gmail.com](mailto:ur.abuammar99@gmail.com)

---

Submitted: March ; Revised: June ; Approved: August ; Available Online: September

---

**Abstract.** A prototype of an automatic tractor control navigation system using a microcontroller has been designed. This study aims to design a prototype of an automatic tractor control navigation system. The design involves initializing ESP32, reading GPS (Ublox Neo M8N), and compass (QMC5883L). Subsequently, the system waits for commands from the wifi network, reads waypoints, moves the motor, and then the motor drives the tractor prototype. Tests conducted include GPS and compass testing, control response testing, and waypoint navigation testing. The test results show that the accuracy of the coordinates of GPS UBlox Neo M8N is 0.04 meters from the Android smartphone GPS. The QMC5883L compass test shows a difference of 0.4 degrees and 1.0 degrees between the analog compass and the Android smartphone compass. Testing the navigation system using the waypoint method demonstrates that it is capable of mapping an area or location with a distance of less than 5 meters while following the waypoint route, providing accurate coordinate information to the server during the trip as a source of map information. The automatic tractor control navigation system operates well.

**Keywords:** *ESP 32, Microcontroller, Tractor, Waypoint, Wifi.*

**DOI :** [10.15408/fiziya.v6i1.31593](https://doi.org/10.15408/fiziya.v6i1.31593)

## INTRODUCTION

Indonesia is an agricultural country, many people in Indonesia work as farmers. One of the problems that arise for farmers is in terms of plowing the fields before farming. In general, farmers use tractors to plow the fields. However, the use of tractors in plowing the fields requires a lot of energy and time in the process. Because the tools owned by farmers are still traditional, it requires a touch of technology that can facilitate farmers in plowing fields, especially on a large scale. One of the technologies currently being developed is an autonomous system. Autonomous is a mode that refers to GPS coordinate data on an electronic device that can move automatically without using a remote control in its movement. The system used in the development of autonomous systems is a waypoint navigation system. Waypoints are usually used to remember or store a position point from a place on the map. In this study, a waypoint navigation system is used to correct the position obtained from the GPS. And so that the tractor can move properly, a compass is also needed which can set the direction of the tractor's



rotary motion. The data is then processed in the ESP32 microcontroller which is then sent to the DC motor to drive the wheels of the tractor prototype.

This study aims to design a prototype of a tractor control navigation system automatically using a microcontroller. With the prototype of this tractor control navigation system, it is hoped that it will become an innovative technological design that can later help farmers in plowing the fields, namely by using a tractor that can plow the fields automatically. Tractors are specially designed vehicles used to pull low-speed implements commonly used in agriculture [1]. The tractor used in this research is a type of hand tractor or two-wheeled tractor. A hand tractor or two-wheeled tractor is a machine that is used to cultivate land with a tillage tool mounted on the back of the machine [2]. The main components of a two-wheeled tractor or hand tractor can be grouped into three, namely propulsion, power transmission, and control levers. Generally, hand tractors use a single-cylinder motor as a drive unit with a power output of around 3-12 hp [3]. The power successor is divided into two, namely the frame and transmission. The frame is the seat of the transmission, drive motor, other parts of the tractor. While the transmission is the part that transfers power to other moving devices from the driving motor. There are several types of transmission used, namely belts, pulleys, chains, gears, clutches, and others. Control levers are several levers that are used as control devices when the tractor is running [1]. Tractors are specially designed vehicles that are used to pull implements at low speed which are commonly used in the agricultural field. has been loaded into it [4]. ESP 32 is a microcontroller introduced by Espressif System. ESP 32 is the successor to the previous version, namely ESP8266 [5]. The advantage of ESP 32 compared to other microcontrollers is that ESP 32 is equipped with wifi so it can make it easier to connect to the internet. Wi-fi (Wireless Fidelity) is a medium that is used to communicate or transfer data and programs wirelessly [6]. An internet connection is needed to create an IoT-based application system [7]. IoT is a system where an object in everyday life can communicate with other objects [8]. GPS is a system that uses satellite technology by receiving signals from several interconnected satellites. GPS can be applied as a navigation service, time (PNT), and position [10].

GPS is widely used in various fields, including mapping surveys, geology, geodesy, geodynamics, geophysics, deformation monitoring, transportation and navigation, forestry, agriculture, and even in sports to recreation [11]. One of the important tools in the navigation system is a compass. The compass functions to determine the direction based on the position of the earth's poles [12]. Digital compasses, especially those found on Android smartphones, are activated by a sensor commonly referred to as a magnetic sensor [13]. The working principle of a digital compass is generally almost the same as an analog compass, namely that both work by detecting magnetic field values around the compass [14]. DC motor or direct current motor is a type of electric actuator that uses a DC voltage source [15]. There are two main parts that are owned by a DC motor, namely the rotor and stator. The rotor is a coil through which electric current flows. The stator is a fixed part of a DC motor that generates a magnetic field [16]. In DC motors, energy changes from electrical energy to mechanical energy (motor) take place through the medium of a magnetic field [15]. A waypoint is a point on the GPS that has been marked in the form of a location point based on the coordinates of the latitude (y) and longitude (x) axes [17]. Waypoint navigation works by making coordinate points for the location that the machine will go through, then from the path that has been formed, the machine can follow it to the coordinate points for the next location that has been determined [18].

The important components needed in this waypoint navigation system are GPS which is used to determine the position and compass which is used to determine direction and can also be used to find the bearing direction of the tractor [19]. Based on the aforementioned background, this research develops a prototype of an automatic tractor control navigation system using ESP32 sensors.

### RESEARCH METHODS

The instruments used in this study were ESP32, Smartphone/Android, DC Motor, Jumper Cables, BreadBoard, Ublox M8N GPS, QMC5883L Compass, Batteries, and Arduino IDE software. The design begins with initializing the ESP 32 microcontroller, followed by reading the GPS (Ublox Neo M8N) and compass (QMC5883L). After that, waiting for commands from the wifi network (manual or automatic). If the command is automatic, it is followed by reading the waypoint and if the order is manual, then it is continued by reading the command from the operator to move the motor, then the motor will drive the tractor prototype.

To obtain a good result, the stages in this study follow the flowchart as shown in the following figure:

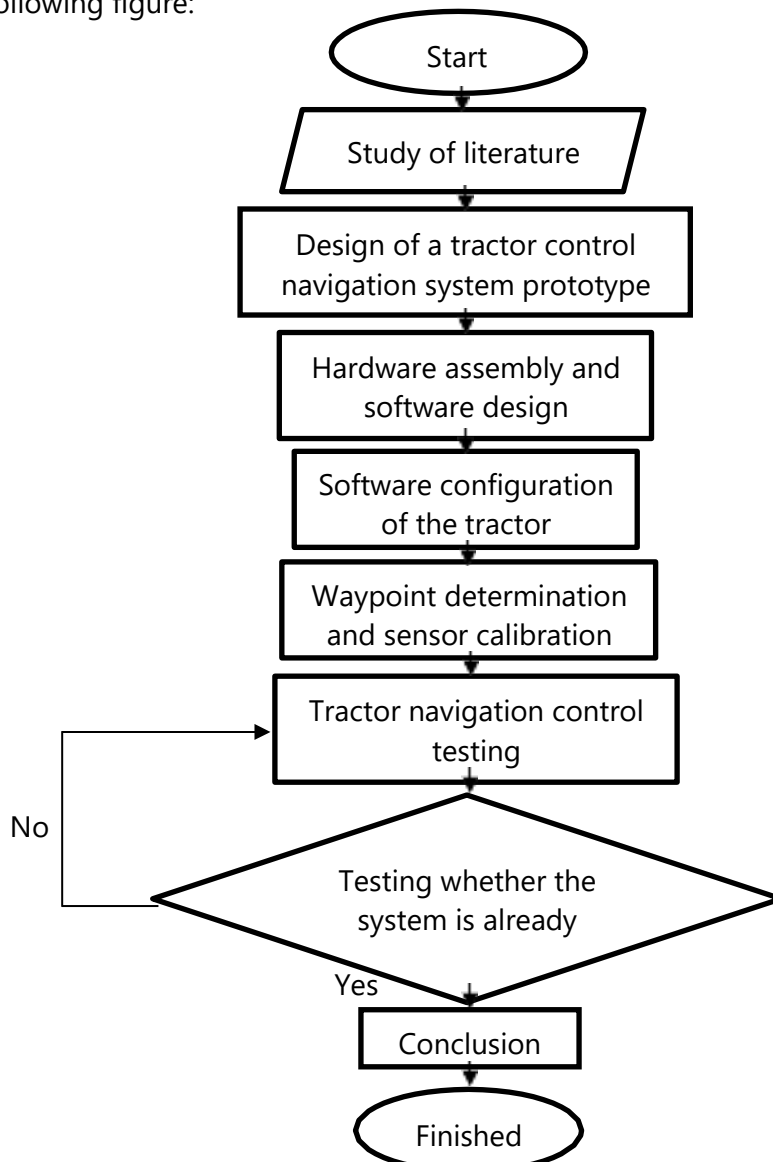


Figure 1. Research Flowchart

## RESULTS AND DISCUSSIONS

### Design Results

Hardware design includes combining electronic components, microcontroller, DC motor, compass, and GPS. The results of the hardware design can be seen in Figure 2.



**Figure 2.** Results of the prototype tractor design

The results of this prototype design consist of several parts, namely, the ESP32 microcontroller, GPS, compass and driving motor (DC motor). The ESP microcontroller is used to store the Arduino IDE program and as a firebase communication liaison device as a data and history store with the controller application via the internet. GPS is used to determine the coordinates that will see the position of the tractor prototype. The compass functions to determine the angle that corresponds to the path to be taken. Finally, the driving motor is used to move the prototype towards a predetermined point or direction.

### GPS Test Results

GPS testing is done by comparing the value of the GPS sensor on the device with the reference GPS value. The GPS sensor used in this study is a GPS sensor with the Ublox Neo M8N type. while the reference GPS used in this study is GPS on the oppo A54 android smartphone (GPS GLONASS, GALILEO, BDS). This test is carried out by taking five sample points from different locations. The data obtained is then poured into Table 1. Table 1 contains a comparison of the location point readings (latitude and longitude) between the GPS sensor and the reference GPS. Then from the two data it is calculated what is the difference in the distance between the two location point readings.

**Table 1.** GPS Sensor Test Results

No	GPS Sensor		GPS Reference		Difference (Meter)
	Latitude	Longitude	Latitude	Longitude	
1	-5.370141	120.334926	-5.3701642	120.334926	0.000025
2	-5.370153	120.334912	-5.3701576	120.334930	0.00002
3	-5.370143	120.334893	-5.5701582	120.334927	0.2
4	-5.370136	120.334904	-5.3701657	120.334934	0.000046
5	-5.370121	120.334883	-5.3701546	120.334921	0.000031
Average					0.04

Table 1 shows that the difference between the GPS sensor readings and the reference GPS readings is quite small, except for data number 3. The difference seems to reach 0.2 meters. Nevertheless, the overall difference obtained is still relatively small. This can be seen by the average difference value obtained by 0.04 meters.

### Compass Test Results

Compass sensor testing is done by comparing the reference compass reading with the compass sensor reading on the tool. The compass sensor used in this study is a compass sensor with the QMC5883L type. While the reference compass used is an analog compass and a compass sensor on an Android smartphone. Testing is done by taking five data with different compass angles. Furthermore, the data obtained is entered into Table 10.

**Table 2.** Compass Sensor Test Results.

No	Analog Compass	Android Compass	QMC5883L Compass	Difference with Analog Compass	Difference with Android Smartphone Compass	% Error with Analog Compass	% Error with Compass Android smartphones
1	0	0	0	0	0	0	0
2	30	31	30.2	0.2	0.8	0.67	2.58
3	60	60	60.3	0.3	0.3	0.50	0.50
4	90	90	90.1	0.1	0.1	0.11	0.11
5	120	119	120.3	0.3	1.3	0.25	1.09
6	150	152	150.5	0.5	1.5	0.33	0.99
7	180	180	180.7	0.7	0.7	0.39	0.39
8	210	211	210.9	0.9	0.1	0.43	0.05
9	240	241	240.3	0.3	0.7	0.13	0.29
10	270	268	270.5	0.5	2.5	0.19	0.93
11	300	303	301	1.0	2.0	0.33	0.66
12	330	332	330.1	0.1	1.9	0.03	0.57
Average				0.4	1.0	0.3	0.7

Table 2 shows that the error for each angle between the reference compass reading value and the compass sensor reading value has a small percentage error. This can be seen by the average error value obtained, which is equal to 0.3% using a manual compass as a reference and 0.7% using a cellphone compass as a reference. Although there are several angles that have quite large errors, such as at angle 30 with an error of 2.8%, and at angle 120 with an error of 1.09%. This can be caused because at these angles there are metal objects and disturbing magnetic fields around the compass sensor so that it can affect the reading results. Table 2 also shows that the difference between the compass sensor reading value and the reference compass reading value is quite small for the two reference compasses. This can be seen by the difference in value which is not up to one degree using an analog compass reference. Although the reference compass using a cellphone compass has quite a large difference, such as at angles of 120, 150, 270, 300, and 330. The difference seems to reach 1 to 2 degrees. Nevertheless, the overall difference obtained is still relatively small. This can be seen by the average difference value obtained by 0.4 degrees for the analog compass reference and 1 degree for the smartphone compass reference.

### Control Response Test Results

Control response testing is carried out to find out how long it takes for the tractor to adjust its angle towards a predetermined target angle. Control response testing is done by determining the starting angle of the tractor (the angle must be different or even opposite to the destination angle). Then it is calculated how long it takes the tractor to adjust its angle so that the angle matches the target angle.

**Table 3.** Control Response Test Results

angle of the tractor	destination angle	Time (s)
0	270	13
90	270	10
180	270	5
270	270	3
360	270	14

Table 3 contains how long it takes for the tractor's direction to adjust to the destination direction. The tractor angle is the direction angle of the tractor at the start, while the destination angle is the direction angle of the destination point that the tractor will go through. The time is obtained from how long it takes the tractor to adjust its angular direction.

Based on Table 3, it can be seen that the shortest time needed for the tractor to adjust its direction is when the starting angle of the tractor is 270 degrees, which is 3 seconds. The longest time it takes the tractor to adjust its direction is when the starting angle of the tractor is 360, which is 14 seconds.

### Waypoint Navigation Test Results

Waypoint testing is carried out to find out how accurate the prototype tractor is in navigating to a predetermined waypoint.

**Table 4** List of Waypoints

	<i>Latitude</i>	<i>Longitude</i>
Waypoint 1	-5.203794	119.495729
Waypoint 2	-5.203787	119.495639
Waypoint 3	-5.203728	119.495645
Waypoint 4	-5.203685	119.495666
Waypoint 5	-5.203692	119.495738

The plot results for the application based on the waypoints in Table 4 are as follows:

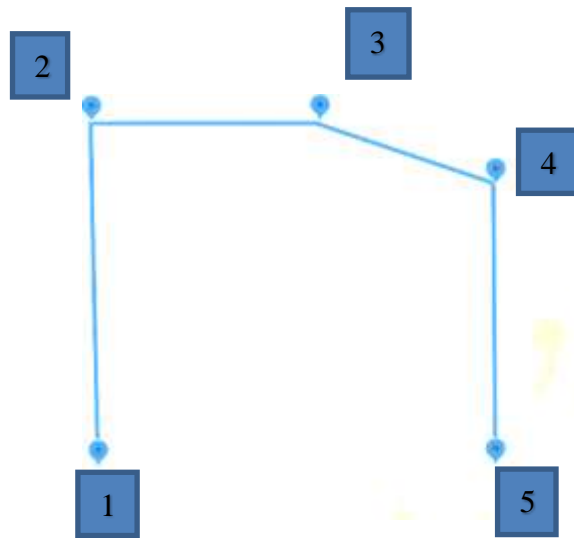


**Figure 3.** Waypoint Coordinate Plot

After the waypoint is entered, the tractor prototype will move and send the movement coordinates. The coordinates of the movement of the tractor can be seen in Table 5 below.

**Table 5.** Tractor Prototype Travel Coordinate Data

No.	<i>Latitude</i>	<i>Longitude</i>	No.	<i>Latitude</i>	<i>Longitude</i>
1	-5.203794	119.495718	15	-5.203738	119.495647
2	-5.203796	119.495707	16	-5.203732	119.495648
3	-5.203797	119.495697	17	-5.203721	119.495645
4	-5.203794	119.495686	18	-5.203705	119.495649
5	-5.203790	119.495669	19	-5.203698	119.495652
6	-5.203787	119.495662	20	-5.203691	119.495657
7	-5.203784	119.495652	21	-5.203686	119.495664
8	-5.203788	119.495642	22	-5.203680	119.495667
9	-5.203791	119.495633	23	-5.203678	119.495678
10	-5.203781	119.495632	24	-5.203682	119.495688
11	-5.203773	119.495633	25	-5.203685	119.495697
12	-5.203765	119.495637	26	-5.203689	119.495705
13	-5.203757	119.495642	27	-5.203692	119.495722
14	-5.203747	119.495645	28	-5.203691	119.495731

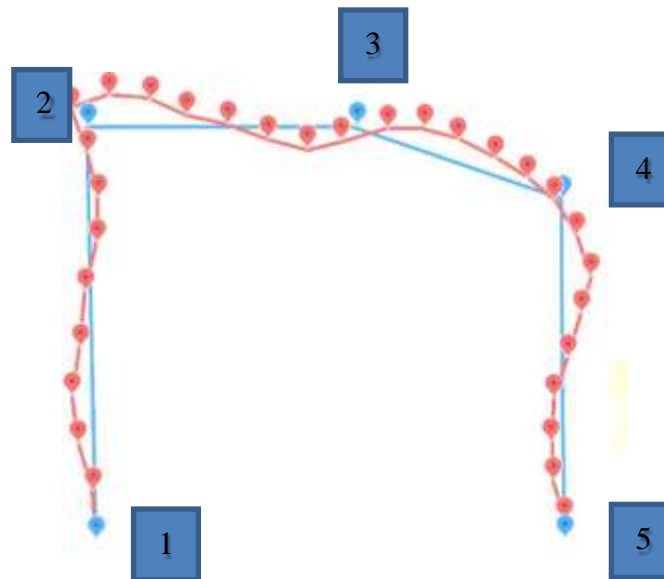


**Figure 4.** Tractor Prototype Path Plot Data

The trip data and waypoint data are then plotted as shown in Figure 5 to show the paths that have been passed by the tractor prototype with the paths that should have been traversed. The red line shows the travel line, while the blue line shows the waypoint line. At several points there was a deviation between the path that should have been and the path passed by the prototype tractor. This could be due to the deviation of the compass sensor. Then the number of satellites that lock GPS is also very influential. The more the number of satellites locked, the higher the accuracy of the GPS.

## CONCLUSIONS

The conclusion of this study is that a navigation system has been obtained using the waypoint method to make paths traversed by the prototype tractor with the help of GPS sensors and a compass. From the tests carried out, it shows the accuracy of the GPS coordinates of the UBlox Neo M8N with a difference of 0.04 m from the reference GPS, the QMC5833L compass test shows a difference from the reference compass of 0.4 degrees, and from the waypoint navigation test it can already map an area or location with a distance deviation less than 5 meters to follow the waypoint route and provide accurate coordinate information to the server during the trip as a source of map information.

## REFERENCES

- [1] Wibowo, N. "Traktor Pertanian". Pusat Pengembangan Dan Pemberdayaan Pendidik Dan Tenaga Kependidikan Pertanian, 2017.
- [2] Nurmawati, I., Nova, M. A., and Norita, L. "Mesin Traktor dan Alat Tradisional Pengolah Tanah". Universitas Muhammadiyah Gresik, 2017.
- [3] Kementerian Pertanian. "Modul Traktor Roda Dua (Hand Traktor)". Badan Penyuluhan dan Pengembangan SDM Pertanian, 2015.
- [4] Musaddiq, M. "Rancang Bangun Alat Pengusir Kalelawar Menggunakan Mikrokontroler

- Berbasis Android (Doctoral dissertation". Universitas Islam Negeri Alauddin Makassar, 2021.
- [5] Muliadi, M., Imran, A., and Rasul, M. "Pengembangan Tempat Sampah Pintar Menggunakan ESP32". *Jurnal Media Elektrik*, vol. 17, no. 2, pp. 73-79, 2020.
- [6] Karim, R., Sumendap, S. S., and Koagouw, F. V. I. A. "Pentingnya Penggunaan Jaringan Wi-Fi Dalam Memenuhi Kebutuhan Informasi Pemustaka Pada Kantor Perpustakaan Dan Kearsipan Daerah Kota Tidore Kepulauan". *Acta Diurna Komunikasi*, 2016.
- [7] Hermana, R., Setyoadi, Y., and Aza, M. F. "Kaji Eksprimental Perbandingan Ketelitian Mesin CNC Milling Dengan Kontrol SMC Dan Mesin CNC Milling Dengan Kontrol ESP32 Wifi". *Majalah Ilmiah Gema Maritim*, vol, 24, no. 2, pp. 105-113, 2021.
- [8] Syamsuddin, M., Imansyah, F., Marpaung, J., and Yacoub, R. R. "Analisis Kinerja Komunikasi Modul Transceiver ESP32 Pada Frekuensi 2, 4 GHz yang Akan di Terapkan pada Jaringan IoT". *Jurnal Teknik Elektro Universitas Tanjungpura*, vol. 1, no. 1, 2022.
- [9] Adelianthi, N. "Pendeteksi Kebakaran Hutan Menggunakan komunikasi LoRa (Long Range) Wireless Network". Doctoral dissertation, Universitas Islam Negeri Alauddin Makassar, 2019.
- [10] Rohman, Q. A. H. H., and Salahuddin, N. S. "Rancang Bangun Prototipe Mobil Penjelajah Dengan Kendali Jarak Jauh Melalui Jaringan Wi-Fi Berbasis Antarmuka Web". *Teknika*, vol. 7, no. 1, pp. 1-7, 2018.
- [11] Pramono, H. S. "Pembacaan Posisi Koordinat Dengan GPS Sebagai Pengendali Palang Pintu Rel Kereta Api Secara Otomatis untuk Penambahan Aplikasi Modul Praktik Mikrokontroler". *Jurnal Pendidikan Teknologi dan Kejuruan*, vol. 20, no. 2, 2011.
- [12] Arief, F. F., Muchlas, M., and Sutikno, T. "Kompas Digital Dengan Output Suara Berbasis Mikrokontroler AT89S52". *TELKOMNIKA (Telecommunication Computing Electronics and Control)*, vol. 61, no. 1, pp. 1-6, 2008.
- [13] Musthafa, A. R. "Sistem Navigasi Indoor Menggunakan Sinyal Wi-fi dan Kompas Digital Berbasis Integrasi dengan Smartphone untuk Studi Kasus pada Gedung Bertingkat". Doctoral dissertation, Institut Teknologi Sepuluh Nopember Surabaya, 2016.
- [14] Triwibowo, Aries. "Penerapan Navigasi Kompas Android Pada Robot Sepak Bola Beroda Berbasis Arduino". Universitas Negeri Semarang, 2016.
- [15] Setiawan, D. "Sistem Kontrol Motor Dc Menggunakan Pwm Arduino Berbasis Android System". *SITEKIN: Jurnal Sains, Teknologi dan Industri*, vol. 15, no. 1, pp. 7-14, 2017.
- [16] Anggoro, B., and Munadi, D. "Desain Pemodelan Kinematik dan Dinamik Humanoid Robot". Doctoral dissertation Diponegoro University, 2013.
- [17] Rachmawati, P., and Asyam, M. H. "Sistem Kontrol Pesawat Tanpa Awak Untuk Menentukan Waypoint Berbasis Ardupilot". *Quantum Teknika: Jurnal Teknik Mesin Terapan*, vol. 2, no. 2, pp. 80-86, 2021.
- [18] Saputra, F. R., and Rivai, M. "Autonomous Surface Vehicle sebagai Alat Pemantau Lingkungan Menggunakan Metode Navigasi Waypoint". *Jurnal Teknik ITS*, vol. 7, no.1, pp. A76-A81, 2018.
- [19] Fikri, A. R., Anam, K., and Cahyadi, W. "Rancang Bangun Sistem Navigasi Robot Beroda Pemandu Disabilitas Netra Menggunakan Metode Waypoint". *Jurnal Rekayasa Elektrika*, vol. 16, no. 3, 2020.
- [20] Amari,S.: Characteristics of Randomly Connected Threshold Element Networks and Network Systems. *Proc. IEEE* 59, 35-47 (1971).
- [21] Adamopoulos, 2011,Adamopoulos T."Transportation Costs, Agricultural Productivity, and Cross-Country Income Differences" *Int. Econ. Rev.*, 52 (2) (2011), pp. 489-521
- [22] Adkins K.A., Sescu A. "Analysis of Near-Surface Relative Humidity in a Wind Turbine Array Boundary Layer Using an Instrumented Unmanned Aerial System and Large-Eddy Simulation" *Wind Energy*, 21 (11) (2018), pp. 1155-1168
- [23] Yuniarti, Elvan, and Dewi Lestari. "Design and Build Underwater Robot Control System Based on PID (Proportional Integral Derivative)." *Al-Fiziya: Journal of Materials Science, Geophysics, Instrumentation and Theoretical Physics* 4.2 (2021): 115-123.
- [24] Subrata, I. Rancang Bangun Sistem Kendali Otomatis Traktor Roda Empat.
- [25] Ratu, A. G. L. Modifikasi Sistem Navigasi Otomatis Pengendalian Traktor untuk Pengolahan Lahan Kering.



[26] Rahman, C. S. Development of Automatic Guidance for Agricultural Tractor Based on GPS  
Navigatio

---

## Design and Control Underwater Robot Based on Smartphone

Lamin Rene Loua<sup>1</sup>, Dewi Lestari<sup>2\*</sup>, Elvan Yuniarti<sup>3</sup>, Rista<sup>4</sup>

<sup>1</sup>EcoSolutions Research Group-The Gambia

<sup>2</sup>Universitas Trilogi, Indonesia

<sup>3,4</sup>Universitas Islam Negeri Syarif Hidayatullah Jakarta, Indonesia

\*[dewy24@trilogi.ac.id](mailto:dewy24@trilogi.ac.id)

---

Submitted: May ; Revised: August ; Approved: August ; Available Online: September

---

**Abstract.** Underwater robot is a type of robot specially designed and configured to operate underwater, especially in seas, rivers, and lakes. The main purpose of underwater robots is to perform various tasks and missions underwater, which are often difficult or dangerous for humans to carry out. The method used to design the underwater robot is with a smartphone control system. The robot can move according to the user's commands by being connected through a internet network, allowing the robot and smartphone to be interconnected. This underwater robot is equipped with a camera and two lamps, and the images captured by the camera are displayed on a personal computer. Meanwhile, the lights are controlled by the user using a smartphone. The research results show that the underwater robot can be controlled to a depth of 0.5 meters with an average button press speed of 1 second in floating conditions and 2.9 seconds at a depth of 15 centimeters. The application of this robot can take photos, display good images, and monitor activities underwater. In addition, the captured image from underwater robot are also good and the image produced are clearly visible both on land and in the water.

**Keywords:** Blynk, Smartphone, Underwater Robot, WiFi.

**DOI :** [10.15408/fiziya.v6i1.32368](https://doi.org/10.15408/fiziya.v6i1.32368)

## INTRODUCTION

Indonesia has a very wide water area that reaches more than 3000000 Km<sup>2</sup>. The breadth of Indonesian waters certainly has abundant fishery potential such as various freshwater fish in lake waters. The large role of Indonesian waters certainly needs a monitoring system to be able to monitor the conditions and potential of underwater fisheries, one of which conditions and potential of underwater fisheries, on of which is by using an underwater robot equipped with camera. So that, every condition and potential of fisheries can always be monitored without having to dive into the water. Underwater robot is a robot that is intended specially for activities in the water. Where this robot is usually used to make observations or underwater surveys. Based on the working system, underwater robots consist of two types, namely AUV (Autonomous Underwater Vehicle)

and ROV (Remotely Operated Vehicle). Autonomous Underwater Vehicle (AUV) is an underwater robot that is autonomous based on the program that has been given to the robot chip [1]. This robot makes it easier for users to operate, which it can send data to users wirelessly [2]. Meanwhile, Remotely Operated Vehicle (ROV) is an unmanned underwater robot that can maneuver in water and it's controlled by an operator above the water surface [3]. The application of ROV can help humans in various research and engineering activities in the water [4]. In this research, an underwater robot based on ROV is designed which it's controlled using a smartphone connected to WiFi network. Electronic communication underwater Robot [16],[21]. An underwater electronic communication robot, often referred to as an underwater communication system or underwater robot, is a specialized device designed to transmit and receive information in aquatic environments. These robots play a crucial role in various applications, including ocean exploration, environmental monitoring, underwater research, and industrial tasks. Technology continues to increase, ranging from means of communication to means of transportation. Technology can provide comfort and convenience for humans to carry out activities. Along with the rapid development of technology, a concept has emerged that can help human activities with the help of network commonly referred to as IoT [5]. Internet of Things (IoT) is a concept where objects can communicate with each other such as transferring data using the internet network in real time without involving human intervention [6][7]. One of the application of IoT can be done by using the blynk application on a smartphone. Where the blynk application can control various controllers such as Arduino, ESP32, ESP8266, Raspberry, etc. With blynk application, it is easier to control other devices using only a smartphone. So users can control anything remotely by staying connected to the internet. Blynk itself provides a limit of 2000 points for each new user in accessing the features in the application without having to pay (free) [8]. However, if we want to use it on a commercial scale and for a long period of time, we need to add limit points by buying an energy pack that is available on the blynk application.

## RESEARCH METHODS

### **Underwater Robot System Requirements Design**

Designing an underwater robot system requires careful consideration of various factors to ensure its functionality, reliability, and efficiency in the challenging underwater environment.

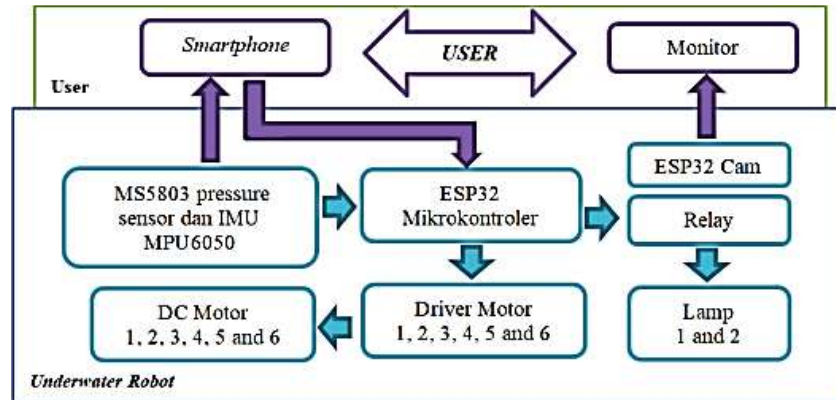


**Figure. 1** Underwater Robot System Block Diagram

In this system consists of two parts of the function, where the first function is performed by the user and the second function is performed by the system.

1. Functions performed by user

In this part of the function is carried out directly by user, where user control the system using a smartphone. In addition, the user can see and monitor data from pressure sensor in the form of depth position robot. Monitoring movement and stability of the of the robot by looking at roll and pitch data from IMU MPU6050 contained in blynk application display. Then user can also monitoring underwater conditions in the form of streaming video from those captured by ESP32 Cam.

2. Function performed by the system

This function is carried out by the system such as reading commands from user via a smartphone, reading roll and pitch data values of IMU MPU6050 and reading data from pressure sensor which is the processed by DOIT ESP32 DEVKIT. Furthermore, the reading of data is poured in output of PWM value on the DC motor and the light condition.

**Hardware Design**

The following is a series of hardware on the underwater robot

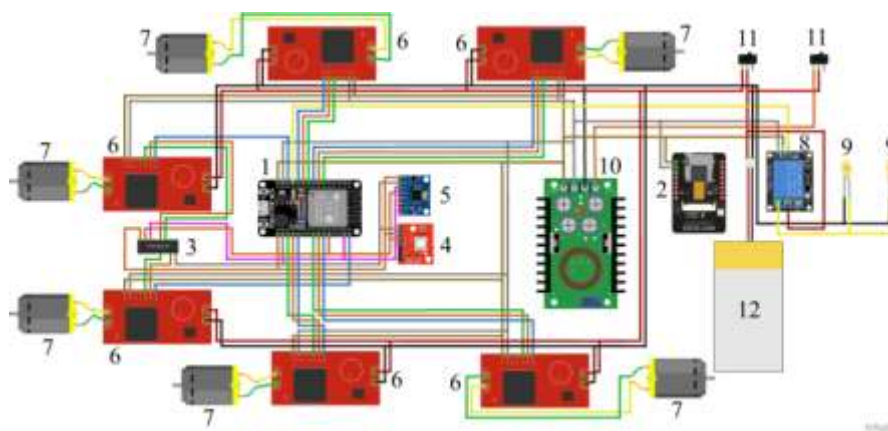


**Figure. 2** The Overall Circuit of Underwater Robot Hardware

The explanation of the components contained in Fig. 3, including:

1. DOIT ESP32 DEVKIT is used as the main controller of the control system.
2. ESP32 Cam and OV2640 camera are used as image and video image data capture.
3. PCF8574 IO module is used as an additional GPIO pin.
4. MS5803 pressure sensor is used to measure depth position robot.
5. IMU MPU6050 sensor module is used to measure the tilt of robot and maintain the stability of robot.
6. VNH2SP30 driver motor is used as a DC driver motor.
7. 1100goh bilge pump DC motor is used to drive the robot.
8. Relay is used as a regulator of condition the lamp.
9. Lamps is used as a robot lighting.
10. Buck converter XL4015 is used to lower voltage from 11.1 Volt to 5 Volts.
11. On off switch is used to disconnect and connect electric current.
12. LiPo (Lithium Ion Polymer) battery is used as a voltage source for the robot.

The following is a flow diagram of the underwater robot as shown in Fig. 3.

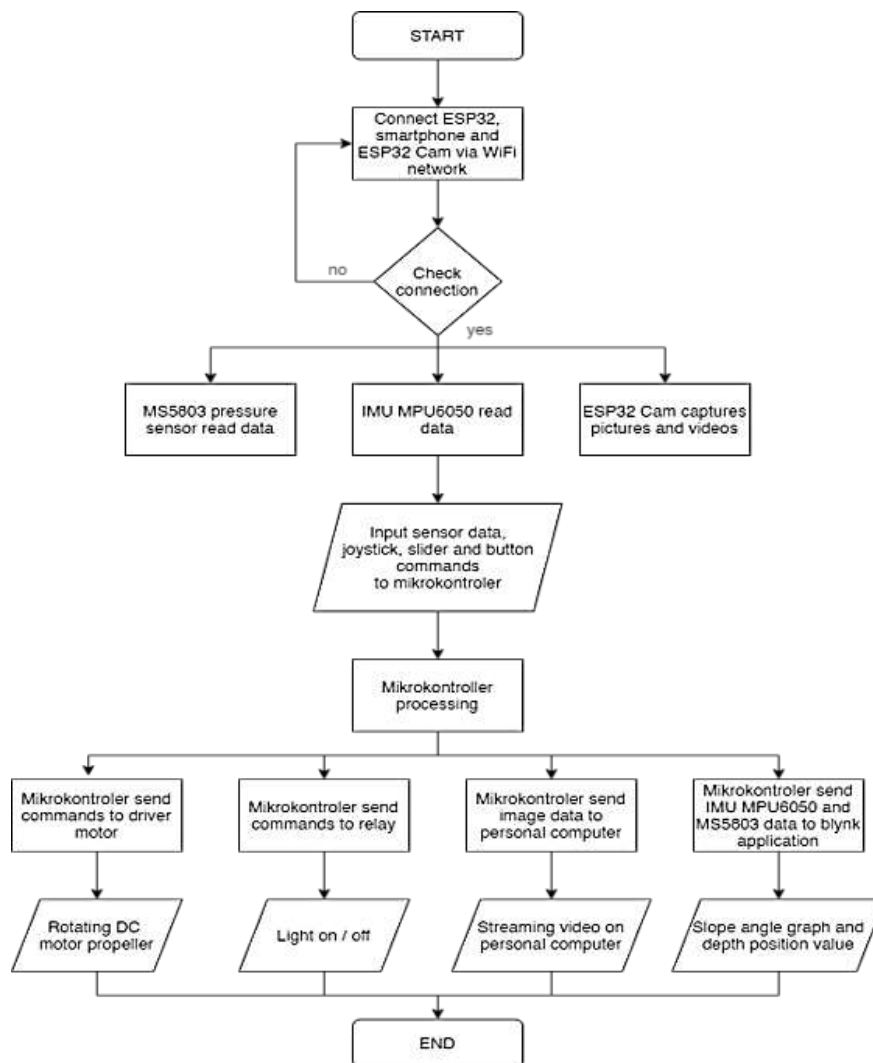


**Figure. 3** Flowchart Design System Underwater Robot

### Control System Design with Blynk Application

In addition, the control system design was also carried out using the blynk application which was previously installed on smartphone. After the installation is successful, it is continued by registering via email until it is finished according to the instructions in the application. After successful registration, the next step is to create a new project by clicking the "New Project" button and then naming the project as desired, in this research it was named "Underwater Robot". Then, in the choose device section, select the type of device used namely "ESP Dev Board" and select the WiFi communication media, then click the "Create" button. So, blynk will send an auth token to the previously registered email address. The appearance of the new project can be seen in Fig. 4.

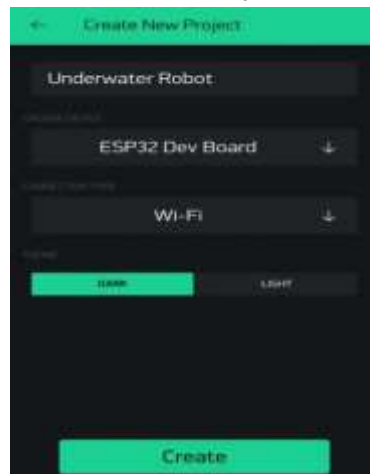


Figure. 4 Create New Project Display on Blynk

The next step is to create command buttons and display on blynk. In this research, a joystick widget is used to adjust the direction of the robot's movements such as forward, backward, and turn. In addition, using a slider widget to adjust the robot's up and down when in water, a button widget to adjust the robot's lighting, a value display widget to display the depth position robot and a superchart widget to display a graph of roll angle and pitch angle of the robot in water. So that, the robot stabilizer control system can always be monitored. The overall appearance of the widget on blynk used in this research can be seen in Fig. 5.

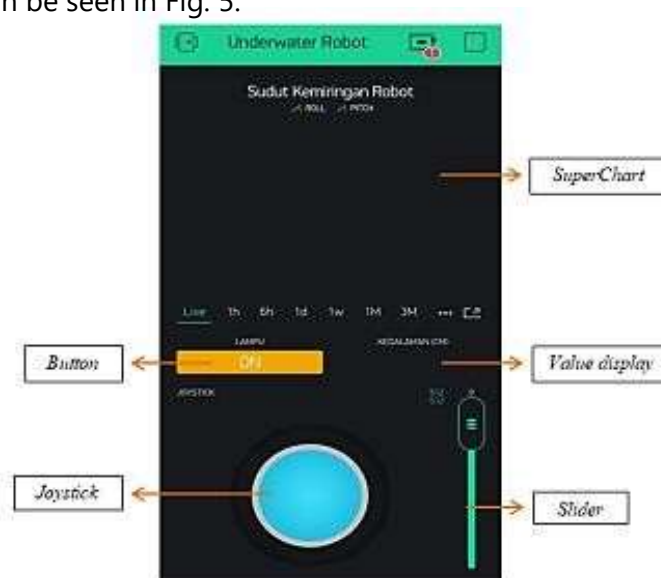


Figure. 5 Underwater Robot Control System Widget Display

After the design of control system on blynk is complete, next step is to configure the control system for blynk application to the personal computer. The steps for configuring blynk application control system to PC are as follows:

1. Copy the auth token sent to email.
2. Connect ESP32 to PC using a USB cable.
3. Enter the auth token, WiFi name and password according to the WiFi used on smartphone into program that we created on Arduino IDE, then upload it to completion.

## RESEARCH METHODS

### Underwater Robot Design Result

The design of an underwater robot can vary depending on its intended purpose and application. Below is the design of the underwater robot that has been created.



**Figure. 6** Robot Design Result Front View

The specifications of the robot that has been made in this research can be seen in Table 1.

**Table 1.** Underwater Robot Specifications

<b>Robot size</b>	<b>Title of second column</b>
Robot size	45 cm x 38 cm x 24 cm
Input voltage	11.1 Volts
Number of motors	6
Number of lamps	2
Number of camera	1
Robot mass	8 Kg

### Camera Test Results

The shooting test was carried out using an OV2640 cam mounted on the ESP32 cam. In shooting, image data is captured by the camera and processed by the ESP32 cam which is then sent and displayed on a personal computer using auth token with the help of WiFi network.

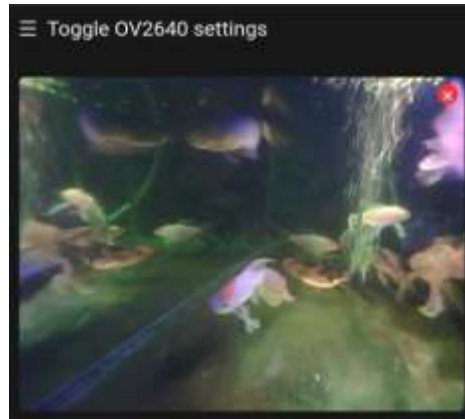


**Figure. 7** Image Result of ESP32 Cam

### Lighting Control Test Results

In the lighting control test, it is carried out to determine the response speed of pressing button on smartphone to the condition lights. In this research, two DC lamps are installed in series on relay with NO (Normally Open) mode. So, when relay is active, the lamps also be ON. Lighting system testing is done using button on smartphone application. When the button is pressed to ON then lights will turn ON and the button is pressed to OFF then the lights will go out. The data on the results of lighting testing on system can be seen in Table 2 and Table 3.

**Table 2.** Respon Speed Button Pressing to Light Conditions (Depth 0 cm or Floating)

No	Command	Button Press Time	Light Condition Time	Time Difference
1	ON	16.35.39	16.35.40	1 second
2	OFF	16.37.05	16.37.06	1 second
3	ON	16.39.32	16.39.33	1 second
4	OFF	16.40.10	16.40.11	1 second
5	ON	16.42.05	16.42.06	1 second
6	OFF	16.42.21	16.42.22	1 second
7	ON	16.44.13	16.44.14	1 second
8	OFF	16.45.28	16.45.29	1 second
9	ON	16.47.02	16.47.03	1 second
10	OFF	16.47.53	16.47.54	1 second
Average Time				1 second

**Table 3.** Respon Speed Button Pressing to Light Conditions (Depth 15 cm)

No	Command	Button Press Time	Light Condition Time	Time Difference
1	ON	17.34.10	17.34.13	3 second
2	OFF	17.37.18	17.37.22	4 second
3	ON	17.49.21	17.49.25	4 second
4	OFF	17.52.19	17.52.22	3 second
5	ON	17.55.03	17.55.06	3 second
6	OFF	18.21.18	18.21.20	2 second
7	ON	18.23.06	18.23.08	2 second
8	OFF	18.24.17	18.24.20	3 second



9	ON	18.25.32	18.25.35	3 second
10	OFF	18.27.13	18.27.15	2 second
Average Time				2.9 second

Based on Table 2 and Table 3, it can be seen that the response speed of pressing the button to the condition of lights when the system is at a water depth of 0 cm (floating) is faster than when the system is at a water depth of 15 cm. This happens because the molecular density in water is denser than in air, so it is making difficult for electromagnetic waves to penetrate when in water. Thus, the deeper diving robot, longer response speed of pressing the button to the condition of lights.

### Control System View on Blynk Application

The display of experimental results on blynk application can be seen in Fig. 9.



**Figure. 8** Overall Control System View on Blynk

In monitoring the stability of robot, superchart widget available in blynk application used. Which every time is a change in the stability of the slope and the change in depth position of robot, the graph will be formed according to magnitude of the slope and the depth position that occurs. In lighting control, a widget button is used, if the button pressed to ON then light condition will turn ON, while if the button is pressed to OFF then light condition will go out. Then in controlling the movement of robot, two widgets are used, namely joystick and slider widgets. Joystick widget is used to control horizontal movement of robot, like forward, backward and turn. While slider widget is used to control vertical movement of robot, like diving, hovering and floating. In the blynk application, a value display is also used which it is used to display the depth position of robot in cm.

## CONCLUSION

Based on the results of testing and data analysis that has been carried out in this research, several conclusions can be obtained including the following: Based on experimental data, the underwater robot has an average button response speed of 1 second in floating conditions and 2.9 seconds at a depth of 15 cm. The blynk application can display a graph of stability and depth position robot in real time. In addition, the captured image from underwater robot are also good and the image produced are clearly visible both on land and in the water.

## REFERENCES

- [1] M. S. Gitakarma, K. U. Ariawan, and N. A. Wigraha, "Alat Bantu Survey Bawah Air Menggunakan Amoba , Robot Berbasis ROV," vol. 3, no. 2, p. 393, 2014.
- [2] Jamaluddin, A. K. F. Rustam, A. Sahwawi, A. Sultan, D. T. Pratama, and A. P. Alimuddin, "Desain Robot Observasi Karang Autonomous dengan Sistem Artificial Intelligence," *Hasanuddin Student J.*, vol. 2, no. 1, p. 90, 2017.
- [3] I. Sobary, R. Nugraha, and S. Sumaryo, "Desain Implementasi Sistem Navigasi dan Monitoring pada Remotely Operated Vehicle (ROV)," *e-Proceeding Eng.*, vol. 6, no. 3, p. 10045, 2019.
- [4] B. S. Saputro, E. Djunarsjah, J. Setiyadi, and A. K. Negara, "Pengoperasian Remotely Operated Vehicle (ROV) Mendukung Pekerjaan Bawah Air (Studi Kasus Pendeteksian Kabel Bawah Laut Menggunakan Rov H800 Di Perairan Selat Bangka Belitung)," p. 96.
- [5] P. D. Lestari, L. Karlitasari, and S. Maryana, "Pengendali Pintu Gerbang Berbasis IoT (Internet of Things ) Gate Controller Berbasis IOT ( Internet of Things )," vol. 1, no. 2, pp. 62–63, 2021.
- [6] Y. Efendi, "Internet of Things (IoT) Sistem Pengendalian Lampu Menggunakan Raspberry PI Berbasis Mobile," vol. 4, no. 1, p. 20, 2018.
- [7] M. A. Robbith, "Mengenal Apa Itu Internet of Things dan Control Penerapannya," 2020. <https://www.google.co.id/amp/s/www.sekawanmedia.co.id/pengertian-internet-of-things/amp/>.
- [8] "Mengenal Blynk Platform IoT, Instalasi dan Penerapannya," *CauseAR*. <https://www.google.co.id/amp/s/www.anakkendali.com/mengenal-blynk-platform-iot-instalasi-dan-penerapannya/amp/> (accessed Jun. 12, 2021).
- [9] A. Faudin, "Mengenal Aplikasi Blynk untuk Fungsi IOT," 2017. <https://www.nyebarilmu.com/mengenal-aplikasi-blynk-untuk-fungsi-iot/> (accessed Jun. 12, 2021).
- [10] Huang, C., Zhao, J., Yu, Y., Zhang, H. "Comprehensive Sample Augmentation by Fully Considering SSS Imaging Mechanism and Environment for Shipwreck Detection Under Zero Real Samples, (2022) *IEEE Transactions on Geoscience and Remote Sensing*, 60. [Cited 10 times](https://ieeexplore.ieee.org/servlet/opac?punumber=36). <https://ieeexplore.ieee.org/servlet/opac?punumber=36>, doi: 10.1109/TGRS.2021.3116671
- [11] Yuniarti, Elvan, and Dewi Lestari. "Design and Build Underwater Robot Control System Based on PID (Proportional Integral Derivative)." *Al-Fiziya: Journal of Materials Science, Geophysics, Instrumentation and Theoretical Physics* 4.2 (2021): 115-123.
- [12] Heidemann, John, Milica Stojanovic, and Michele Zorzi. "Underwater Sensor Networks: Applications, Advances and Challenges." *Philosophical Transactions of the Royal Society A: Mathematical, Physical and Engineering Sciences* 370.1958 (2012): 158-175.
- [13] Windiastik, Shania Putri, Elsha Novia Ardhana, and Joko Triono. "Perancangan Sistem Pendeteksi Banjir Berbasis IoT (Internet of Thing)." *Seminar Nasional Sistem Informasi (SENASIF)*. Vol. 3. 2019.

- [14] Hasanah, Ana, Sitti Ahmiatri Saptari, and Dewi Lestari. "Sistem Deteksi Banjir Dan Pintu Air Otomatis Menggunakan Raspberry Pi 3 Berbasis Website." *InfoTekJar: Jurnal Nasional Informatika dan Teknologi Jaringan* 4.2 (2020): 250-254.
- [15] Wang, J., Wu, Z., Dong, H., Tan, M., Yu, J. Development and Control of Underwater Gliding Robots: A Review, (2022) *IEEE/CAA Journal of Automatica Sinica*, 9 (9), pp. 1543-1560. doi: 10.1109/JAS.2022.105671
- [16] Che, Xianhui, et al. "Re-evaluation of RF Electromagnetic Communication in Underwater Sensor Networks." *IEEE Communications Magazine* 48.12 (2010): 143-151.
- [17] Yan, Hai, Zhijie Jerry Shi, and Jun-Hong Cui. "DBR: Depth-Based Routing for Underwater Sensor Networks." *NETWORKING 2008 Ad Hoc and Sensor Networks, Wireless Networks, Next Generation Internet: 7th International IFIP-TC6 Networking Conference Singapore, May 5-9, 2008 Proceedings* 7. Springer Berlin Heidelberg, 2008.
- [18] Heidemann, John, et al. "Research Challenges And Applications for Underwater Sensor Networking." *IEEE Wireless Communications and Networking Conference, 2006. WCNC 2006.* Vol. 1. IEEE, 2006.
- [19] Lee, Uichin, et al. "Pressure Routing for Underwater Sensor Networks." *2010 Proceedings IEEE INFOCOM*. IEEE, 2010.
- [20] Lestari, Dewi, and M. R. Daimunte. "Rancang Bangun Home Automation Berbasis Ethernet Shield Arduino." *Al-Fiziya: Journal of Materials Science, Geophysics, Instrumentation and Theoretical Physics* 3.1 (2020): 21-28.
- [21] Xie, Peng, Jun-Hong Cui, and Li Lao. "VBF: Vector-Based Forwarding Protocol for Underwater Sensor Networks." *NETWORKING 2006. Networking Technologies, Services, and Protocols; Performance of Computer and Communication Networks; Mobile and Wireless Communications Systems: 5th International IFIP-TC6 Networking Conference, Coimbra, Portugal, May 15-19, 2006. Proceedings* 5. Springer Berlin Heidelberg, 2006.
- [22] Vasilescu, Iuliu, et al. "Data Collection, Storage, And Retrieval With An Underwater Sensor Network." *Proceedings of the 3rd international conference on Embedded networked sensor systems*. 2005.
- [23] Li, Shaonan, et al. "Survey On High Reliability Wireless Communication For Underwater Sensor Networks." *Journal of Network and Computer Applications* 148 (2019): 102446.
- [24] Hoang, K.A., Vo, T.Q. A study on fuzzy based controllers design for depth control of a 3-joint Carangiform fish robot (2013), *2013 International Conference on Control, Automation and Information Sciences, ICCAIS 2013*, art. no. 6720570, pp. 289-294. [Cited 7 times](#). ISBN: 978-147990572-0 doi: 10.1109/ICCAIS.2013.6720570
- [25] Yu, J., Liu, J., Wu, Z., Fang, H. Depth Control of a Bioinspired Robotic Dolphin Based on Sliding-Mode Fuzzy Control Method (Open Access), (2018) *IEEE Transactions on Industrial Electronics*, 65 (3), art. no. 8017458, pp. 2429-2438. [Cited 74 times](#). <http://ieeexplore.ieee.org/xpl/tocresult.jsp?isnumber=5410131>  
doi: 10.1109/TIE.2017.2745451

## 3D Visualization of Geothermal System Structure Based on Inversion Model of Gravity Data. Case Study: Mt. Salak Region, West Java

Nanda Ridki Permana<sup>1,\*</sup>, Belista Gunawan<sup>2</sup>

<sup>1</sup>PT Minelog Services Indonesia, Industrial Estate and Warehouse Techno Park, Indonesia.

<sup>2</sup>GeoXplore Indonesia, Indonesia.

\*[nandaridki836@gmail.com](mailto:nandaridki836@gmail.com)

Submitted: July ; Revised: July ; Approved: August ; Available Online: September

**Abstract.** The geothermal power plant located in Mount Salak plays a crucial role in increasing the electricity supply transmitted to the Java-Bali region, as the energy demand continues to rise. The objective of this research is to determine the 3D subsurface structure of Mount Salak, specifically the distribution of the reservoir as the target for geothermal energy using the Gravity method. Gravity data, including gravity disturbance (gd), geoid, and Digital Elevation Model (DEM), were obtained from the ICGEM website with a total of 48740 data each. Based on the results of the residual anomaly map, the low anomalies beneath Mount Salak have values from -5.15 to -1.88 mGal, which are suspected to be associated with the magma chamber. The high anomalies beneath the manifestations have values from 0.92 to 5.01 mGal, indicating andesitic basalt intrusive rocks believed to be the reservoir rock. Through the 3D inversion modeling of the subsurface structure of the Mount Salak geothermal system, a clay cap with a density from 2.47 to 2.5 gr/cc at depths of 0 to 700 m and andesitic basalt rock as the reservoir with a density from 2.74 to 2.91 gr/cc at depths of 700 to 3000 m have been identified.

**Keywords:** Geothermal, Gravity, Inversion, Mt. Salak, Reservoir

**DOI :** [10.15408/fiziya.v6i1.33439](https://doi.org/10.15408/fiziya.v6i1.33439)

### INTRODUCTION

Geothermal is a renewable energy source that shows an increasing role and mix of primary energy supply in Indonesia [1], because it is relatively environmentally friendly for electricity generation compared to other sources such as fuel oil [2]. Geothermal potential in Indonesia is estimated to reach more than 27,000 Mw or the equivalent of 219 million barrels of petroleum [3]. Where almost 40% of the world's geothermal potential is in Indonesia [4] and around 21.7% is in West Java [5].

Geothermal power plants have an important role in the Java-Bali network as they require a large supply of electricity for the local population. The Geothermal Power Plant in Mount Salak supplies electricity to the surrounding areas, particularly in the Jawa-Bali region, with a capacity of not less than 180 MWe. [6]. The Geothermal Power Plant in Mount Salak consists of three units with a capacity of 60 MW each. Electrical power from these three units is transmitted to the New Bogor 150 kV transmission network for interconnection with the Java-Madura-Bali system. Part of the generated power is also used for self-consumption [7].

©2023 The Author (s) This is an Open-access article under CC-BY-SA license  
(<https://creativecommons.org/licenses/by-sa/4.0/>)

AI-Fiziya: Journal of Materials Science, Geophysics,  
Instrumentation and Theoretical Physics  
P-ISSN: 2621-0215, E-ISSN: 2621-489X

Previous research has been carried out using the Active Directory Magnetotelluric (ADMT) geophysical method which aims to identify the geothermal potential of Mount Salak through 2D modeling, the result is a layer of clay cap at an average depth of 200 – 700 m and a reservoir layer that starts to appear from a depth of 700 – 1000 m. Therefore, this research is a form of development from previous research which aims to provide information in 3D inversion model of geothermal system structure based on gravity satellite data, especially the depth of the reservoir as a geothermal target using the gravity method.

### Geothermal System

Geothermal systems are usually associated with volcanic systems that occur due to the movement of tectonic plates on the earth's surface which causes volcanoes [8]. Geothermal systems are formed as heat transfer from surrounding heat sources which can occur by conduction and convection [9]. This system stores and transports heat generated from geological processes within the Earth's crust.

The geothermal system consists of three main elements: (1) permeable reservoir rock, (2) water that carries heat from the reservoir to the earth's surface, and (3) a heat source. In addition, the essential things needed for the existence of a geothermal system are (1) heat source as the primary source, (2) reservoir that stores and transports hot fluids within the Earth, and (3) cap rock as the covering layer that contains the hot fluids [10]. The presence of reservoirs as geothermal targets can be characterized by the presence of manifestations around geothermal areas in the form of hot springs, mud pools, fumaroles, solfatara, etc.

### Regional Geology

Mount Salak is a Quaternary volcano which is still geologically active and is a potential source of geothermal energy as well as a geological disaster. The volcanism of Mount Salak is directly related to the tectonic processes that occur as a result of the collision of the Eurasian and Indo-Australian plates in southern Java [11].

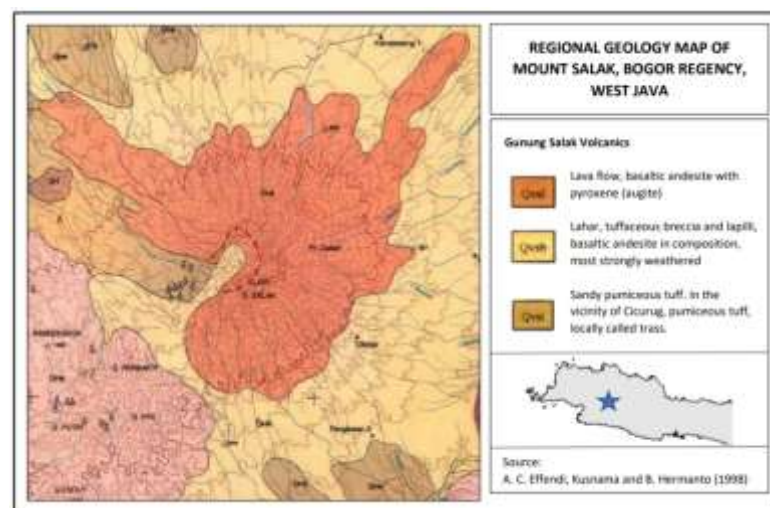


**Figure 1.** Regional Geology of Research Area [15]

Based on the 1:100,000 scale geological map, the geological structure in the study area consists of faults, folds, and lineaments. The fault structure consists of shear faults, reverse faults, and normal faults which generally trend north-south, southwest-northeast, and northwest-southeast [12]. The top to the foot of Mount Salak is composed of rock products of

Mount Salak in the form of sandy pumice tuff covered by lava deposits, tuffaceous breccias, and andesitic-basalt layered lapilli which are generally very weathered, the uppermost part is composed of andesitic lava [13] [14].

### Gravity Method

The gravity method is a geophysical exploration method that is carried out by measuring the acceleration of gravity below the earth's surface caused by differences in rock density from an area [16].

The method of gravity works based on Newton's Law of Gravity which states that the force acting between two objects with masses of  $m$  separated at a distance  $r$  will be directly proportional to the multiplication of the masses of the two objects and inversely proportional to the square of the distance from the center of mass of the two objects [17]. The gravitational force can be written in an equation as follows:

$$F = G \frac{M.m}{r^2} \quad (1)$$

Where  $F$  is the weight of the object in units (N),  $M$  is the mass of the first object in units (Kg),  $m$  is the mass of the second object in units (Kg),  $r$  is the distance between the two masses in units (m), and  $G$  is a constant gravity with a value  $6,67428 \times 10^{-11} Nm^2Kg^{-2}$  atau  $m^2 Kg^{-1} dt^2$  [17].

### Gravity Corrections

Gravity correction refers to the steps or procedures applied to improve or minimize the factors that can affect gravity measurement results [18]. Gravity data obtained from satellites has been corrected by Free Air Anomaly (FAA), so that the corrections needed are only terrain and Bouguer corrections which aim to reduce the rock masses in the earth's crust.

The Bouguer correction is a variation in the pull of rock masses on the earth's surface that can be calculated from the results of the derivation process [19]. The Bouguer correction can be written as follows:

$$BC = 0.000419\Delta hp \quad (2)$$

BC is the Bouguer correction (mGal),  $h$  is the difference between the height of the measurement point and the datum (m), and  $\rho$  is the density ( $gr/cm^3$ ). The average density value in the study area was carried out using the parsnis density method and the results obtained were  $2.6 gr/cm^3$  [20].

Terrain correction is caused by topographical factors in the measurement point area because there are topographical effects as well as large elevation differences, such as hills and valleys around the measurement station [21].

$$TC = G \rho \theta [(r_2 - r_1) + \sqrt{r_1^2 + z^2} - \sqrt{r_2^2 + z^2}] \quad (3)$$

TC is Terrain Correction (mGal),  $G$  is universal constant,  $\rho$  is density of rock mass ( $kg/m^3$ ),  $r_1$  radius of inner circle (m),  $r_2$  radius of outer circle (m),  $z$  is height of hill or depth of valley (m) [20].

### Inversion Modeling

Inverse modeling is a process used to obtain information about subsurface structures based on observation or measurement data collected at the surface. Inverse modeling involves the use of algorithms and mathematical methods to transform observation data into a model or representation that approximates the actual conditions beneath the surface [22]. In general, inversion modeling is based on the following equation:



$$m = F^{-1} \quad (4)$$

where  $F$  is the operator associated with the model,  $m$  is the model calculation data, and  $d$  is for the observation data, where the value of the calculation data and the observation data is done by trial and error so that the shape of the curve is the same [21].

## RESEARCH METHOD

The research location is on Mount Salak which is located between Bogor Regency and Sukabumi Regency, West Java with predetermined boundaries with an area of 587 km<sup>2</sup> (Figure 2). Gravity anomaly data in the form of gravity disturbance (gd), geoid, and Digital Elevation Model (DEM) were obtained from the website of the International Center for Global Earth Models (ICGEM) with a total of 48740 data each. The ICGEM was established in 2003 as a new service under the umbrella of the new International Gravity Field Service (IGFS). This website has a pretty good resolution up to 100 m and the distance resolution can also be set, one of its uses is collecting and long-term archiving of existing global gravity field models and solutions from dedicated time periods (e.g., monthly GRACE models). While, for the data processing process, from data collection to 3D modeling, can be seen in the flowchart below (Figure 3).



Figure 2. Research Area Map

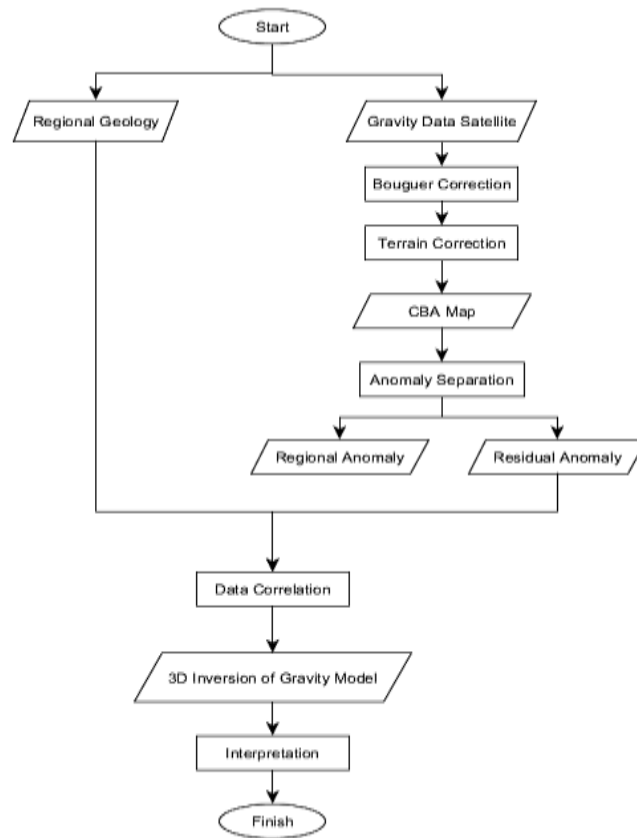


**Figure 3.** Research Flowchart

## RESULTS AND DISCUSSION

### ***Topography***

On the topographic map of the research area, it can be observed that the distribution of topographic values ranges from 306.4 to 1448.1 meters. The low-lying topography is found north of Mount Salak, with values ranging from 306.4 to 459 meters. The high-lying topography is located on Mount Salak and in several surrounding manifestations, with values ranging from 694.2 to 1448.1 meters (Figure 4).



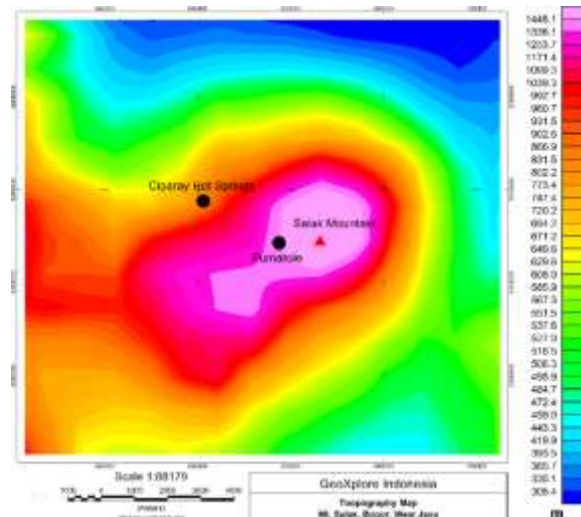


**Figure 4.** Topography Map

**Complete Bouguer Anomaly (CBA)**

On the CBA map, it can be observed that the distribution of gravity anomaly values at the research location ranges from 25 to 134.6 mGal. The low anomalies in the central part of the research area have values ranging from 25 to 68.6 mGal, which are believed to be associated with the overlying clay cap layer and alteration zone due to subsurface hydrothermal flow. High anomalies surround Mount Salak with values ranging from 99.6 to 134.6 mGal, which are believed to be associated with the Mount Salak caldera consisting of lava flows and pyroxene-containing basaltic andesite (augite). This CBA map still contains a mixture of shallow residual anomalies and deep regional anomalies, so to eliminate ambiguity in the interpretation, separation of these anomalies needs to be performed (Figure 5). Separation of regional and residual anomalies using a bandpass filter is used to reduce noise from regional anomalies by passing data that has a wavelength with a certain range [23].

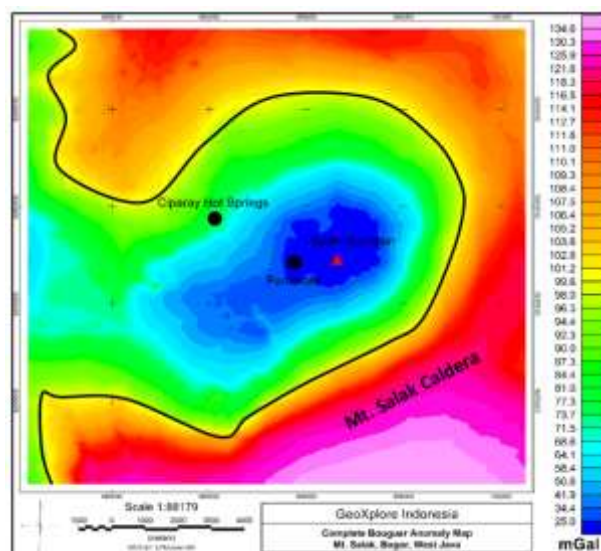


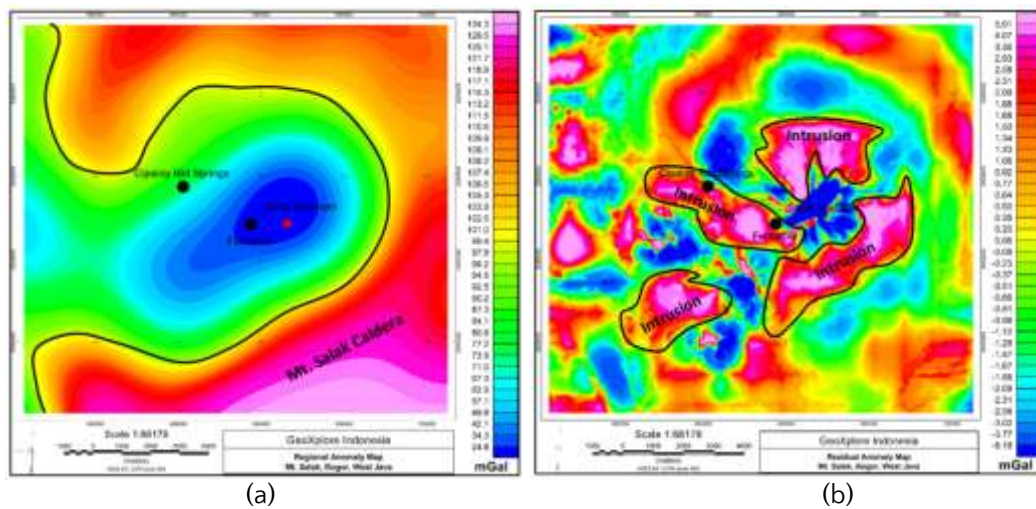
**Figure 5.** Complete Bouguer Anomaly Map

**Regional and Residual Anomaly**

On the regional anomaly map in the research area, the distribution of gravity anomaly values ranges from 24.8 to 134.3 mGal. This regional anomaly is caused by the response of

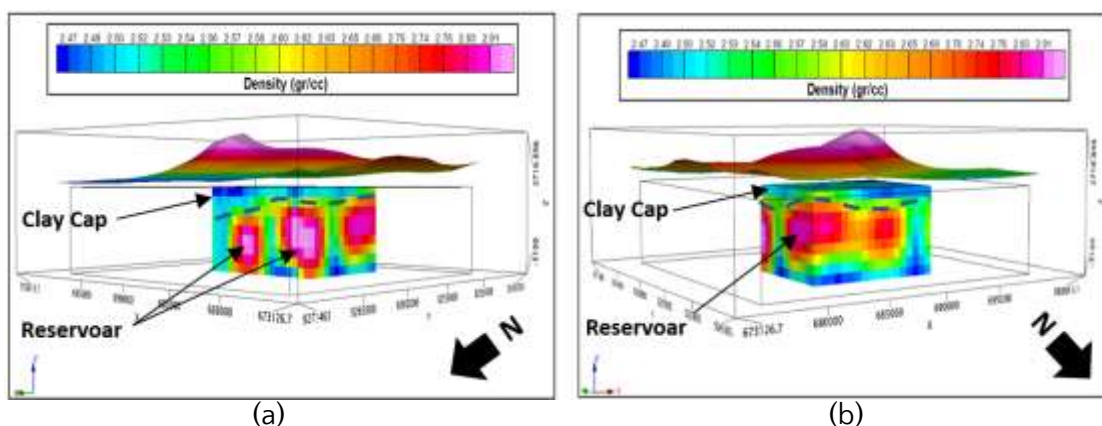
deep rocks beneath the Earth's surface and has contour shapes similar to the CBA map, but the contours on this regional anomaly map are smoother (Figure 6a).

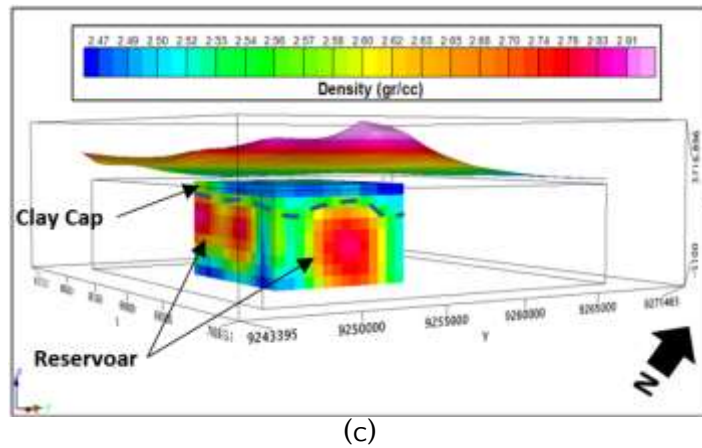
On the residual anomaly map, the distribution of gravity anomaly values ranges from -5.15 to 5.01 mGal. The low anomalies located directly beneath and around Mount Salak have values ranging from -5.15 to (-1.88) mGal, which are believed to be associated with the magma chamber of Mount Salak containing fluids and the distribution of the overlying clay cap layer with alteration minerals. The high anomalies located directly beneath and around Mount Salak have values ranging from 0.92 to 5.01 mGal, which are believed to be associated with the Mount Salak caldera composed of Salak volcanic rock formation (Qvsl), consisting of lava flows and pyroxene-containing basaltic andesite (augite). The high anomaly located directly beneath the manifestations (Fumarole and Ciparay Hot Springs) is believed to be an intrusive andesitic basalt rock, which is considered a reservoir rock containing hot fluids as the target of this research (Figure 6b).



**Figure 6.** (a) Regional Anomaly Map, and (b) Residual Anomaly Map

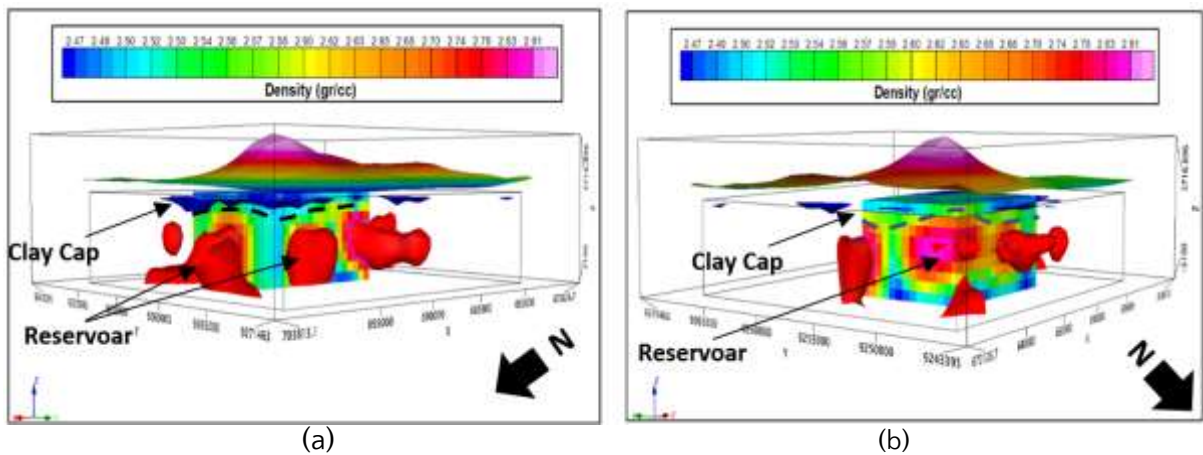
3D Inverse Modeling In this stage, 3D inverse modeling is conducted to depict the subsurface structure of the geothermal system in the Mount Salak region, West Java, correlated with the regional geological map. In the 3D model image below the surface of Mount Salak, it can be observed from different perspectives that the clay cap has a density ranging from approximately 2.47 to 2.5 gr/cc with a depth of 0 to 700 meters, while the andesitic basalt rock serving as the reservoir has a density ranging from approximately 2.74 to 2.91 gr/cc with a depth of 700 to 3000 meters (Figure 7).





**Figure 7.** Model 3D Gravity (a) Northwest View, (b) Northeast View, (c) Southeast View

In this 3D Isosurface model, it is conducted to visualize the shape and structure of the geothermal system in a three-dimensional manner, including the clay cap and reservoir beneath the surface. It is evident that the clay cap forms thin layers, while the reservoir appears as intrusive rock. Additionally, the model allows us to observe the shape of the magma chamber within Mount Salak, which has a density value ranging from 2.47 to 2.5 gr/cc with a depth of 0 to 3000 meters (Figure 8). If these results are correlated with previous research using the electromagnetic method, namely ADMT (Active Directory Magnetotelluric), the target depth results are reservoirs containing hot fluid at a depth of 700 m - 1000 m. It can be said that the results of the inversion model of the gravity method are validated.



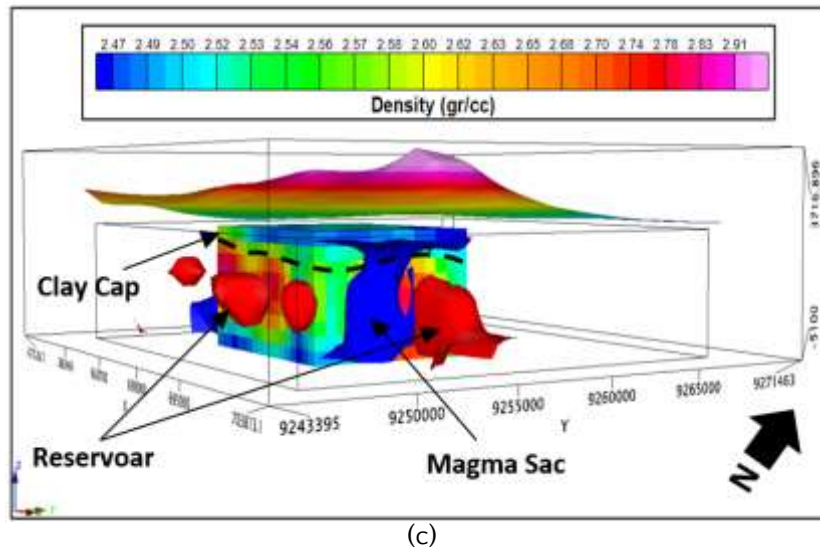


**Figure 8.** Model 3D Isosurface (a) Northwest View, (b) Northeast View, (c) Southeast View

## CONCLUSIONS

Based on the residual anomaly map, the low anomalies located beneath and around Mount Salak have values ranging from -5.15 to -1.88 mGal, which are suspected to be associated with the magma chamber of Mount Salak containing fluids and the distribution of the clay cap layer. The high anomalies located directly beneath and around Mount Salak have values ranging from 0.92 to 5.01 mGal, which are believed to be associated with the caldera of Mount Salak consisting of lava flows and andesitic basalt with pyroxene content (augite). The high anomalies beneath the manifestations are believed to be andesitic basalt intrusive rocks, which are considered as the reservoir containing hot fluids.

Based on the results of 3D inverse modeling to depict the subsurface structure of the geothermal system in the Mount Salak region, West Java, correlated with the regional geological map, there is a clay cap as the overlying rock with a density ranging from 2.47 to 2.5 gr/cc at depths of 0 to 700 m. Meanwhile, the andesitic basalt rock serves as the reservoir with a density ranging from 2.74 to 2.91 gr/cc at depths of 700 to 3000 m. these results have been validated from the results of previous researchers who used the electromagnetic method, namely ADMT (Active Directory Magnetotelluric) with quite the same depth of 700 - 1000 m.

## REFERENCES

- [1] Ermawati. T, and N. D Siwage., 2014. "Policy Analysis of Geothermal Energy Development in Indonesia", Jakarta: Lipi Press.
- [2] S. Mirwanda, et al., 2021. "Pemetaan Suhu Permukaan Anomali Panas Bumi Daerah Mount Ciremai Menggunakan Data Inframerah Termal Landsat 8". Jurnal Geosains dan Remote Sensing (JGRS), Vol. 2, Number 2, pp. 92-99.
- [3] I. R. Dewi., et al., 2022. "Anomali Bouguer Lengkap untuk Mengidentifikasi Sistem Panas Bumi Mount Pandan Jawa Timur". Evolusi: Journal of Mathematics and Sciences, Volume 6, Number 1, pp. 48-57.

- [4] R. D. Goenawan., et al., 2018. "Studi Potensi Panas Bumi Dan Teknologi Modifikasi Cuaca Alternatif Di Pantai Parang Tritis Yogyakarta". Seminar Sains dan Teknologi Kelautan, Fakultas Teknik UNHAS Gowa, pp. 2-7.
- [5] I. Adhitia dan M. A. Karmadi, 2021. "Studi Potensi Panas Bumi di Wilayah Kabupaten Bogor Ditinjau Dari Geologi Dan Geokimia". Jurnal Teknik, Vol. 22, No. 1, pp. 27-37.
- [6] R. Adiprana, Izzuddin, E. Yuniarto, 2010. "Mount Salak Geothermal Power Plant Experience of Scaling/Deposit: Analysis, Root Cause and Prevention". Proceedings World Geothermal Congress 2010 Bali, Indonesia, pp. 1-11.
- [7] A. R. Swastika, 2012. "Analisa Monitoring Arus Penggiat Pada Operasi Generator Di Unit Pembangkit Listrik Tenaga Panas Bumi (PLTP) Mount Salak". Depok: Universitas Indonesia.
- [8] M. Nafian, N. R. Permana, B. Gunawan, 2022. "Identification of the Subsurface Structure of Geothermal Working Area of the Hamiding Mountain, North Maluku through Land Surface Temperature (LST) Data and Forward Modeling with the Gravity Method". J. Nat. Scien. & Math. Res, Vol. 8, No. 1, pp. 10-19.
- [9] Hermawan, D., Widodo, S., Mulyadi, E., 2012. "Sistem Panas Bumi Daerah Candi Umbul-Telomoyo Berdasarkan Kajian Geologi Dan Geokimia". Buletin Sumber Daya Geologi, 7(1), pp. 1-6.
- [10] A. Firdaus, U. Harmoko, S. Widada., 2014. "Pemodelan Steady State Sistem Panas Bumi Daerah Sumber Air Panas Diwak-Derakan Dengan Menggunakan Software Hydrothrem 2.2". Youngster Physics Journal, 3(4), pp. 243- 250.
- [11] D. Zaenudin M., et al., 2019. "Karakteristik Endapan Vulkanik Sub DAS Cigombang Lereng Timur Mount Salak". Bulletin of Scientific Contribution: GEOLOGY, Vol. 17, No. 2, pp. 109 – 120.
- [12] S. Mawardi, E. Sukiyah, and I. Haryanto., 2019. "Karakteristik Morfotektonik Daerah Aliran Sungai Cisadane Berdasarkan Analisis Citra Satelit". Jurnal Geologi dan Sumberdaya Mineral, Vol. 20, No. 3, pp.175 – 186.
- [13] B. R. Suganda and V. Isnaniawardhani., 2014. "Karakteristik Geologi Daerah Vulkanik Kuarter Kaki Tenggara Mount Salak". Bulletin of Scientific Contribution, Vol. 12, No. 2, pp. 99-106.
- [14] D. Zaenudin M., et al., 2019. "Stratigrafi Vulkanik Sub DAS Cibadak Implikasinya Terhadap Kegiatan Mountapi Salak Lereng Timur". Bulletin of Scientific Contribution: GEOLOGY, Vol. 17, No. 1, pp. 9 – 20.
- [15] Effendi, A. C., 1974. "Peta Geologi Lembar Bogor, Jawa". Direktorat Geologi.
- [16] Jamaluddin, et al., 2019. "Pemodelan Geologi Bawah Permukaan Bantar Karet, Jawa Barat Menggunakan Metode Gravitasi". Jurnal Geocelebes Vol. 3 No. 2, pp. 59 – 65
- [17] M. Nafian, B. Gunawan, N. R. Permana., 2021. "2D Forward Modeling Geothermal System Gravity Data in South Solok Region, West Sumatra. Al-Fiziya: Journal of Materials Science, Geophysics, Instrumentation and Theoretical Physics, pp. 36-44.
- [18] N. R. Permana, B. Gunawan, M. Nafian., 2022. "Analysis of Subsurface Structure of Sembalun Geothermal Prospect Area, East Lombok with 2D and 3D Gravity Modeling". Al-Fiziya: Journal of Materials Science, Geophysics, Instrumentation and Theoretical Physics, Vol. 5, No. I, pp. 10 – 22.
- [19] Rachmawati, F. A., Haryanto, A. D., Hutabarat, J., Sumaryadi, M., 2019. "Penentuan Sumber Panas Sistem Panas Bumi Mount Api Talang, Sumatera Barat Berdasarkan Sejarah Panas dan Geokimia Air". Padjajaran Geoscience Journal. 3 (1), pp. 44-50.
- [20] Aji D. M., 2019. "Analisa Matematis pada Koreksi Bouguer dan Koreksi Medan Data Gravitasi Satelit Topex dalam Penentuan Kondisi Geologi Studi Kasus Sesar Palu Koro, Sulawesi Tengah". Jurnal Geosaintek, Vol. 5, No. 3, pp. 91-100.
- [21] B. Gunawan, A. Anjani, and A. Anjalni, 2022. "Identifikasi Pemodelan 2D dan Suhu Permukaan Daerah Panas Bumi Mount Gede-Pangrango, Jawa Barat menggunakan Metode Gravitasi", J. of Engineering Environmental Energy and Science, vol. 1, no. 1, pp. 1-14.
- [22] Hartini, 2020. "Pemodelan Inversi Linier Least Square (LS) Pada Anomali Geomagnet Model Dyke," J. Hadron, vol. 2, no. 2, pp. 49-53.
- [23] N. Agustin, and A. Wibawa, 2022. "Analisis Data Gravitasi Untuk Identifikasi Struktur Bawah Permukaan Daerah Potensi Panas Bumi Cipari", Jambura Geoscience Review, Vol. 4, No. 1, pp. 22-32.



---

## Library Visitor Noise Monitoring System Design With Warning Using LED and Telegram

Nur Fitriani<sup>1</sup>, Sitti Ahmiatri Saptari<sup>1</sup>, Elvan Yuniarti<sup>1\*</sup>

<sup>1</sup>Universitas Islam Negeri Syarif Hidayatullah Jakarta, Indonesia

[\\*elvan.yuniarti@gmail.com](mailto:*elvan.yuniarti@gmail.com)

---

Submitted: August ; Revised: August ; Approved: August ; Available Online: September

---

**Abstract.** *The library supports education and is a place to learn and gain knowledge. To maximize its use, visitors need comfort by not making noise or upheaval that can disturb other visitors. According to the decision of the Ministry of Environment in 1996, the maximum standard for noise levels in libraries is 55 dB. This research was conducted to design a tool that can monitor the noise that occurs in the library by providing information on room conditions using LED (Light Emitting Diode), LCD (Liquid Crystal Display), and giving notifications to librarians in the form of messages on the Telegram application if the noise exceeds the limit maximum. The tool is designed using ESP32 as a control, a GY-MAX4466 sensor to detect sound, and the output system uses red, yellow, and green LED (Light Emitting Diode), LCD (Liquid Crystal Display) 16x2, and the Telegram application. The results of this study concluded that the noise monitoring system was running well, with a GY-MAX4466 sensor error rate of 0.4%, and the best R Square value was obtained at a distance of 1 meter from the sound source with an R Square value of 0,7202.*

**Keywords:** ESP32, GY-MAX4466, LCD, LED, Library, Noise, Telegram.

**DOI :** [10.15408/fiziya.v6i1.34280](https://doi.org/10.15408/fiziya.v6i1.34280)

### INTRODUCTION

The library functions as a medium for education, research, preservation, information, and entertainment and acts as a promoter of literacy culture with the hope of creating conditions for cultural literacy to become a basic need in the daily lives of Indonesian people. If literacy culture is practiced as a way of life, then the Indonesian nation will become an educated society, thirsty for knowledge and ready to become a developed country [1]. Libraries have several types, namely national libraries, academic libraries, public libraries, community libraries, school libraries, and other libraries[2][3].

In every library, there is always a librarian who plays an important role in the management, service, and organization of library activities, and he is responsible for improving services, implementing program promotions, assisting customers in finding information, replacing damaged books, and sending them to the bookbinding department, monitoring the use of collections, verifying the correct arrangement of collections on shelves, making statistical

©2022 The Author (s) This is an Open-access article under CC-BY-SA license  
(<https://creativecommons.org/licenses/by/4.0/>)

Al-Fiziya: Journal of Materials Science, Geophysics,  
Instrumentation and Theoretical Physics  
P-ISSN: 2621-0215, E-ISSN: 2621-489X

reports on activities, maintaining order and cleanliness of the room[4]. To maintain order, librarians give guests the freedom to carry out any activity as long as they don't disturb other guests. A warning is needed to remind the state of the room caused by visitor activity. Of course, the warning given shouldn't add to the noise in the room. In addition to warning visitors, it is also important to notify the librarian if room conditions exceed the noise limit values in the library. The minimum number of employees in a large room can cause the room to go unnoticed, requiring notification to provide reports even if the distance between staff and visitors is far.

As for several previous noise detection studies, Nurwati's first research was in 2018 regarding noise detection using a microcontroller similar to Arduino Uno, the LM393D sound sensor as a noise detector and a speaker as an alarm if noise is detected [5]. Then, in the same year, research was also carried out by Theodorus and his friends regarding a noise detection device using an Arduino Uno-type microcontroller, a condenser mic sound sensor as a sound detector, and a speaker as an alarm if noise is detected [6]. Using the Arduino Nano 33 BLE microcontroller and ESP32-WROOM32U using the DFROBOT Analog Sound Level sensor. The system was built by classifying machine training using the Convolutional Neural Network algorithm by utilizing a Feature Extraction [7].

In this study, the telegram application. This telegram application has been widely used in monitoring systems, such as monitoring electricity users, accessing smart agricultural data, monitoring traffic violations, monitoring automatic home keys, and Home automation[8][9][10][11][12]. Telegram is a cloud-based application in the form of instant messaging that focuses on speed and security. The use of Telegram is designed to be able to send text, audio, video, images, and stickers messages to each other safely. Its use is designed to be quite easy. [13].

For the problems above, the author intends to design a noise detector for library visitors based on sound pressure parameters using an amplified sound sensor so that it is able to detect not only loud sounds but also the GY-MAX4466 sensor. This sensor has been widely used to detect sound noise [14][15][16]. Research on monitoring noise in the library has been carried out using the ESP32 microcontroller with the WhatsApp application [17]. In other studies, noise measurement has also been carried out with the NODEMCU ESP8266 sensor [18]. The difference between this study and previous research is the application used is different. In this study, the telegram application. In this study, the ESP 32 microcontroller was used. To warn visitors, of course, warning signs were used so as not to cause additional noise, so 3 LEDs (light emitting diodes) with different colors were used to clearly indicate when one of them was on.

And for librarians, a system has also been created to notify when conditions exceed the limit. For this reason, the messaging application Telegram is used because it can be accessed on many devices so that many librarians can access it.

## **RESEARCH METHODS**

This research was conducted at the Physics Laboratory Center, the Integrated Laboratory Center at UIN Syarif Hidayatullah Jakarta, and the Siliwangi University Library, Tasikmalaya City, West Java. The tools and materials used include an esp32 microcontroller, GY-MAX4466 sensor, LED (Light Emitting Diode), LCD (Liquid Crystal Display), laptops, Arduino IDE applications, telegram applications, etc. The research phase consists of the preparation stage, analyzing the tools and materials needed, designing hardware (hardware) and software (software), then calibrating and testing the accuracy of the sensor, testing the tool as a whole, analyzing data, and making conclusions.

## RESULTS AND DISCUSSION

### Hardware Design Results

The hardware design for the library visitor noise monitoring system is designed by making the esp32 microcontroller the brain or control center for all components, including the GY-MAX4466 sensor, LED (Light Emitting Diode), and LCD (Liquid Crystal Display). The results of the hardware design can be seen in Figure 1 and Figure 2.



**Figure 1. Hardware Design Results**

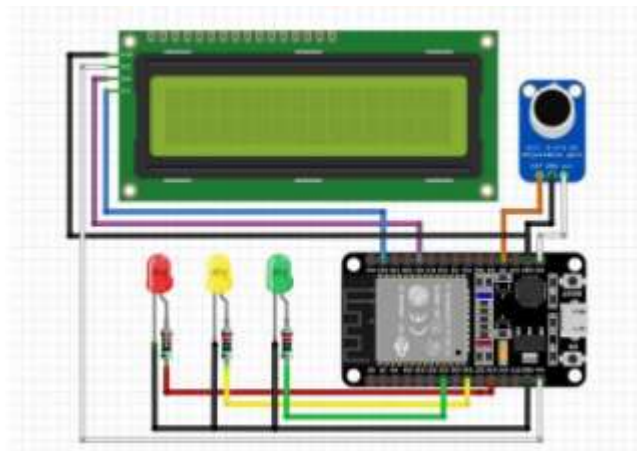


**Figure 2. Series of noise monitoring systems**

In Figure 1, you can see from the outside that a black circle, the GY-MAX4466 sound sensor, receives sound waves from the surrounding environment. Then, an LCD screen displays the results of the esp32 microcontroller process, which processes sound wave value data received by the sound sensor so that room conditions and sound intensity can be displayed. Finally, a red, yellow, and green LED (Emitting Diode) functions as a warning sign. The red LED will light up when the surrounding sound intensity is above 55 dB. The yellow LED will light up when the surrounding sound intensity is between 50 and 55 dB, and the green LED will light up when the surrounding sound intensity is below 50 dB.



## Software Design Results

The library visitor noise monitoring system software is designed by making the esp32 microcontroller, which is a microcontroller with a wifi module as the control center so that it can send noise alerts via the Telegram application. The design uses the Arduino IDE application as a programming medium and the Telegram application to receive warnings regarding room conditions. Here is a picture. 3 is a display of the design results for the Telegram application.

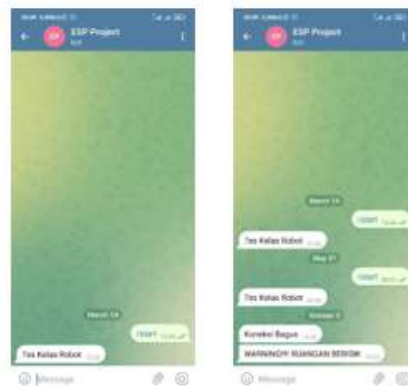


**Figure 3.** The results of the Telegram Messenger Application Software Design

Figure 3 shows that at the beginning of the message, type `"/start"` to start a chat on the Telegram bot so that the smartphone can receive a warning message when it is noisy with the sentence `"WARNING!!! NOISY ROOM"`.

## Tool Testing Results

test the noise monitoring tool for library visitors, and several stages were carried out, namely by testing the sensor's accuracy, then conducting a linear regression test, and finally testing the entire system, including LCD, LED, and the Telegram application.

### GY-MAX4466 Sensor Accuracy Test Results

The GY-MAX4466 sensor is a sound sensor that identifies the sound intensity values around it. Testing the accuracy of the GY-MAX4466 sensor is carried out by taking sound intensity data in a library room measuring approximately 150 m<sup>2</sup> and accommodating a maximum of 30 visitors. Retrieval is done by placing the GY-MAX4466 sensor in the middle of the room when the number of people in it is one person, ten people, 20 people, and 30 people, with data retrieval intervals every second. At the same time, data is also collected using a factory-made sound level meter, then the results from the GY-MAX4466 sensor are compared with the results of the factory-made device to determine the accuracy value of the GY-MAX4466 sensor.

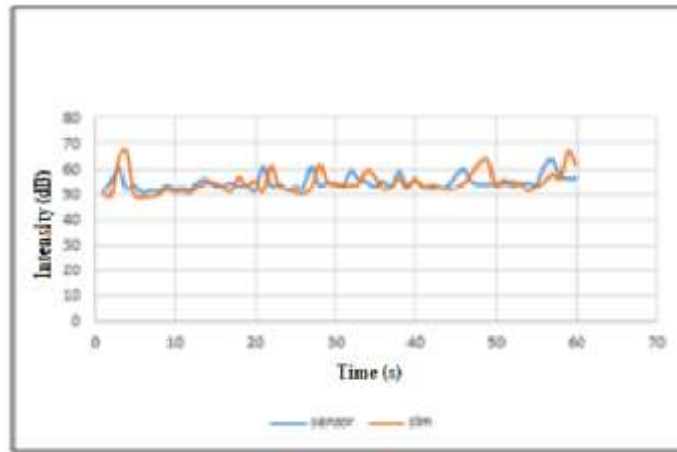


**Figure 4.** Graph of Comparison of Measurement Results of the GYMAX4466 Sensor with factory sound level meters in the library (20 people)

Figure 4 shows a graph of the results of sound intensity measurements carried out in the library room with one visitor. The blue line shows the measurement results using the GY-MAX4466 sensor, and the orange line shows the results using a factory-made sound level meter. The graph shows that the blue and orange lines have almost the exact shape of peaks and valleys, but there are gaps or differences between the two. Some lines intersect, which means that the measurement results with both tools have the same results, so the error rate is 0.1%. This system has an accuracy value of 99.9%. This value is higher than the monitoring system with the Blink application, with an accuracy of 97.58% [14].

#### Linearity Test Results

Another static characteristic test is a linearity test. In this test, the sound measurement is carried out using a higher audio sound source sensor. The measured level is 10% to 100% at 10% intervals. This test is also carried out for variations in the distance between the sound source and the GY-MAX4466 sensor. The distances tested were 1 meter, 2 meters, and 3 meters in a room with an area of about 30 m<sup>2</sup>.

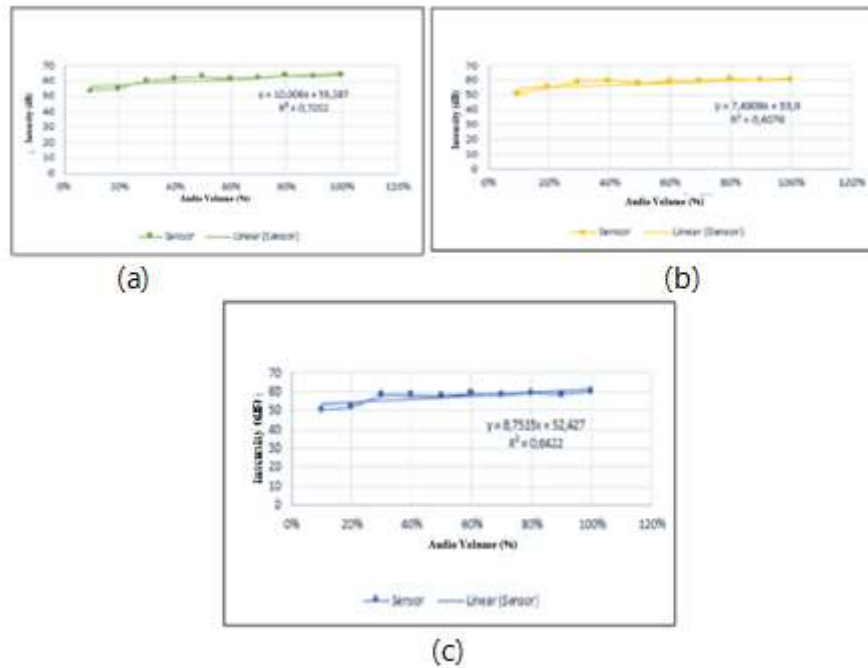


**Figure 5.** Graph of the Relationship Between Audio Volume and Sound Intensity at a Distance of (a) 1 Meter, (b) 2 Meters and (c) 3 Meters

Figure 5 shows a graph of the relationship between audio volume and sound intensity. It is then known that the higher the audio volume, the higher the measured intensity value. At a distance of 1 meter, an R-Square value of 0.7202 is obtained, which means that it is above the value of 0.67, so the results are categorized as vital. At a distance of 2 meters, an R-Square value of 0.6076 is also obtained, which means that between 0.33 and 0.67, the results are categorized as moderate. At a distance of 3 meters, an R-Square value of 0.6422 is also obtained, which means that between 0.33 and 0.67, the results are categorized as moderate [19].

It can be concluded that the data obtained at a distance of 1 meter is better than at a distance of 2 meters and 3 meters, with the R-Square value closest to number 1, namely at 0.7202. This value is much different from other studies conducted with variations of distances above 10m, 20m, 30m, 40m, and 50m. This study detects traffic noise using a sound level meter with a linearity of 0.98 for a distance of 10 m[20]. However, the trend obtained in this study has something in common with this study, namely experiencing a decrease in linearity with increasing distance.

### Overall System Test Results

The final test is testing the entire system, which consists of the output LCD, LED, and warning messages that enter the Telegram application. When the sensor detects sound intensity below 50 dB, the LCD screen will display a notification "Quiet" with a green LED that lights up. When the sensor detects the sound intensity between 50 dB and 55 dB, the LCD screen will display the word "Caution" with a yellow LED that lights up, which means visitors are expected to be careful because the sound generated is close to the noise level. When the sensor detects the sound intensity is above 55 dB, the LCD screen will display a warning with

the sentence "No noise" and a red LED that lights up as a warning to visitors to stop causing noise, and there will also be an incoming message via the Telegram application to notify the librarian that noisy room conditions. The test was carried out in an empty room 6 times with different sound sources, namely, without any sound interference, human voices talking, music from smartphones, the sound of clapping hands, the sound of turning book pages, and the sound of whistling with the distance of the sound source and the instrument. 1 meter away.

**Table 1. Test Results for the Whole System**

NO	Voice Description	Intensity (dB)	Telegram warning	LCD Detection Results	LED			Delay Telegram (s)	Information
					Red	Yellow	Green		
1	No sound disturbance	44,2 dB	-	Quite	-	-	✓	-	Succeed
2	Human Voice Talking	50,6 dB	-	Attention	-	✓	-	-	Succeed
3	Smartphone Music Sound	55,5 dB	✓	Do not be noisy	✓	-	-	3 s	Succeed
4	Applause	70 dB	✓	Do not be noisy	✓	-	-	3 s	Succeed
5	Turning Book Pages	54,5 dB	-	Attention	-	✓	-	-	Succeed
6	Whistling	52,5 dB	-	Attention	-	✓	-	-	Succeed

Table 1 shows the results of the first test without any additional sound disturbance; the measured sound intensity value is 44.2 dB, and the word "Quiet" is displayed on the LCD screen with a green LED that lights up, indicating that the room conditions are calm or conducive. The second test, with a human voice speaking, measured a sound intensity value of 50.6 dB, so the word "Caution" is displayed on the LCD screen with a yellow LED that lights up, indicating that the room conditions are at a moderate level. The third test was with a music sound source from a smartphone; the measured sound intensity value was 55.5 dB, so the word "Noise Prohibited" is displayed on the LCD screen with a red LED that lights up. The message has successfully entered the Telegram application with the interval between the color change of the LED light and the entry of the message. For 3 seconds, it indicates that the room condition is noisy. The fourth test is with the sound source of clapping. The measured sound intensity value is 70 dB. The word "No noise" is displayed on the LCD screen with a red LED that lights up well as the message successfully entering the Telegram application with the time interval between the color change of the LED light and the entry of the message for 3 seconds indicates that the condition of the room is noisy. The fifth test, with the book sound source, turned upside down, measured a sound intensity value of 54.5 dB; the word "Caution" is displayed on the LCD screen with a yellow LED that lights up, indicating that the room condition is at a moderate level. The sixth test, with a whistling sound source, measured a sound intensity value of 52.5 dB, so the word "Caution" is displayed on the LCD screen with a yellow LED that lights up, indicating that the room conditions are at a moderate level.



**Figure 6.** Display of Telegram Overall System Test Results

Table 1 shows the first test's results without any additional sound disturbance; the measured sound intensity value is 44.2 dB, and the word "Quiet" is displayed on the LCD screen with a green LED that lights up, indicating that the room conditions are calm or conducive. The second test, with a human voice speaking, measured a sound intensity value of 50.6 dB, so the word "Caution" is displayed on the LCD screen with a yellow LED that lights up, indicating that the room conditions are at a moderate level. The third test was with a music sound source from a smartphone; the measured sound intensity value was 55.5 dB, so the word "Noise Prohibited" is displayed on the LCD screen with a red LED. Figure 6 displays the message that entered the telegram in the sentence "WARNING!!!!" NOISE ROOM" when the sensor detects the sound source of smartphone music and hand clapping. From all the test results, it can be concluded that the design of the library visitor noise monitoring tool using LED (Light Emitting Diode) as a warning to visitors and messages sent via the Telegram application as notifications to guards can run well as planned.

## CONCLUSION

The design of a tool for monitoring the noise of library visitors has been successfully carried out using LED (Light Emitting Diode) as a warning to visitors and messages via the Telegram application as notifications to guards. From the results of the characterization carried out on the GY-MAX4466 sensor, an average error value of 0.4% is obtained. The linear regression test obtains the R square value when the distance between the sound source and the GY-MAX4466 sensor is 1 meter. .6076 and 0.6422.

All components and systems in this noise monitoring tool are going well as planned. The sensor can identify the environment well so the warning LED can function correctly. Also, notification messages for the Telegram application can be received correctly with an average delay time of receiving messages of 3 seconds.

## REFERENCE

- [1] Tunardi, "Memaknai Peran Perpustakaan dan Pustakawan dalam Menumbuhkembangkan Budaya Literasi," *Media Pustakawan*, vol. 25, no. 3, p. 79, 2018.
- [2] IFLA, "Definitions of Library Types," 30 Juli 2019, p. 2789, 2019, [Online]. Available: <https://librarymap.ifla.org/files/lmw-library-types-definitions-es.pdf>.

- [3] A. Iztihana and M. Arfa, "Peran Pustakawan MTSN 1 Jepara Dalam Upaya Mengembangkan Minat Kunjungan Siswa Pada Perpustakaan," *Ilmu Perpust.*, vol. 9, no. 1, 93–103, 2020, [Online]. Available: <https://ejournal3.undip.ac.id/index.php/jip/article/download/29974/25002>.
- [4] N. J. Azmar, "Peran Pustakawan Dalam Meningkatkan Kualitas Layanan Di Perpustakaan," *Jurnal Iqra*, vol. 9, no. 2, pp. 227-231, 2015.
- [5] Nurwati, "Pendeteksi Tingkat Kebisingan Dan Pemberi Peringatan Pada Perpustakaan Berbasis Arduino," in SEMINAR NASIONAL ROYAL (SENAR), Asahan, 2018.
- [6] Kalengkongan, T. S, D. Z, Mamahit and dkk, "Rancang Bangun Alat Deteksi Kebisingan Dan Pemberi Peringatan Pada Perpustakaan Berbasis Arduino Uno," *Teknik Elektro dan Komputer*, vol. 7, no. 2, pp. 183-188, 2018.
- [7] D. Eridani, A. F. Rochim, and A. Z. Firdananta, "Noise Monitoring System Development in a Library Based on The Internet of Things," *Proc. - 2022 2nd Int. Conf. Electron. Electr. Eng. Intell. Syst. ICE3IS 2022*, no. November, pp. 24–28, 2022, doi: 10.1109/ICE3IS56585.2022.10010007.
- [8] S. Abdurrahman, "Rancang Bangun Sistem Monitoring Penggunaan Daya Listrik Berbasis Aplikasi Telegram," *Kumpul. Karya Ilm. Mhs. ...*, 2021, [Online]. Available: <http://jurnal.pancabudi.ac.id/index.php/fastek/article/view/1673>.
- [9] R. P. Astutik, "Aplikasi Telegram Untuk Sistem Monitoring pada Smart Farming Telegram Application Monitoring System for Smart Farming," *J. Teknol. dan Terap. Bisnis*, vol. 2, no. 1, pp. 1–6, 2019.
- [10] D. P, I. Santoso, and Fardan, "Perancangan Dan Implementasi Website Dan Telegram Untuk Pemantauan Pelanggaran Lalu Lintas Berbasis Internet Of Things," *e-Proceeding Eng.*, vol. 8, no. 6, p. 3523, 2022, [Online]. Available: <https://openlibrarypublications.telkomuniversity.ac.id/index.php/engineering/article/view/19043>.
- [11] G. D. Ramady et al., "Rancang Bangun Sistem Monitoring Pintu Rumah dan Kontrol Lampu Berbasis Telegram," vol. 16, no. 2, pp. 52–58, 2021. *Isu Teknologi Stt Mandala Vol.16 No.2 Desember 2021 P-Issn 1979-4819 E-Issn 2599-1930*
- [12] A. Sedayu, E. Yuniarti, and E. Sanjaya, "Rancang Bangun Home Automation Berbasis Raspberry Pi 3 Model B dengan Interface Aplikasi Media Sosial Telegram sebagai Kendali," *Al-Fiziya J. Mater. Sci. Geophys. Instrum. Theor. Phys.*, vol. 1, no. 2, pp. 42–47, 2019, doi: 10.15408/fiziya.v1i2.9254.
- [13] V. F. Dr. Vladimir, "Penggunaan Aplikasi Telegram Untuk Kegiatan Pembelajaran Jarak Jauh Pada Mata Kuliah Bahasa Inggris Materi Speaking Pada Mahasiswa Universitas Maritim Amni Semarang," *Pros. Kematriman 2021*, vol. 1, no. 1, pp. 245–256, 2021.
- [14] L. Wilani, M. Peslinof, J. Pebralia, P. Studi Fisika, F. Sains dan Teknologi, and U. Jambi, "STRING (Satuan Tulisan Riset dan Inovasi Teknologi) Rancang Bangun Sistem Monitoring Kebisingan Pada Ruangan Dengan Sensor Suara Gy-Max4466 Berbasis Internet Of Things (IoT)," vol. 7, no. 3, 2023, [Online]. Available: <https://journal.lppmunindra.ac.id/index.php/STRING/article/view/15492>.
- [15] B. Nodemcu et al., "Implementasi Sensor GYMAX4466 Pada Sistem Monitoring Kebisingan Menggunakan Internet of Things (IOT) Berbasis Nodemcu," *J. Cyber*
- [16] C. M. Achsan and D. Krisbiantoro, "Rancang Bangun Alat Pendeteksi Dan Pemberi Peringatan Kebisingan Suara Berbasis Arduino (Studi Kasus: Perpustakaan Universitas Amikom Purwokerto)," *Simetris J. Tek. Mesin, Elektro dan Ilmu Komput.*, vol. 11, no. 2, pp. 551–559, 2021, doi: 10.24176/simet.v11i2.5013.
- [17] R. N. Sayaifah, B. S. Nugroho, and B. Aditya, "Rancang Bangun Alat Pendeteksi Kebisingan di Perpustakaan Berbasis Mikrokontroler Esp32 Notifikasi Whatsapp," *e-Proceeding Eng.*, vol. 8, no. 6, pp. 3821–3827, 2022. *Tech*, vol. 4, no. 8, 2021, [Online]. Available: <https://ojs.trigunadharma.ac.id/index.php/jct/article/view/4323>.
- [18] H. Heri and H. Khotimah, "Rancang Bangun Alat Deteksi Kebisingan Pengunjung Perpustakaan Berdasarkan Parameter Tekanan Suara Menggunakan Nodemcu Esp8266," *J. Ilmu Komput.*, vol. 10, no. 1, pp. 20–26, 2021, doi: 10.33060/jik/2021/vol10.iss1.204.

- [19] W. Wynne, *The Partial Least Square Approach To Structural Equation Modeling*, London: Lawrence Erlbaum Associates, 1998.
- [20] S. Bahri, A. Saputra, and M. R. Razali, "Pengaruh Distansi Terhadap Tingkat Kebisingan Yang Bersumber Dari Bunyi Mesin Kendaraan (Studi Kasus Pada Jalan Suprpto Kota Bengkulu)," *Inersia, J. Tek. Sipil*, vol. 11, no. 2, pp. 34–40, 2019, doi: 10.33369/ijts.11.2.34-40.

---

## Lithofacies Interpretation Of Sediment Rocks In The Cipamingkis River Outcrop, Jonggol Area, Bogor District, West Java

Suwondo <sup>1\*</sup>, Mill Sartika Indah<sup>2</sup>, Afzalurrahman Assalam<sup>3</sup>, M. Nafian <sup>1</sup>, Andika Perbawa<sup>4</sup>

<sup>1</sup>State Islamic University Syarif Hidayatullah Jakarta, Indonesia

<sup>2</sup>PT Pertamina Research and Technology Innovation, Indonesia.

<sup>3</sup>PT Pertamina Hulu Sanga Sanga, Indonesia.

<sup>4</sup>King Abdullah University of Science and Technology, Saudi Arabia.

\*[suwondo@uinjkt.ac.id](mailto:suwondo@uinjkt.ac.id)

---

Submitted: August ; Revised: August ; Approved: August ; Available Online: September

---

**Abstract.** This research aims to study sedimentary structures and determine the depositional environment of the outcrop in the Cipamingkis River, Jonggol area, Bogor Regency, West Java. The method in this study includes literature studies, field surveys, data interpretation, and facies analysis. The result shows the outcrop in the Cimangkis River can be divided into four (4) sedimentation sequences unit: Claystone Unit (Sequence 1), Limestone/Calsirudit Unit (Sequence 2), Limestone/calcarenite-Calcilutite Unit (Sequence 3), Mudstone/ Calsilutite Unit (Sequence 4). Based on the depositional environment analysis, this outcrop displays characteristics of a shallow marine environment. The Interpretation of facies from outcrops can be used as a reservoir analog and can support subsurface interpretation in the Northwest Java Basin.

**Keywords:** *facies, cibulakan, cipamingkis river, carbonate.*

**DOI :** [10.15408/fiziya.v6i1.34280](https://doi.org/10.15408/fiziya.v6i1.34280)

### INTRODUCTION

The outcrop is located along the Cipamingkis River in the Jonggol area of West Java. Its coordinates are approximately 6°31'57.64"S and 107°2'8.71"E. This outcrop is covered by the Jatiluhur Formation, which is equivalent to the Cibulakan Formation in the Northwest Java Basin. The Cibulakan Formation plays a significant role in hydrocarbon [1] exploration. The Jatiluhur Formation is composed of siliciclastic rocks intercalated with limestone, forming a slope-shelf system or continental shelf environment with ages ranging from Middle Miocene to early Late Miocene [2]. According to [3], this basin is situated between the Sunda Shelf in the North, the Pergulungan - Bogor Line in the South, the Karimun Jawa Lifting Area in the East, and the Seribu Island Shelf in the West. The North West Java Basin is influenced by a north-south trending block faulting system. This system divides the basin into graben or several sub-basins, namely Jati Barang, Pasir Putih, Ciputat, Rangkas Bitung, and several

©2022 The Author (s) This is an Open-access article under CC-BY-SA license  
(<https://creativecommons.org/licenses/by-sa/4.0/>)

**Al-Fiziya: Journal of Materials Science, Geophysics,  
Instrumentation and Theoretical Physics**  
P-ISSN: 2621-0215, E-ISSN: 2621-489X



basemen elevations, Arjawinangun, Cilamaya, Pamanukan, Kandanghaur–Waled, Rengasdengklok, and Tangerang Based on its stratigraphy, structural patterns, and its location within a subduction arc pattern over time, it becomes evident that the West Java Basin has undergone multiple sedimentation and tectonic phases from the Eocene to the present [3].



**Figure. 1** Geological map of the Cipamingkis area [4], the research study is covered by the Jatiluhur formation which is shown by a red box line.



**Figure. 2** Location map of the outcrop in the Cipamingkis River [5]

This formation consists of alternating shales, sandstones, and limestones. The limestone within this unit is primarily clastic limestone and locally developed reef limestone. This type of limestone is referred to as Mid Main Carbonate (MMC). The formation was deposited during the Early Miocene to Late Miocene period. It is further divided into three members:

a) Massive

This member is deposited unconformably above the Baturaja Formation. The lithology of this member consists of intercalations of claystone and sandstone with fine to medium





**Figure 2.1** Response of gamma-ray log to variations in grain size and depositional environment [9]

The cylindrical shape of the GR or SP logs may indicate the presence of thick and homogeneous sediment, bounded by channel-fills or channel-fills with sharp contacts. The cylindrical form represents homogeneity and ideal properties. It is associated with braided channel sediment deposits, estuarine or sub-marine channel fills, anastomosed channels, eolian dunes, and tidal sands. This shape is a representation of reservoir rock presence. Irregular shapes are associated with alluvial plain sediments, floodplains, tidal sands, shelves, or back barriers. Generally, this pattern is identified as thin interbedded layers. Thin deposit elements may include crevasse splays, overbank deposits in lagoons, and turbidites.

The bell-shaped profile shows upward smoothing, possibly due to channel fills. Observations indicate that the grain size at each level tends to be the same, but the number shows a gradation towards fine-grained with more radioactive clays upwards. The bell shape is produced by point bar deposits, tidal deposits, transgressive shelf sands (shallow sea), sub marine channels, and turbidite deposits. The profile in the form of a funnel or funnel shows upward roughness, which is the opposite of the bell shape. The funnel shape may result from progradation systems such as sub-marine fan lobes, regressive shallow marine bars, barrier islands or front reef carbonate prograding on top of mudstone, delta fronts or distributary mouth bars, crevasse splays, beach and barrier beach, strandplain, shoreface, prograding shelf sands, and submarine fan lobes.

The upward smoothing of the bell shape or bell shape is an indication of a regression event, while the upward roughening of the funnel shape represents a transgression event. Meanwhile, the constant cylindrical shape indicates a transition. The determination of the depositional environment is initially directed on a large scale and is further analyzed on a smaller scale using a combination of available data, such as cutting data and wireline log characters [9].

The Grabau classification is grounded in a straightforward characteristic of limestone or carbonate rock—the size of its constituent grains (Table 2.1) [10]. The concept behind this classification method aligns with general approaches used in categorizing clastic sedimentary rocks. The underlying idea of this method is associated with the potential deposition energy level of carbonate material [11]. The simplest categorization of limestone/carbonate rock is determined by the grain size of its components [10].

**Table 2.1.** Grabau Classification [10]

Grain Size	Carbonate Classification
>2 mm	Calcirudite
63 μm - 2mm	Calcarenite
< 63 μm	Calcilutite

This classification is founded on the concept of textural maturity in carbonate rocks, encompassing the type of rock composition (refer to Figure 2.2) [12]. The evolution of this classification stems from petrographic analysis of limestone, necessitating a more specific basis for determining depositional environments. Understanding the rock's fabric enables the interpretation of sediment deposition energy levels [13]. The Folk classification (1959) is rooted in the fabric and composition of carbonate rocks, categorizing them into three primary types: grains (allochems), matrix (micrite), and cement (sparite). Based on the allochem type—namely, intraclast, ooid, bioclast, and peloid—limestone is categorized into four groups. Furthermore, coherent, organically structured in-situ limestones are termed biolithites (as modified by [14]).

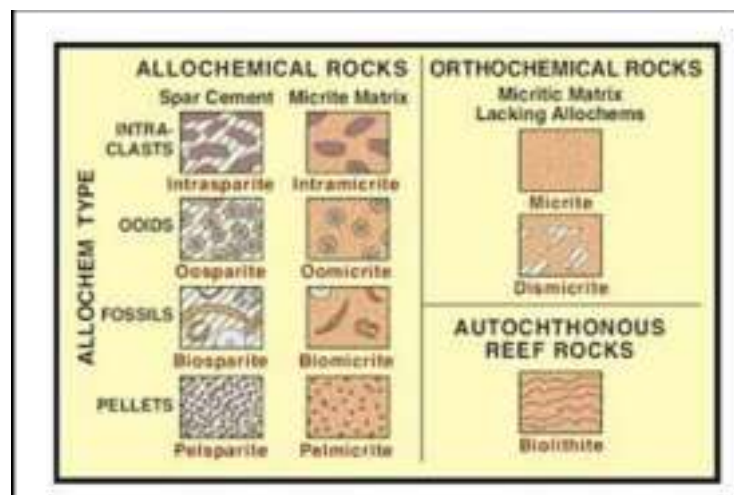


**Figure 2.2.** Folk Classification (1959) [12]

Dunham's classification is based on the fabric and composition of the carbonate rock. The three main divisions consist of limestone which has matrix-supported, grain-supported, and biological bound. The fourth category in addition is limestone that has undergone crystallization, namely crystalline carbonate [15].

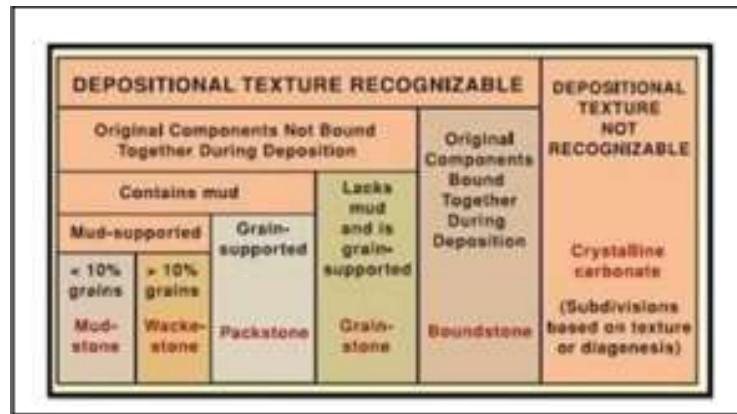


**Figure 2.3** Dunham's classification of carbonate rocks [15]

This classification is founded upon the same characteristics as Dunham's classification, encompassing rock fabric, texture, the proportion of silt content in the rock, and the structural framework of the rock—both mechanical and biological in nature. This classification represents a refinement of Dunham's classification, which previously lacked specific categorization for boundstones [16]. Boundstone resulting from the organic framework of coral colonies is categorized into several types based on the composing organisms. By combining texture and composition, this classification offers insights into the conditions under which the rock was formed [13].

### RESEARCH METHODS

This study can be divided into several research stages, as follows: Preparation Stage: This stage involves studying the literature related to the research area and obtaining permits for research locations. Description of Outcrops Stage: Field research is conducted through the following steps: General observations are made concerning sediment materials, sedimentation processes, and the environment around the study area. Rock samples are collected, and changes in rock facies are observed both vertically and laterally.

Rock Sedimentology Analysis Stage: In this stage, the data collected and recorded during field research are summarized in an article or report containing interpretations, discussions, and conclusions drawn from the data. Interpretation of Facies and Depositional Environment: The flow of these stages is illustrated in Figure 3.1.

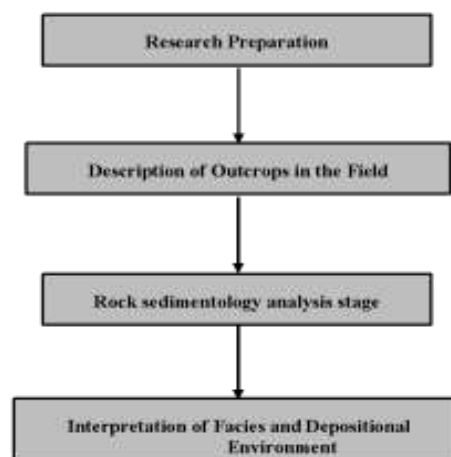
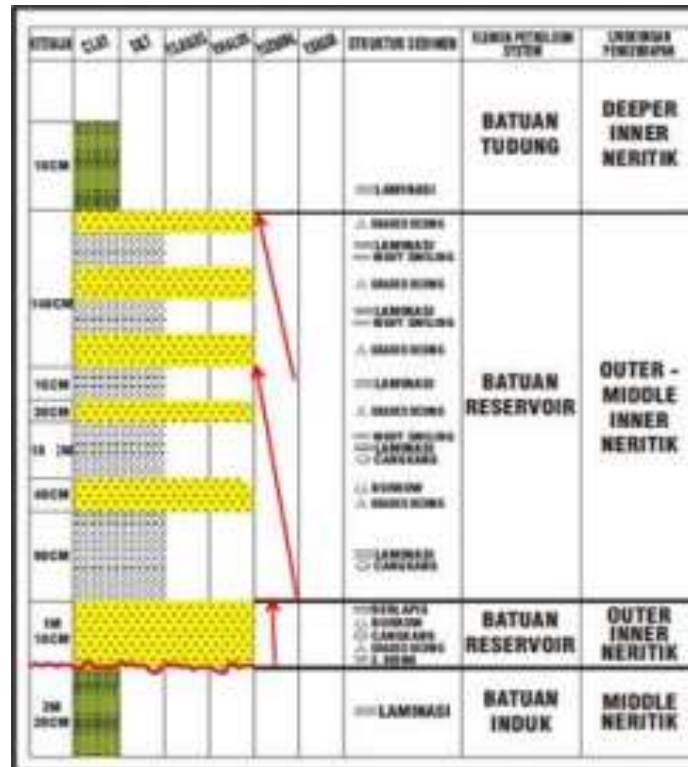


**Figure 3.1** Research workflow



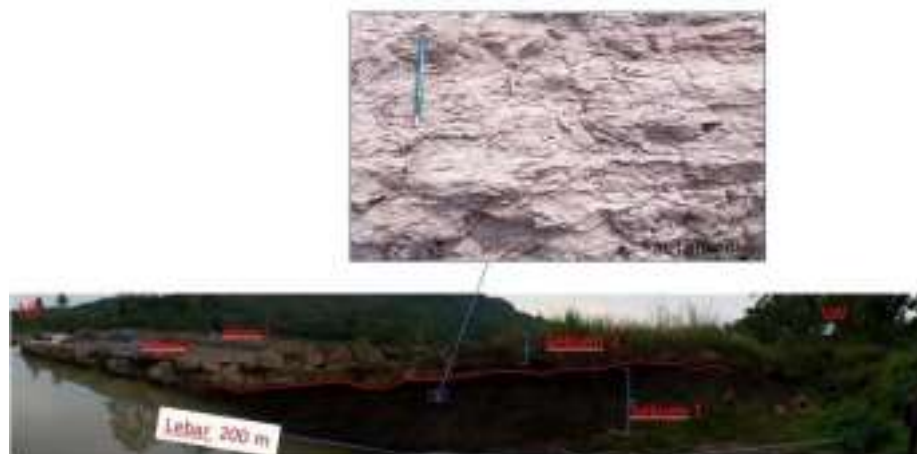
## RESULTS AND DISCUSSIONS

The stratigraphic column represents a stacking pattern that fining upwards due to sediment deposition processes that have occurred in the Cipamingkis River over geological timescales. The appearance of the Cipamingkis River outcrop aids in constructing a history of sediment deposition by revealing the condition of the sediment structure, which possesses distinct characteristics shown in Figures 4.1.



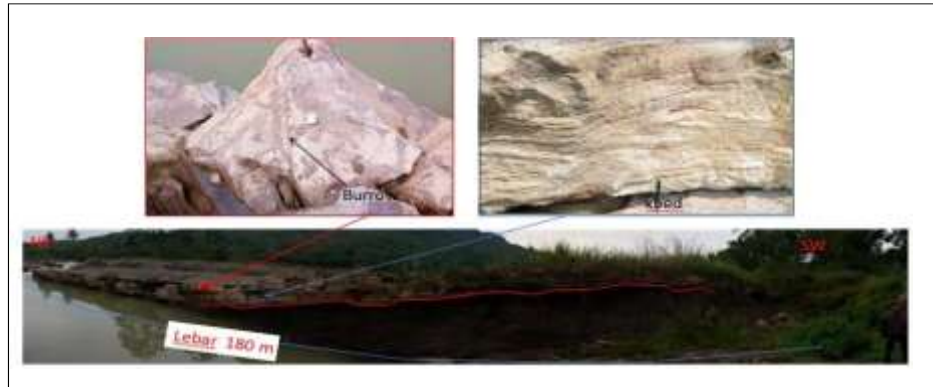
**Figure 4.1** The Outcrop Stratigraphic Column (without scale)

Figure 4.2 show in the stratigraphic column outcrop reveals that, based on the stacking pattern of sediment layers and the ratio of thickness of each lithofacies fining upward, it can be subdivided into four sequences of sediment deposition as follows: Black color, clay grain size, texture : clay grain shape, good sorting, closed packing, mineral composition : slightly visible quartz very fine size, parallel-layered laminated sedimentary structure.



**Figure 4.2** Sediment structure of parallel laminations in Sequence 1

The carbonate rock is bright yellowish brown in color, grain size of fine sand-very fine sand, texture: angular-sub, rounded grain shape, moderately-good sorting, closed packing, mineral composition: slightly visible quartz, very fine size, coarse shell fragments very abundant, very abundant foraminifera grains, sedimentary structures in the form of cross-bedding, graded bedding, bedding, and burrowing, there is the appearance of erosional fields on the lower sequence boundaries, good porosity.



**Figure 4.3** Crossbed, erosional and burrow sedimentary structures in Sequence 2

**Calcarenit** : Bright blackish-gray color, grain size of fine sand-very fine sand, texture: rounded-sub. rounded grain shape, moderately-good sorting, sealed packing, mineral composition : slightly visible quartz very fine size, shell fragments very slightly coarse, very abundant foraminifera grains, graded bedding, burrowing, good porosity sediment structure.  
**Cal silutite**: Dark gray-black color, clay grain size, texture: clay grain shape, well sorted, sealed packing, mineral composition: very fine quartz, parallel lamination sedimentary structure, abundant shell fragments at the bottom and top Ripples and wavy smiles appear due to storms and waves show in figure 4.3..

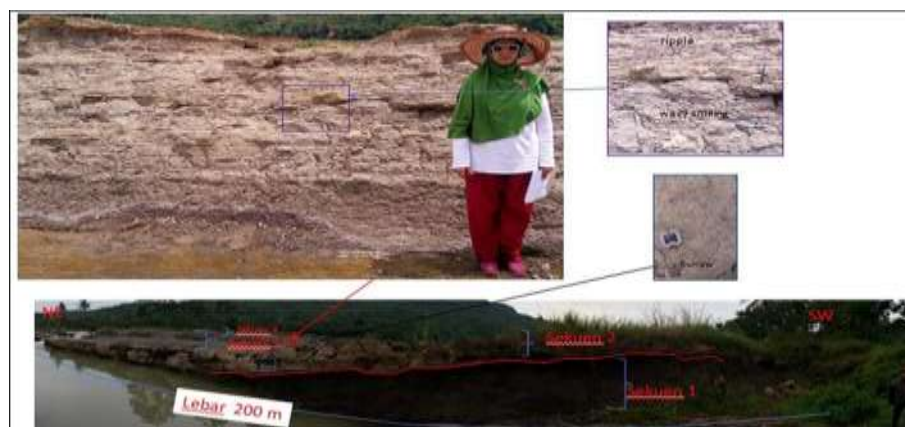


**Figure 4.4** Sediment structure of parallel laminations in Sequence 3

Figure 4.4 show in texture: clay grain shape, good sorting, closed packing, mineral composition: slightly visible quartz, very fine size, parallel lamination sedimentary structure. Generally, carbonate rocks form in aquatic environments that meet criteria suitable for carbonate formation, such as warm ambient temperatures and the presence of carbonate-

producing organisms. This sedimentation process results in carbonate facies exhibiting variations in depositional texture, mineralogy, chemical composition, and shape. These characteristics are associated with the distribution and pore size features within the rock. Carbonate rock facies are categorized into two types based on their forming materials: loose carbonate sedimentary materials and the products of organismal activities [17]. The presence of carbonate facies indicates a shallow marine depositional environment.



**Figure 4.5** Sediment structure of parallel laminations in Sequence 4

The identification of depositional environments and lithofacies in the stratigraphic column of STA 2 refers to the classification of depositional environments and lithofacies in shallow seas by [18]. The lithofacies units are named according to Dunham's Classification (1962). The stacking pattern in Sequence 1 exhibits a blocky pattern with a 1-meter thickness, identified as a Calsirudit Unit or Grainstone Unit (Dunham, 1962). The thickness ratio of each lithofacies aids in determining the environment show in figure 4.5.

Cibulakan

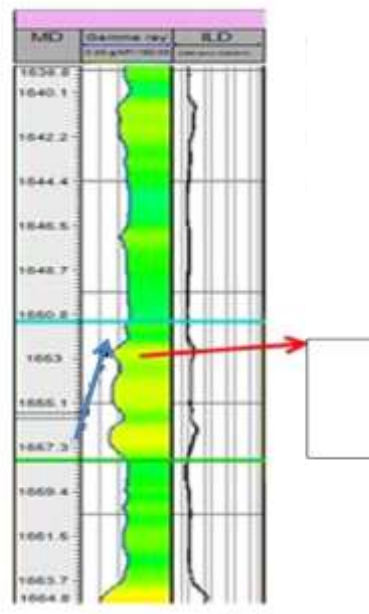


**Figure 4.6** Gamma ray log pattern in Cibulakan Formation (modified from [21])



An analysis of the depositional environment in the Cimangkis River outcrops, based on [18], places it in the Outer–Deeper Inner Neritic and Middle Neritic environments. This assessment is derived from observations of grain size, sediment structure characteristics, and a comparison of the thickness ratio of sand-shale lithofacies. According to [19], the study area's depositional environment is categorized as shallow marine show in figure 4.6.

According to [1], the Jatiluhur Formation is equivalent to the Cibulakan Formation. The deposition of the Jatiluhur Formation took place during the middle Miocene to early Late Miocene (N13 – N16) [20]. The description of the outcrop indicates an upward-fining pattern. Figure 4.7 illustrates an example of a gamma ray log pattern within the Cibulakan interval [21]. The gamma log pattern in the Cibulakan Formation interval exhibits an upward-fining pattern. This interval is dominated by sandstone lithology deposited in a shallow marine environment, specifically an inner littoral environment.

## CONCLUSIONS

Based on the observed stratigraphic column, the outcrops in the Cimangkis River are divided into four sequences of sedimentation: Claystone Unit (Sequence 1), Grainstone/Calsirudit Unit (Sequence 2), Calcarenit-Calsilutite Unit (Sequence 3), and Mudstone/Calsilutite Unit (Sequence 4). The analysis of the depositional environment indicates that the outcrops in the Cimangkis River were deposited in a shallow marine environment, specifically interpreted as the Outer–Deeper Inner Neritic area.

## ACKNOWLEDGMENTS

We thank to members of the Committee 'Al-Fiziya: Journal of Materials Science, Geophysics, Instrumentation and Theoretical Physics' for selecting this paper to be published.

## REFERENCES

- [1] Abdurrokhim. "Stratigrafi Sikuen Formasi Jatiluhur di Cekungan Bogor, Jawa Barat". (Bulletin of Scientific Contribution, 2017). 15(2), 167–172.
- [2] Abdurrokhim, & Ito, M. "The role of slump scars in slope channel initiation: A case study from the Miocene Jatiluhur Formation in the Bogor Trough, west java". (Journal of Asian Earth Sciences, 2013). 73, 68–86.
- [3] Martodjojo, S., "Parigi Limestone Field Trip, Karawang-Jatiluhur", In House Field Trip ARII-ITB, 23PP. 1990
- [4] Achdan, A. dan Sudana, D., Peta Geologi Lembar Karawang, Jawa, Direktorat Geologi, Departemen Pertambangan dan Energi, Republik Indonesia, Bandung. 1992
- [5] www. Google earth. Diakses jam 20.00 WIB 12 oktober 2017
- [6] Arpandi, D., Patmosukismo, S., "The Cibulakan Formation as One of the Most Prospective Stratigraphic Units in the Northwest Java Basinal Area". (IPA Proceeding. Vol 4th Annual Convention. Jakarta, 1975)
- [7] Budiyan et al., "Konsep Eksplorasi Untuk Formasi Parigi di Cekungan Jawa Barat Utara". (Makalah IAGI. Vol 20th, Indonesia., .1991) hal 45-67.
- [8] Pertamina BPPKA, "Petroleum Geology of Indonesian Basins: Principles, Methods and Application". Pertamina BPPKA. Indonesia. 1996
- [9] Walker, R. G., & James, N. P. Facies Model: Response to Sea Level Change. Geological Association of Canada. 1992.
- [10] Grabau, A., On The Classification of Sedimentary Rocks, New Jersey: Princeton University. 1904.

- [11] Nichols, G., *Sedimentology and Stratigraphy* 2nd Edition, San Antonio: Willey-Blackwell. 2009
- [12] Folk, R.L. *Practical petrographic classification of limestones*. Bulletin of the American Association of Petroleum Geologists, 1959. 43(1): 1-38
- [13] Tucker, M.T., dan Wright, V.P., *Carbonate Sedimentology*, Blackwell Science Ltd, Oxford. 1990.
- [14] P. A. Scholle and D. S. Ulmer-Scholle, "A Color Guide to the Petrography of Carbonate Rocks: Grains, Textures, Porosity, Diagenesis," AAPG Memoir, Vol. 77, 2003
- [15] Dunham, R.J. *Classification of Carbonate Rocks According to Depositional Texture*. In: Ham, W.E., Ed., *Classification of Carbonate Rocks*, AAPG, Tulsa, 108-121. 1962
- [16] Embry, A., dan Klovan, J., 1971, A Late Devonian Reef Tract on Northeastern Banks Island, *Bulletin of Canadian Petroleum Geology* vol.4, 730 – 781.
- [17] Lucia, F. Jerry, *Carbonate Reservoir Characterization "An Integrated Approach"* 2nd edition, Springer-Verlag, Berlin. 2007.
- [18] Tipson, H. L, Setzer, F. M, and Smith, F. L. JR. "Interpretation of Depositional Environment in Gulf Coast Petroleum Exploration from Paleocology and Related Stratigraphy." *Gulf Coast Assoc. Geol. Socs. Trans.* 1966.
- [19] W Imanda, et al., "Lithofacies analysis, ichnofacies analysis and depositional environment of Jatiluhur Formation in Cipamingkis area" (IOP Conf. Series: Earth and Environmental Science 846, 2021) 012021 doi:10.1088/1755-1315/846/1/012021
- [20] Mohamad Solihin, et al., "Biozonasi Foraminifera Planktonik Di Lintasan Sungai Cipamingkis, Daerah Jonggol, Provinsi Jawa Barat," *Bulletin of Scientific Contribution*, Volume 14, Nomor 1, April 2016: 55 – 62.
- [21] Firman Herdiansyah, et al., "Low Resistivity Zone Pada Reservoir Batupasir Formasi Cibulakan Atas, Cekungan Jawa Barat Utara Low Resistivity Zone In Sandstone Reservoir Upper Cibulakan Formation, North West Java Basin", *Bulletin of Scientific Contribution*, Volume 14, Nomor 1, April 2016: 97 – 116

---

## 2D JOINT INVERSION OF GRAVITY AND MAGNETIC DATA TO EVALUATE A GEOLOGICAL STRUCTURE IN TANIMBAR ISLAND

Arkanu Andaru <sup>1</sup>, Praditiyo Riyadi <sup>2,\*</sup>, Farah Aliya Rahma <sup>2</sup>, Muhammad Nafian <sup>2</sup>

<sup>1</sup>School of Computing, College of Engineering and Computer Science, Australian National University, Australia

<sup>2</sup>Physics Study Program, Faculty of Sciences and Technology, State Islamic University Syarif Hidayatullah Jakarta, Indonesia

\*[praditiyo.riyadi@uinjkt.ac.id](mailto:praditiyo.riyadi@uinjkt.ac.id)

---

Submitted: August ; Revised: August ; Approved: August ; Available Online: September

---

**Abstract.** Tanimbar Island is located in the eastern part of Indonesia, where this region is very famous for its immensely complex subsurface geology. The structure of the formed fold thrust belt is the biggest challenge for exploration, especially for oil and gas in the area. In this research, an innovation is carried out using joint inversion modeling by correlating physical parameters from two geophysical data: gravity and geomagnetic. This research aims to determine the subsurface mapping of the research area, determine the density and susceptibility values of rocks, and determine the structural patterns that exist in the subsurface. The results of subsurface mapping of the Tanimbar Islands based on the results of Joint Inversion modeling have found a geological structure pattern in the form of a fold-thrust belt due to the Banda Arc subduction zone. Section A-A has a sequence of fold-thrust belts with ten structural patterns, including six structures in the northwest-southeast direction and four in the northeast-southwest direction. In section B-B' there are nine structural patterns in the northeast-southwest direction. High anomalies obtained density values ranging from 2.77 - 2.81 gr/cm<sup>3</sup> and susceptibility ranging from 0.00125 - 0.0013 SI are thought to be caused by high basement in the form of volcanic rocks, while low anomalies obtained density values ranging from 2.45 - 2.49 gr/cm<sup>3</sup> and susceptibility ranging from 0.0008 - 0.00085 SI are thought to be caused by thick sedimentary layers of the Batimafudi Formation.

**Keywords:** *fold thrust belt, Geomagnetic, Gravity, Joint Inversion, Tanimbar*

**DOI :** [10.15408/fiziya.v6i1.34293](https://doi.org/10.15408/fiziya.v6i1.34293)

### INTRODUCTION

As in 2012, oil consumption reached 1.6 million barrels per day while production was only around 900 thousand barrels [1]. Therefore, exploration is needed to find potential hydrocarbon or oil and gas reserves in Indonesian areas that have not been exploited, especially in the eastern part of Indonesia. Complex geology and being on the fold thrust belt (FTB) route as a result of tectonic evolution [2] makes the Tanimbar Islands, Maluku interesting to study and selected to be the research area. Structurally the

Tanimbar Islands occupy part of the forearc of the banda arc (Figure 1) which is a collision zone between the Australian continental margin which causes deformation accompanied by diversion and fold and thrust processes along 23,000 km resulting from the mass of the Australian continental margin experiencing a roll back under the Banda trench. [3][4][5]. The characteristic of FTB in the study area is a thin-skinned anticline with a complex structure [6]. In some cases, the FTB contains accumulations of oil and gas in structural traps [7]

To see the oil and gas potential in the Tanimbar area, various efforts have been made, including the seismic reflection method. However, the results obtained in the study area are not clear enough to describe the complexity of geology because, and the seismic data does not show a clear subsurface image because the seismic reflector is poor due to the fold-thrust belt structure [2]. Therefore, other geophysical data such as gravity and geomagnetic data are needed. Even though the resolution of gravity and magnetic data is lower than the seismic method, the range of both methods is deep enough to see subsurface images. An approach using the forward modeling method with gravity data has been carried out [8], so an update was made using joint inversion modeling using gravity and geomagnetic data. This joint inversion combines physical parameters from different geophysical data which aims to increase data resolution and reduce the ambiguity of inversion modeling separately [9]. In this study, applying joint inversion in research areas with complex geology and looking at its effectiveness.

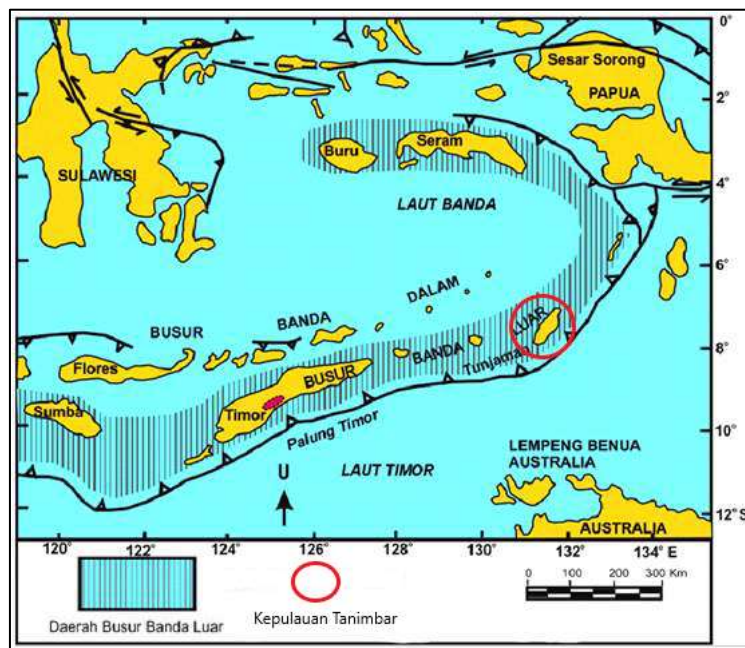


**Figure. 1** Banda Arc Forearc Map (Haryanto et al, 2021)

Joint inversion was carried out by Luis A. Gallard who integrated P-wave, S-wave, DC resistivity and audiomagnetotellurics data, L. Gross (2019) and M. Tavakoli, et al (2020) which combined gravity and geomagnetic data. The three studies above show that joint inversion is a fairly effective method with structurally consistent images of several physical parameters and produces higher image resolution compared to separate inversions [10][11][12]. The research was conducted for a preliminary survey of oil and gas exploration, which aims to determine the subsurface mapping, see the density and susceptibility of the subsurface, and determine the pattern of faults in the study area.

## RESEARCH METHODS

In this study, two secondary data from airborne surveys were used, namely gravity and geomagnetic data. The gravity method is based on measuring variations in the gravitational field caused by variations in rock density in the soil or subsurface [13]. The geomagnetic method is based on measuring variations in magnetic field intensity due to variations in the distribution of magnetized objects beneath the earth's surface [14]. The gravity data obtained has been acquired or the gravity data has been corrected to obtain a Complete Bouguer Anomaly (CBA) value. The geomagnetic data obtained has also been acquired and corrected to obtain a Total Magnetic Intensity (TMI) value. Then the data is processed into CBA and TMI contour maps (Figure 2).

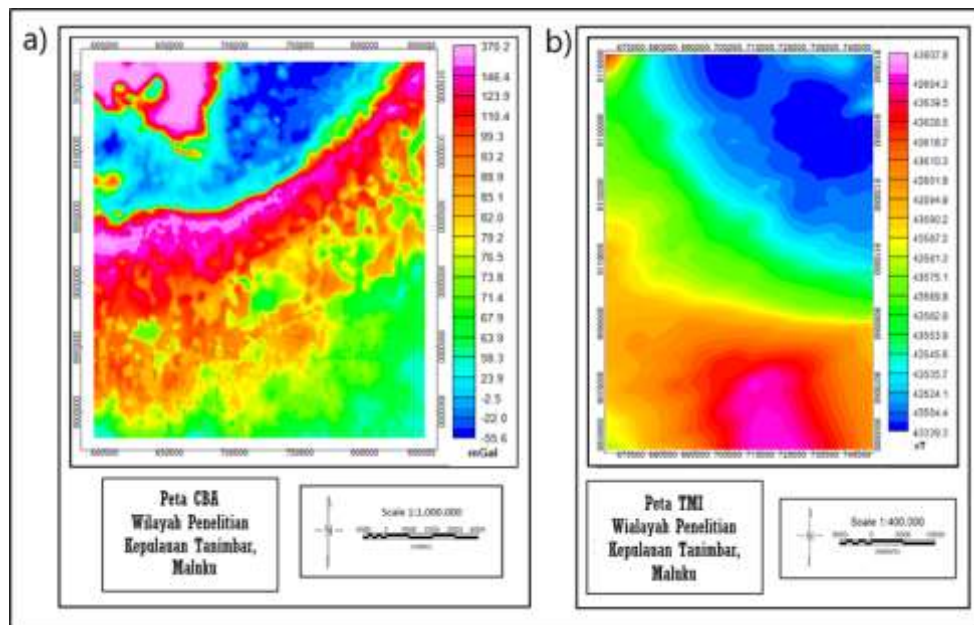


**Figure. 2** (a) CBA Map (b) TMI Map

To facilitate interpretation, the TMI map is processed into a Reduce to pole (RTP) map, namely transforming the dipole anomaly into a monopole by changing the inclination angle of the study area, namely  $-30^{\circ}$  to  $90^{\circ}$  and the declination angle, namely  $-5^{\circ}$  to  $0^{\circ}$  so that it looks as if measurements were made at the north pole. CBA and RTP maps still consist of regional anomaly effects, residual (local) anomalies, and noise. Regional and residual anomalies interact with each other and cause overlapping anomalies, so these anomalies must be separated from each other [15]. Anomaly separation is carried out by analyzing the Radially Averaged Power Spectrum (RAPS) curve at Oasis Montaj using a Bandpass filter, as shown in Figure 3. Bandpass filters are used to separate anomalies produced at different depths by adjusting the desired wave range [16].



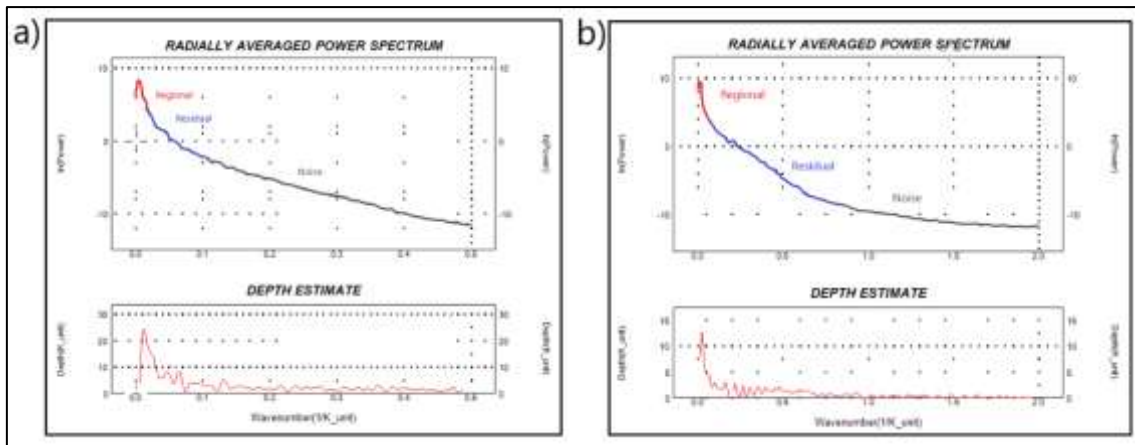


**Figure. 3** (a) RAPS gravity (b) RAPS magnetic

The target of this research is a shallow anomaly (residual) with a depth of approximately 10 km, then the residual anomaly is selected for further processing for modeling. Residual gravity and magnetic anomalies obtained by slicing were carried out at GYM-SYS Oasis Montaj. Slicing is done 2 times as shown in Figure 4. The first digit is A-A' trending northeast - southwest. The second digit is B-B' trending northwest - southeast.

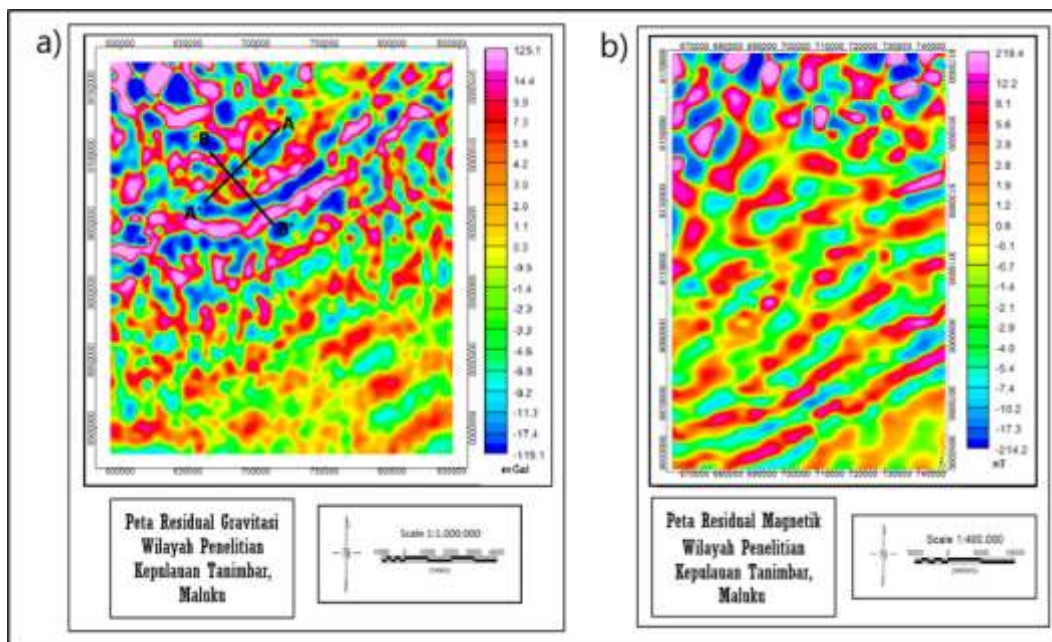


**Figure. 4** (a) Gravity residual slicing (b) Magnetic residual slicing

Then the data obtained is modeled separately inversion in ZondGM2d software. After that, a joint inversion was performed by correlating the two physical parameters from the gravity and magnetic data using a cross-gradient in ZondGM2d. The inversion modeling process is carried out by matching the curve (curve fitting) between the mathematical model and the data from observations or measurements. The result of inversion modeling is a subsurface model to estimate rock physical parameters [17].

## RESULTS AND DISCUSSIONS

The inversion modeling results show a heterogeneous subsurface pattern and the presence of low and high anomaly contrasts which might be caused by the fold thrust belt. Comparison of the results of single inversion and joint inversion is shown in Figure 5 (section A-A') and Figure 6 (section B-B'). It can be seen that there is a change in the model from the results of single inversion and joint inversion. Visible model changes are marked with red circles for gravity anomalies and also white circles for geomagnetic anomalies. There are several high anomalies that fade or become lower, and vice versa, namely low anomalies that fade to become higher. The error value generated by joint inversion is greater than that of single inversion, namely in section A-A' the gravity error is 6.41 and the geomagnetic error is 1.12. In section B-B' the gravity error is 3.33 and that of the geomagnetic is 4.40. Model changes and increasing error values are caused by joint inversion to establish a flexible balance between data discrepancies from different methods and structural similarity. However, there are also insignificant model changes which are thought to be due to the good results from a single inversion, and the limitations of joint inversion modeling in fold thrust belt areas or in areas with complex geology.

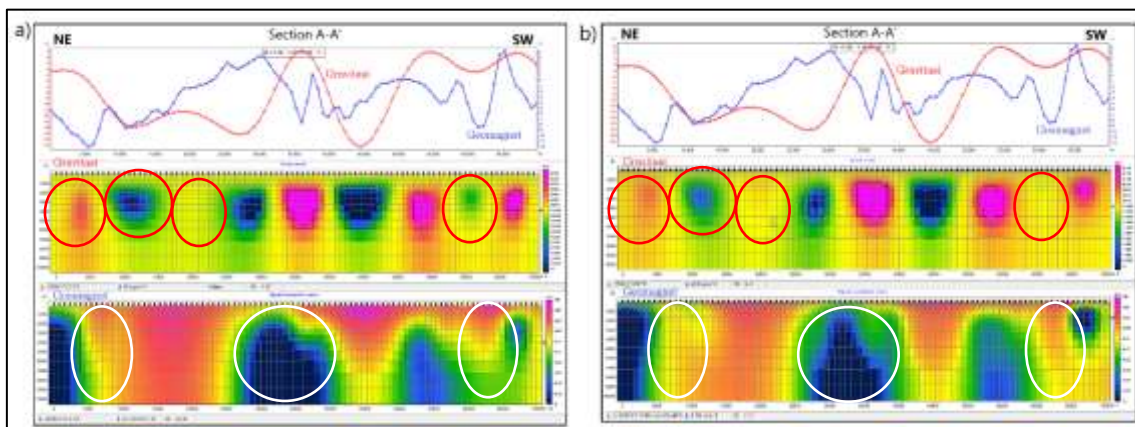


**Figure. 5** Comparison of Sections A-A': (a) Single Inversi (b) Joint Inversi

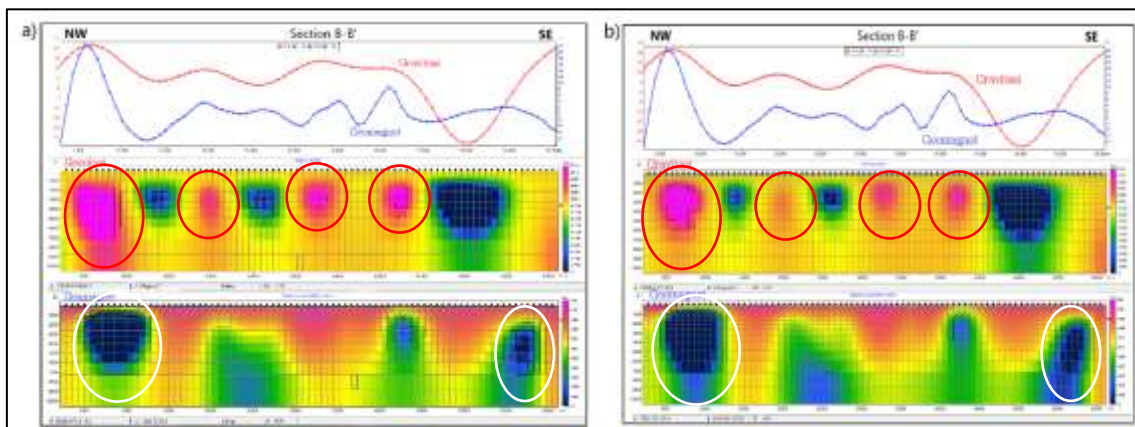


**Figure. 6** Comparison of Section B-B': (a) Single Inversi (b) Joint Inversi

From the results of the joint inversion, an interpretation of the subsurface mapping in the study area was carried out. The results of the joint inversion show the value of the

distribution of density and susceptibility values which can be seen from the contrast of the anomaly model obtained. In section A-A' and section B-B' (Figure 7) there is a high anomaly in the gravity and geomagnetic modeling which is marked with a red circle presumably due to the presence of a basement high with a high density of around 2.79 - 2.81 gr/cm<sup>3</sup> (section A-A'), and 2.77 - 2.79 gr/cm<sup>3</sup> (section B-B') and susceptibility with values ranging from 0.00125 – 0.0013 SI, which are suspected volcanic rocks from the Selu Formation of Permian age. This is the effect of subduction so that the basement is lifted up to the surface causing a high anomaly response. This usually allows the emergence of anticlinal structures as potential hydrocarbon structures. It is also seen that low anomalies in the gravity and geomagnetic modeling are marked with blue circles, presumably due to thick sedimentary rocks with density values ranging from 2.45 - 2.47 gr/cm<sup>3</sup> (section A-A') and 2.47 - 2.49 gr/cm<sup>3</sup> (section B-B'), and the susceptibility ranges from 0.0008 – 0.00085 SI which is thought to be caused by sedimentary rocks from the Batimafudi Formation consisting of shale and also sandy limestone crosses. In addition, there is also a high gravity anomaly but a low geomagnetic anomaly which is marked with a white circle. This is thought to be due to the subduction or collision of the Asian Continental plate (Banda Arc) with the Australian plate which causes high pressure and temperature so that the rocks experience demagnetization and the susceptibility value becomes low, while the density value becomes high due to the high temperature.

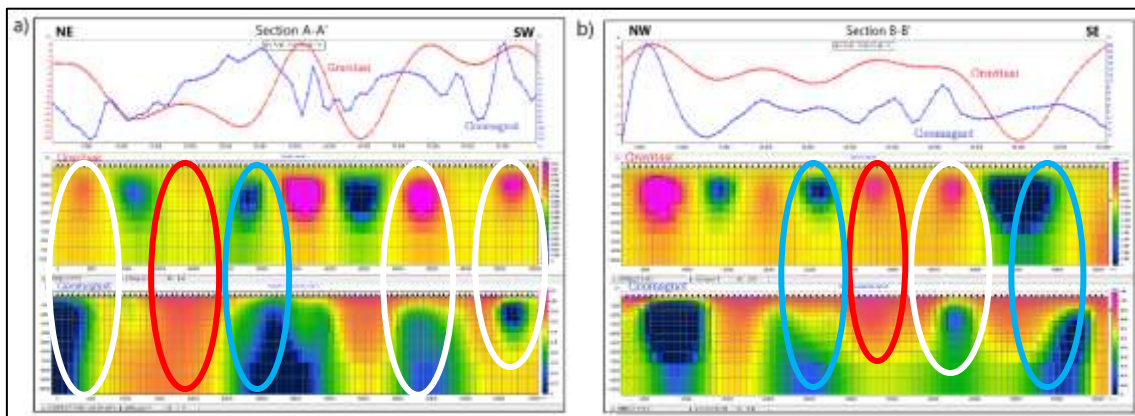


**Figure. 7** Joint Inversion Modeling Results: (a) Section A-A' (b) Section B-B'

The anomalous contrast resulting from the modeling of gravity and geomagnetic data indicated by the contrast of the blue (low) and pink (high) trend colors is thought to be due to the fracture of the fold thrust belt series due to the Banda Arc subduction zone. The model anomaly pattern generated by the gravity data is round in shape, which is suspected to be a fold of the fold thrust belt. This is in accordance with the concept or geological model from Charlton 2004, namely the existence of a fold thrust belt in the Tanimbar Islands. Referring to the geological model from Charlton 2004 [15], and seeing the trend of the anomalous pattern resulting from the joint inversion of gravity and geomagnetic data, a subsurface mapping was made in the study area shown in Figure 8. From the results of the model, a structural pattern can be seen indicating the presence of fold thrust belt in the study area. In section A-A' (Figure 8 (a)) it can be seen that there is a series of folded thrust belts with 10 structural patterns located at the anomaly contrast boundaries. The structure consists of 6 structures trending northwest-southeast and 4 structures trending northeast-southwest. In section B-B' (Figure 8 (b)) it can be seen that there is a series of fold thrust belts with 9 structural patterns trending



northeast-southwest. This pattern was proposed based on the geological model from Charlton 2004 (Figure 2.5) and the forward modeling results from Niluh 2021. Other structural patterns such as subsurface boundaries are not visible, and this is a limitation of inversion modeling.

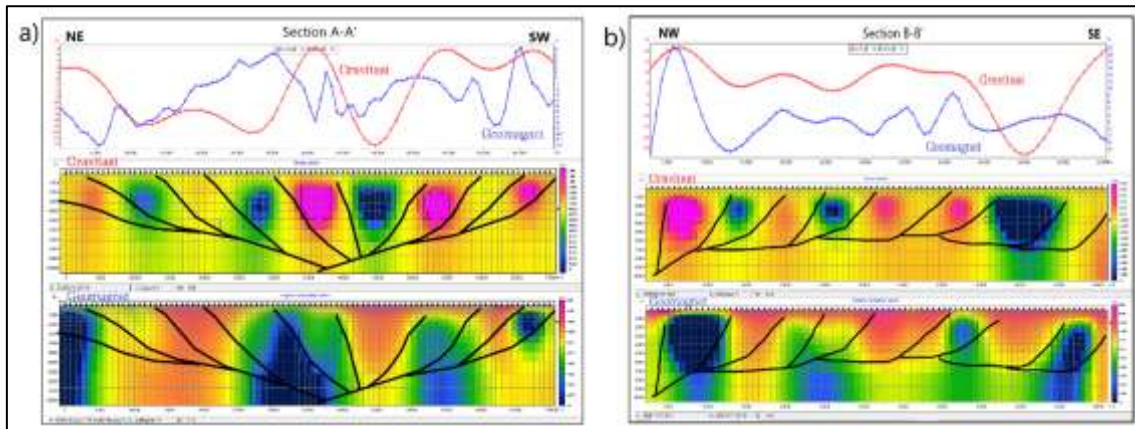


**Figure. 7** Interpretation of Joint Inversion Modeling: (a) Section A-A' (b) Section B-B'

## CONCLUSIONS

The results of the subsurface mapping of the Tanimbar Islands based on the results of Joint Inversion modeling have found a geological structure pattern in the form of a fold thrust belt due to the Banda Arc subduction zone as seen from the contrast of gravity and geomagnetic anomalies with the direction or pattern of folds referring to the Charlton 2004 publication model. From the results of 2 cross sections Joint Inversion modeling obtained high anomalies with density values ranging from 2.77 - 2.81 gr/cm<sup>3</sup> and susceptibility ranging from 0.00125 - 0.0013 SI which is suspected to be due to basement high in the form of volcanic rocks and low anomalies with density values ranging from 2.45 - 2.49 gr/cm<sup>3</sup> and susceptibility ranging from 0.0008 - 0.00085 SI which is thought to be due to thick sedimentary rocks beneath the surface. In section A-A', there are 10 structural patterns, namely 6 structures trending northwest-southeast and 4 structures trending northeast-southwest. In section B-B', it can be seen that there are 9 structural patterns trending northeast-southwest.

## REFERENCES

- [1] H. A. Saputro, "Analisis Produksi Minyak Mentah Indonesia Dengan Pendekatan Error Correction Model," *Econ. Dev. Anal. J.*, vol. 3, no. 1, pp. 36-47, 2014, [Online]. Available: <http://journal.unnes.ac.id/sju/index.php/edaj>
- [2] L. Lamba, I. Haryanto, D. S. Herutomo, N. Ilmi, and E. Sunardi, "Geologi Bawah Permukaan Dan Perhitungan Cadangan Hidrokarbon Dengan Metode Volumetrik Berdasarkan Interpretasi Data Seismik 2D Daerah Cekungan Tanimbar," *Padjadjaran Geosci. J.*, vol. 5, no. 4, pp. 394-404, 2021.
- [3] Koesnama and A. K. Permana, "Sistem Minyak Dan Gas Di Cekungan Timor, Nusa Tenggara Timur Petroleum System In The Timor Basin, Nusa Tenggara Timur," *J.G.S.M*, vol. 16, no. 1, pp. 23-32, 2015, [Online]. Available: <https://jgsm.geologi.esdm.go.id/index.php/JGSM/article/view/48>
- [4] M. G. Audley-Charles, "Geometrical problems and implications of large scale over-

- thrusting in the Banda Arc-Australian margin collision zone," *Geol. Soc. London, Spec. Publ.*, vol. 9, no. 1, pp. 407–416, 1981.
- [5] N. R. Amelia, Supriyanto, and H. Haryanto, "Identifikasi Stuktur Geologi Sebagai Potensi Area Jebakan Hidrokarbon Berdasarkan Integrasi Data Gaya Berat dan Data Seismik di Pulau Timor , Indonesia Timur," *Geosains Terap.*, vol. 4, no. 1, pp. 1–8, 2021.
- [6] T. R. Charlton, T. R. Charlton, and S. Omer, "The petroleum potential of inversion anticlines in the Banda Arc," vol. 5, no. 5, pp. 565–585, 2004, doi: 10.1306/12290303055.
- [7] J. Poblet and R. J. Lisle, "Kinematic evolution and structural styles of fold-and-thrust belts," *Geol. Soc. Spec. Publ.*, vol. 349, pp. 1–24, 2011, doi: 10.1144/SP349.1.
- [8] T. Niluh, "Integrasi Metode Gayaberat Dan Data Seismik Untuk Mengidentifikasi Struktur Perangkap," 2021.
- [9] R. Zhang, T. Li, C. Liu, X. Huang, K. Jensen, and M. Sommer, "3-D joint inversion of gravity and magnetic data using data-space and truncated Gauss–Newton methods," *IEEE Geosci. Remote Sens. Lett.*, vol. 19, pp. 1–5, 2021.
- [10] L. A. Gallardo, "Cross-Gradients Joint Inversion of Disparate Geophysical Data for Improved Subsurface Characterisation: Multiple-Physics Field Examples," *Philosophy*, pp. 1–7.
- [11] L. Gross, "Weighted cross-gradient function for joint inversion with the application to regional 3-D gravity and magnetic anomalies," *Geophys. J. Int.*, vol. 217, no. 3, pp. 2035–2046, 2019, doi: 10.1093/gji/ggz134.
- [12] M. Tavakoli, A. Nejati Kalateh, and M. Rezaie, "Two-Dimensional Cross-Gradient Joint Inversion of Gravity and Magnetic Data By a Sequential Strategy," *82nd EAGE Conf. Exhib. 2021*, vol. 2, no. November, pp. 1112–1116, 2021, doi: 10.3997/2214-4609.202010967.
- [13] M. Syukri, *Pengantar Geofisika*. Syiah Kuala University Press, 2020.
- [14] S. H. Muchtar, "Penerapan Metode Geomagnetik Untuk Identifikasi Sebaran Batubara Daerah Klatak Kecamatan Besuki Kabupaten Tulungagung," Universitas Islam Negeri Maulana Malik Ibrahim, 2018.
- [15] J. Purnomo, S. Koesuma, and M. Yuniyanto, "Pemisahan Anomali Regional-Residual pada Metode Gravitasi Menggunakan Metode Moving Average, Polynomial dan Inversion," *Indones. J. Appl. Phys.*, vol. 3, no. 01, p. 10, 2013, doi: 10.13057/ijap.v3i01.1208.
- [16] J. D. Phillips, *Geosoft eXecutables (GX's) developed by the US Geological Survey, version 2.0, with notes on GX development from Fortran code*. US Geological Survey, 2007.
- [17] Supriyanto, *Analisis Data Geofisika: Memahami Teori Inversi*. 2007.
- [18] W. J. Hinze, R. R. B. Von Frese, R. Von Frese, and A. H. Saad, *Gravity and magnetic exploration: Principles, practices, and applications*. Cambridge University Press, 2013.
- [19] U. Permana, "Pengolahan Data Seismik Refleksi 2d Untuk Memetakan Struktur Bawah Permukaan Lapangan X Prabumulihsumatra Selatan," *ALHAZEN J. Phys.*, vol. 2, no. 1, 2015.
- [20] A. Syafnur and T. A. Sunantyo, "Potensi Airborne Gravity untuk Studi Sesar," *Pros. Semin. Nas. Geotik*, pp. 392–399, 2019.

